Prace Naukowe Instytutu Chemii Organicznej i Fizycznej
Politechniki Wrocławskiej
37
Seria: Monografie
21

Andrzej Miniewicz

Search for molecular-ionic and molecular crystals exhibiting ferroelectric and electrooptic properties

Wrocław 1990

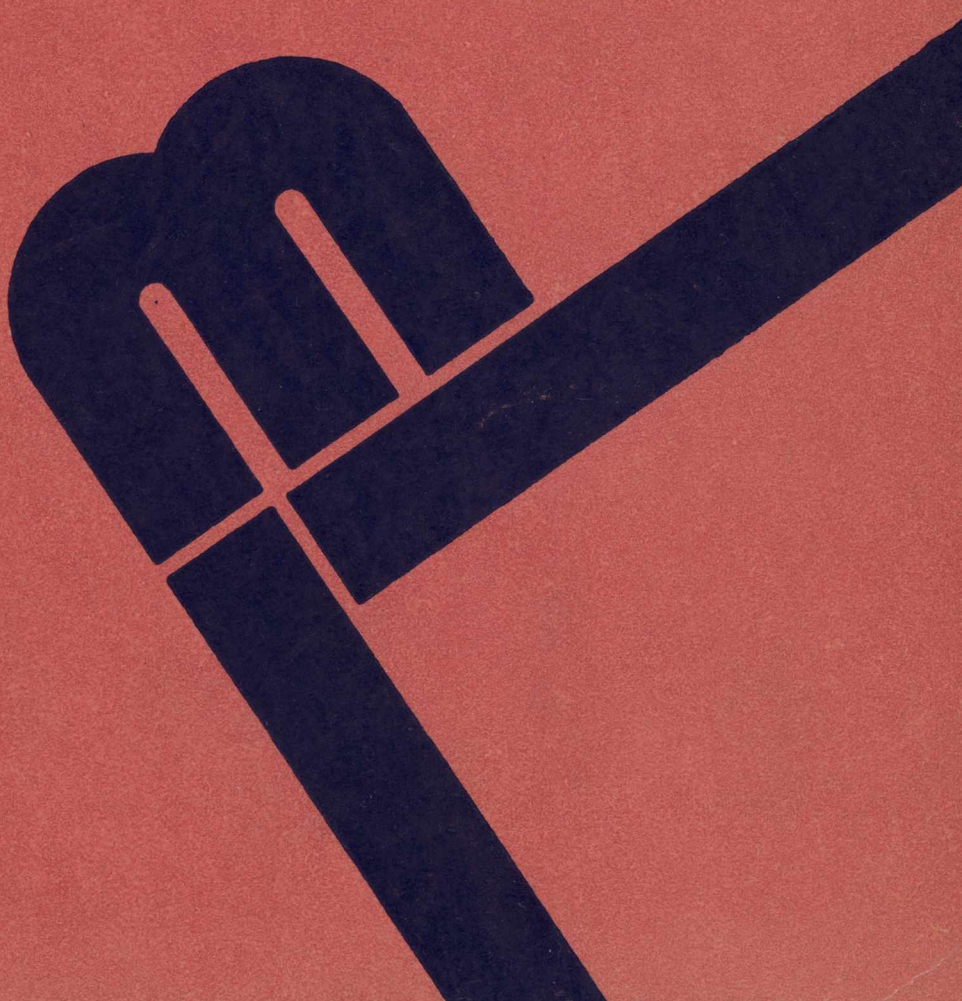

PRACE NAUKOWE POLITECHNIKI WROCŁAWSKIEJ

Scientific Papers of the Institute of Organic
and Physical Chemistry
No. 37 of the Technical University of Wrocław No. 37

Monographs No. 21 1990

Andrzej MINIEWICZ

Search for molecular-ionic and molecular crystals exhibiting ferroelectric and electrooptic properties

Prace Naukowe Instytutu Chemii Organicznej i Fizycznej Politechniki Wrocławskiej 37

Seria:
Monografie 21

Andrzej Miniewicz

Search for molecular–ionic and molecular crystals exhibiting ferroelectric and electrooptic properties

Wydawnictwo Politechniki Wrocławskiej · Wrocław 1990

Recenzenci
Zbigniew CZAPLA
Hubert KOŁODZIEJ
Juliusz SWORAKOWSKI

Redaktor naukowy
Lucjan ACHREMOWICZ

Opracowanie redakcyjne i korekta
Hanna BASAROWA

WYDAWNICTWO POLITECHNIKI WROCŁAWSKIEJ
Wybrzeże Wyspiańskiego 27, 50-370 Wrocław

ISSN 0324-976x

Nakład 180+70 egz. Ark. wyd. 7. Ark. druk. 6½. Papier offset. kl. III, 70 g. B1.
Oddano do druku w kwietniu 1990 r. Druk ukończono w maju 1990 r.
Zakład Graficzny Politechniki Wrocławskiej. Zam. nr 612/90. Cena zł 1500,-

Prace Naukowe Instytutu Chemii Organicznej i Fizycznej
Nr 37 Politechniki Wrocławskiej Nr 37

Monografie Nr 21 1990

Ferroelectricity, pyroelectricity, electrooptic properties, phase transitions, molecular ionic crystals

Andrzej MINIEWICZ*

SEARCH FOR MOLECULAR–IONIC AND MOLECULAR CRYSTALS EXHIBITING FERROELECTRIC AND ELECTROOPTIC PROPERTIES

To my Wife

Author

The monograph reviews the author's work in the field of physics of molecular–ionic and molecular crystals, the emphasis being put on the crystals with polar structures. Three groups of crystals are investigated: organic–inorganic halides, acid phthalates and organic charge transfer complexes. Ferroelectric, pyroelectric, elastic, as well as electrooptic properties of several representatives of the mentioned groups are experimentally determined. Numerous phase transitions are studied using the Raman, Brillouin and IR spectroscopy as well as dielectric, calorimetric and X-ray techniques. Application perspectives for some of the studied materials are discussed.

* Institute of Organic and Physical Chemistry, Technical University of Wrocław, Wybrzeże Wyspiańskiego 27, 50-370 Wrocław

INTRODUCTION

The concept proposed by Hans Kuhn in the early 1960's, nowadays known as "molecular engineering" has succeeded in preparation of many purpose oriented materials. A definition of the molecular engineering was given by Kuhn [1] in 1985: "The design and construction of organized systems of molecules that interlock and interact like the parts of a machine is a great challenge. Materials thus obtained can have basically new properties depending on the exact localization of each component molecule. Tools to manipulate single molecules are of great interest. New fundamental physical and chemical processes can be studied and bioprocesses can be simulated using man-made molecules as well as biomolecules as components. Molecular assemblies are of great interest in developing microelectronics, memories with much higher storage density than chips based on present day's technology, microsensors of high specificity, new catalyst for complex reactions, and arrangements for solar energy conversion".

Such a challenge has been undertaken by scientists skilled in chemistry, physics, X-ray crystallography, crystal growth etc. bringing a wide range of new materials with fascinating properties e.g., high-temperature superconductivity and high nonlinear optical properties. The former phenomenon has been found by Müller and Bednorz as a result of their studies on physical properties of inorganic perovskites (1987, Nobel Prize in physics), whereas the best nonlinear optical materials were found among molecular organic crystals basing on the theory of nonlinear optics developed by Bloembergen (1981, Nobel Prize in physics).

During recent decades it has been established that organic solids have an enormous range of interesting properties that are almost continuously "tunable". For the last 15 years some very interesting properties have been discovered in this class of materials: for example, superconductivity [2], spinless conductivity in "doped" conjugated polymers [3], and large nonlinear optical responses [4]. However, despite tremendous efforts such a phenomenon as ferroelectricity has been documented only for two low-molecular weight molecular crystals: thiourea [5] and tanane [6], whereas it is quite popular among inorganics.

The aim of this and many other basic studies is to search for materials which can be promising candidates for advanced device and system application with the emphasis put on to the field of nonlinear and

electrooptic technology. Developments in the field of nonlinear optics hold promise for important applications in optical information processing, telecommunication, and integrated optics. Particularly important is the more recent recognition that organic and polymeric materials with large delocalized π-electron systems may exhibit extremely large nonlinear responses, in many cases much larger than their inorganic counterparts. Thin films of organic or polymeric materials with large second-order nonlinearities in combination with Si-based electronic circuitry offer the possibility of novel phenomena and devices for laser modulation and deflection, information control in optical circuitry, light valves, optical bistability and all optical switches. However, as with any new class of materials, the existence of certain promising samples does not imply that real applications will necessarily be possible. Real optical materials must exhibit some basic properties, including optical clarity (very low scattering and absorption losses), fabricability, and the potential for mass production. These secondary properties are generally not addressed by fundamental research but they determine usability of materials.

This monograph describes the author's effort to look for suitable classes of materials, growing single crystals, checking their polar properties and measuring various other physical effects necessary to characterize and understand diverse processes taking place in the studied crystals. Among many possible classes of materials, we focused our attention on the poorly recognized, in that respect, classes of organic-inorganic crystals and weak charge transfer complex crystals. In the class of organic salts the Van der Waals bonding, typical of pure organics, is replaced by the ionic bonding, and also partially by H-bonding, typical of inorganics. Such types of materials have already been known, but were not seriously studied as potential candidates for electrooptic devices.

By presenting this work we wish to contribute to the knowledge of the physical properties of ionic-molecular crystals e.g., phthalates and organic-inorganic halides, but also of organic charge transfer (CT) complexes, with the data obtained from several substances. The data were analyzed having in mind the desire to understand the mechanisms underlying various polar properties of the crystals and the nature, and structural aspects of phase transformations taking place in some of the materials. The latter seems to be very important on the ground of molecular engineering able to continuously or dramatically change the properties of respective materials.

The experimental results reviewed here represent a joint effort of our, and at least three other research groups from Institute of Chemistry

of University of Wrocław, Groupe de Physique Cristalline of University of Rennes I and Laboratoire de Dynamique des Cristaux Moleculaires of University of Lille I.

The material has been arranged into several parts. The first of them deals with a brief overview of problems and theories concerning investigations of various polar properties. This is followed by the presentation of experimental work, including a section reviewing the necessary formal background and a section with an appropriate discussion. Although no attempt is made to provide a comprehensive literature data, the presentation is supplemented, whenever necessary, with relevant results taken from the literature. Since the literature on the subject is quite extensive, especially where experimental results are concerned, only selected original papers will be quoted.

1. POLAR PROPERTIES OF CRYSTALS

1.1 Definitions

All the properties which uniquely are characteristic of noncentrosymmetric solids are referred to as "polar properties". Because polar properties such as ferroelectricity, pyroelectricity and piezoelectricity are well recognized their definitions will be only shortly reminded here whereas nonlinear optical properties (NLO) will be described in more detail.

Pyroelectric and piezoelectric crystals form a large class of materials whose electric polarization can be changed or produced by variation of temperature or stress, respectively.

A piezoelectric crystal when exposed to an electric field suffers a deformation (strain η_{ij}) or stress σ_{ij}, both proportional to the applied field. In a linear approximation the equations describing electrical and mechanical state of the piezoelectric sample are

$$\begin{aligned} D_i &= d_{ijk}\sigma_{jk} + \varepsilon_{ij}E_j \,, \\ \eta_{ij} &= s_{ijkl}\sigma_{kl} + d_{kij}E_k \,, \end{aligned} \tag{1}$$

D is the electric displacement, E is the electric field, d is the piezoelectric tensor, ε is the dielectric tensor and s is the compliance tensor. It should be noted that the Einstein convention of summation over

repeated indices is used throughout the text. For further reading on this subject the reader is referred to [7]-[10].

The pyroelectric properties of a material are described by a pyroelectric coefficient p_i which relates the changes of the temperature of crystal, ΔT, with the electric polarization vector, ΔP_i, along the i-th polar axis

$$\Delta P_i = p_i \Delta T \ . \tag{2}$$

Strictly, the pyroelectric coefficient p_i^{σ} at constant stress σ and at constant electric field E is defined by

$$p_i^{\sigma} = \left(\frac{\partial D_i}{\partial T} \right)_{\sigma,E} = \left(\frac{\partial P_i}{\partial T} \right)_{\sigma,E} \ . \tag{3}$$

Here, D_i and P_i, denote the components of the electric displacement and polarization vectors, respectively, and T is the temperature. p_i^{σ} is the sum of the primary pyroelectric coefficient p_i^{η} defined at constant strain η and constant E, and the piezoelectric effect due to the thermal strain (the secondary pyroelectric coefficient p_i^{sec}). This relationship can be expressed by the tensor equation [11]

$$p_i^{\sigma} = p_i^{\eta} + d_{ijk}^{T,E} \cdot c_{jklm}^{T,E} \cdot \alpha_{lm}^{\sigma,E} = p_i^{\eta} + p_i^{sec} \ , \tag{4}$$

where $d_{ijk}^{T,E}$ and $c_{jklm}^{T,E}$ denote, respectively, the tensor components of the piezoelectric and elastic stiffness moduli measured at constant T and E, whereas $\alpha_{lm}^{\sigma,E}$ is the thermal expansion tensor at constant σ and E. The pyroelectric coefficient $\bar{p} = (p_1, p_2, p_3)$ defined above is a vector quantity.

Ferroelectric and ferroelastic crystals are the solids in which the spontaneous polarization P_s or spontaneous strain η_s can be reoriented in an electric or stress field.

A ferroelectric crystal is defined as a crystal which belongs to the pyroelectric family and in which the direction of spontaneous polarization P_s (a polarization at E = 0 and σ = 0) can be reversed by an application of an external electric field, weak as compared to a local crystal field. There are many monographs on ferroelectricity [12]-[15] and it is far beyond the scope of this monograph to give the survey of this large area of knowledge. However, basic theories of ferroelectric-to-paraelectric phase transitions will be treated separately in the next section.

A crystal is ferroelastic if it has several "orientation states", identical or enantiomorphous in their crystal structure but different

with respect to their spontaneous strain [16]. Every orientation state can be considered as a tiny distortion, resulting from minute displacements of the atoms of a certain ideal structure called its "prototype". The spontaneous strain occurs at null stress in the same way as the spontaneous polarization occurs in a ferroelectric material in the absence of an electric field. A ferroelastic crystal generally undergoes a phase transition at some temperature T_o. An appropriate mechanical stress can transform the crystal from one to another of the orientational states. Ferroelastic crystals are characterized by three parameters, the coercive stress σ^c_{ij} required for reorientation, the spontaneous strain η^s_{ij}, and the atomic displacements Δ through which the atoms move during reorientation [17]. The possible orientations of domain walls between orientational states in ferroelastic materials were investigated theoretically by Sapriel [18].

1.2. Phenomenological theory of phase transitions in ferroelectrics

Close to a phase transition various thermodynamical energies used to describe ferroelectric material can be expressed in a Taylor series, e.g.,

$$A = A_o + \left(\frac{\partial A}{\partial T}\right)(T-T_o) + \left(\frac{\partial A}{\partial \eta_{ij}}\right)\eta_{ij} + \left(\frac{\partial A}{\partial P_i}\right)P_i + \frac{1}{2}\left(\frac{\partial^2 A}{\partial T^2}\right)(T-T_o)^2 + \frac{1}{2}\left(\frac{\partial^2 A}{\partial \eta_{ik}\partial \eta_{jl}}\right)\eta_{ik}\eta_{jl} + \ldots + \left(\frac{\partial^2 A}{\partial \eta_{ik}\partial P_j}\right)\eta_{ik}P_j + \text{higher order terms.} \qquad (5)$$

Usually it is sufficient to consider the expansion up to the sixth order. Symmetry considerations allow one to reduce the number of expansion terms and to construct a correct, for a given symmetry, form of energy [19]-[21]. The theory of phase transitions based on the above expansion and employing symmetry rules is known as the Landau-Devonshire one.

Phase transitions usually observed are classified according to the Ehrenfest definition [22]. An n-th order transition is the transition where the (n-1)-th derivative of the Gibbs free energy G is continuous, while the n-th derivative shows discontinuity at the transition temperature T_o. Among several thermodynamic functions, the elastic Gibbs function $G_1(T,\sigma,P)$ is the most useful for discussion of the ferroelectric phase transition due to its relevance to ordinary experimental conditions, that is, under constant temperature and constant external

forces. One can discuss the main results of Landau-Devonshire theory for a simplified case of ferroelectric having only one component of spontaneous polarization P. In such a case G_1 is an even function of P, and its expansion in Taylor series leads to

$$G_1 = G_1^\circ + \frac{\chi}{2} P^2 + \frac{\xi}{4} P^4 + \frac{\zeta}{6} P^6 , \tag{6}$$

where the terms of higher orders of P are neglected. G_1° stands for the elastic Gibbs function for P = 0. χ, ξ and ζ are, generally, functions of temperature but to sufficiently good approximation one usually assumes ξ and ζ to be constant. In order to have a stable phase with the finite polarization we assume that $\zeta > 0$. For E = 0 one gets a solution of Equation (6) in the form

$$P_s^2 = \frac{-\xi \pm (\xi^2 - 4\chi\zeta)^{1/2}}{2\zeta} \qquad \text{and} \qquad P_s^2 = 0. \tag{7}$$

A stable phase is obtained for positive P_s^2 and $G_1 \leq G_1^\circ$. If $\xi > 0$ one deals with a second order phase transition and for $\xi < 0$ one deals with a first order phase transition.

(i) *Second order phase transition ($\xi > 0$)*

In this case $P_s^2 > 0$ only when $\chi < 0$, it is common to assume the temperature dependence of χ as

$$\chi = \beta (T - T_o) \tag{8}$$

where β is a constant ($\beta > 0$) and T_o is the transition temperature, equal to the Curie point T_c. In the vicinity of the phase transition the inverse susceptibility $\chi' = \left(\frac{\partial E}{\partial P}\right)_{P=0}$ is given for weak electric field by

$$\begin{aligned} \chi' &= \chi \qquad \text{for } T > T_o \qquad \text{and} \\ \chi' &= -2\chi \qquad \text{for } T < T_o . \end{aligned} \tag{9}$$

(The above equations are true only within a limited temperature range around T_o.) The temperature dependence of the spontaneous polarization P_s is given by the equation

$$\begin{aligned} P_s &= \left[\frac{\beta}{\xi} (T_o - T)\right]^{1/2} \qquad \text{for } T < T_o \\ P_s &= 0 \qquad\qquad\qquad\quad \text{for } T > T_o . \end{aligned} \tag{10}$$

In the above, we have discussed the case of E = 0, if E is not equal to zero, P depends on temperature smoothly, and there is no special temperature to be called a transition point.

(ii) *First order phase transition* ($\xi < 0$)

If $\xi^2 > 4 \chi \zeta$ and $\chi < 0$ the solution of equation (7) has the form

$$P_s = \left[\frac{|\xi| + \sqrt{\xi^2 - 4 \chi \zeta}}{2 \zeta} \right]^{1/2} . \tag{11}$$

The spontaneous polarization suffers a discontinuity at the Curie point T_c which now is given as

$$T_o = T_c + \frac{3}{16} \frac{\xi^2}{\beta \zeta} , \tag{12}$$

and the value of P_s at T_c is equal to $\left[\frac{3|\xi|}{4 \zeta} \right]^{1/2}$. Just below the Curie point the inverse dielectric susceptibility χ' is approximately equal to

$$\chi' = - 4 \chi \tag{13}$$

and thus it is about four times as large as that just above the Curie point. The phenomenological theories of phase transitions were successfully applied to many ferroelectrics such as triglycine sulfate (TGS) [23], [24], $NaNO_2$ [25], [26], Rochelle salt ($NaKC_4H_4O_6 \cdot 4\ H_2O$) [27], KH_2PO_4 (KDP) [28], [29], $BaTiO_3$ [30], [31] and to many other ones [15].

The Landau theory of phase transitions is now a serious tool for studying different types of transitions, not necessarily ferroelectric ones. The recent book by Toledano and Toledano [32] has been devoted to its full formulation and many applications. Of course, as no phenomenological approach is sufficient for a proper description of diverse details of physical properties of a ferroelectric crystal a number of molecular, statistical and dynamical theories were employed as well [33]-[36].

1.3. Nonlinear optical phenomena (NLO)

The NLO phenomena will be discussed in more detail than the other polar properties, simply because they are much less recognized and rarely studied in Poland.

Nonlinear properties of Maxwell's constitutive relations $D = \varepsilon(E)E$ and $B = \mu(H)H$ are well known. The dielectric permittivity and magnetic

permeability can be functions of the field strength. Nonlinear properties in optical region have been demonstrated by harmonic generation of light. As early as in 1961, Franken et al. [37] detected ultraviolet light (λ = 347 nm) at twice the frequency of a ruby laser beam (λ = 694 nm) when this beam traversed a quartz crystal.

The nonlinear properties of the material are described by expanding the polarization in a power series in the electric field. This procedure is useful because the optical nonlinearities are small, and were discovered only after the development of powerful lasers. High electric fields with peak amplitudes of about 10^8 V/m, corresponding to a flux density of about 10^{13} W/m^2, are now available at optical frequencies using Q-switched lasers.

1.3.1. Linear electrooptic effect

The first observed nonlinear optical phenomena were electrooptic effects (Kerr, 1875; Pockels, 1906) [38], [39]. The electrooptic effect is defined by the change in the electric impermeability induced by an applied electric field [40]

$$B_{ij}(E) - B_{ij}(0) = \left[\frac{1}{\epsilon(E)}\right]_{ij} - \left[\frac{1}{\epsilon(0)}\right]_{ij}$$

$$= r_{ijk}E_k + t_{ijkl}E_kE_l + .., \qquad (14)$$

where B_{ij} is the impermeability tensor, ϵ the dielectric tensor, and E_m the applied electric field; r_{ijk} is the linear electrooptic or Pockels coefficient, and t_{ijkl} is the quadratic electrooptic or Kerr coefficient. The early discovery of these two nonlinear optical effects is consistent with the fact that laser light is not required, and that very small changes in the optical indicatrix can be readily observed through a phase retardation between the two polarizations of light propagating in a birefringent medium. Note that r_{ijk} is symmetric with respect to the first two indices, and thus r_{ijk} can be written in reduced tensor notation, r_{uk} [11]. Kleinman symmetry rules [41] do not apply to the linear electrooptic effect.

With the advent of lasers, a host of other nonlinear optical phenomena was discovered [42]. These phenomena are defined by the electric polarization of the medium, and thus are described by so called nonlinear optical susceptibilities [43]

$$P_i = P_o + \chi_{ij}^{(1)}E_j + \chi_{ijk}^{(2)}E_jE_k + \chi_{ijkl}^{(3)}E_jE_kE_l + ..., \qquad (15)$$

where P is the polarization induced in macroscopic medium under the influence of field E, and the $\chi^{(n)}$ are the macroscopic coefficients (susceptibilities) that reflect the projection of the microscopic molecular tensors on an appropriate direction within the unit cell.

Within this formalism, the linear electrooptic effect is defined by the change in the optical susceptibility

$$\Delta \chi_{ij}^{(1)} = \Delta \varepsilon_{ij} = - \varepsilon_{ii} \Delta B_{ij} \varepsilon_{jj} , \tag{16}$$

for $\Delta\varepsilon_{ij} \ll \varepsilon_{ii}$ and ε_{jj}. The induced polarization is then given by

$$P_i(t) = \varepsilon_o \Delta \chi_{ij}^{(1)} E_j = - \varepsilon_o \varepsilon_{ii} \varepsilon_{jj} r_{ijk} E_j(t) E_k(t) . \tag{17}$$

If the electric field is a periodic function of time, then

$$E_j(t) = E_j \cos(\omega_u t + \Phi_u) = 1/2 \left[e_j(\omega_u) \exp(-i\omega_u t) + e_j^*(-\omega_u) \exp(i\omega_u t) \right] , \tag{18}$$

with $e_1(\omega)$ being the Fourier amplitudes of the electric fields including the overall phase. Taking $\omega_u = \omega$, ω being the optical frequency, and $\omega_w = 0$ (for the applied dc field), then the polarization at the optical frequency is

$$P_i(\omega) = - \varepsilon_o \varepsilon_{ii}(\omega) \varepsilon_{jj}(\omega) r_{ijk} e_j^{\omega} e_k^{0} . \tag{19}$$

If a similar analysis is carried out in the notation of a second order nonlinear optical susceptibility defined by

$$P_i(t) = \varepsilon_o \chi_{ijk}^{(2)} E_j'(t) E_k'(t) , \tag{20}$$

then the following relationship between the nonlinear susceptibility and the electrooptic coefficient is obtained

$$\chi_{ijk}^{(2)}(-\omega;\omega,0) = -1/2 \, \varepsilon_{ii}(\omega) \varepsilon_{jj}(\omega) r_{ijk}(-\omega;\omega,0) , \tag{21}$$

where $\varepsilon_{kk}(\omega) = n_k^2$, n being the principal indices of refraction and in parentheses the output and input frequencies of the electric fields involved are given.

Frequency dependence of a linear electrooptic effect

In general, the electrooptic effect can depend on three distinct processes depending on the modulating frequency. For the linear electrooptic effect, the modulating frequency is lower than the frequencies of acoustic and optical phonon modes, thus both of them will contribute to the electrooptic susceptibility. In the Born-Oppenheimer approximation, the responses of phonon and electronic modes are independent and can be expressed as

$$r = \frac{d\,\chi(\omega_o)}{d\,E(\omega_m)} = \left[\frac{\partial\chi(\omega_o)}{\partial E(\omega_m)}\right]_{Q=0} + \left[\frac{\partial\chi(\omega_o)}{\partial Q}\right]_{E(\omega_m=0)} \times \frac{\partial Q}{\partial E(\omega_m)}. \qquad (22)$$

In the above expression, Q is a lattice displacement, $E(\omega_m)$ is the modulating field, and $\chi(\omega_o)$ is the linear susceptibility at optical frequency ω_o [44]. The first term is the primary electrooptic effect, which is of purely electronic origin. The second term is the secondary effect, which arises from the action of the modulating field on the lattice, which is related to the piezoelectric effect, and from the change in the optical susceptibility due to the lattice deformation, which is related to the photoelastic effect. The frequency dependence of the electrooptic coefficient is shown schematically in Fig. 1.

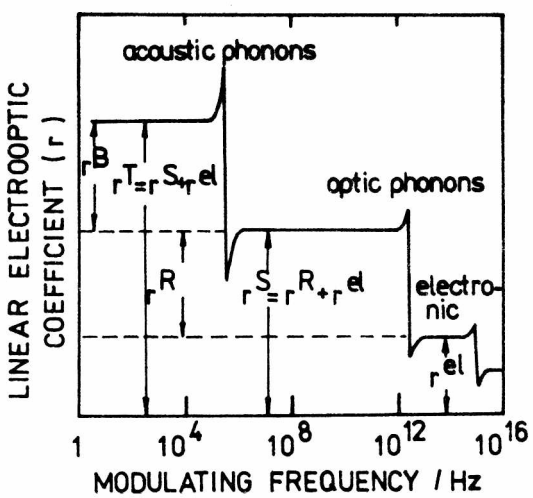

Fig. 1. General dispersion for the linear electrooptic coefficient including contributions from electronic modes, r^{el}, optical phonon modes, r^R, and acoustic phonon modes, r^B. The term r^T is the unclamped and r^S the clamped electrooptic coefficient (after [45])

At low frequencies, acoustic modes appear in the crystal showing characteristic frequencies determined by the size and shape of the particular sample. At these frequencies, the material will deform with the applied field, thus in experiment one determines the unclamped or stress-free coefficient r^T. The coefficient r^T contains contributions due to low-frequency acoustic modes, r^B, optical modes, r^R, and electronic modes, r^{el}. Above frequencies of the acoustic modes and up to the frequencies of optical phonon modes, the material strains are small, yielding the clamped or strain-free coefficient r^S, with contributions from r^R and r^{el}. Above the optical phonon restrahl, only r^{el} is measured, and this is then considered in optical parametric process. It should be noted that the magnitude and sign of the various contributions are material-dependent.

The contribution of the electronic states to the electrooptic coefficient can be determined by measuring an optical parametric susceptibility, such as the second-harmonic generation (SHG) coefficient. (In the second order term of equation (16), a polarization is induced proportionally to the square of the applied electric field, and the nonlinear second order optical susceptibility $\chi^{(2)}(-2\omega;\omega,\omega)$ is responsible for SHG of incoming light.) The residual electrooptic susceptibility is then due to the phonon modes. The contribution of the optical modes can be determined independently by Raman scattering, since it measures fluctuations in the refractive indices due to thermally excited optical phonons. Similarly, the acoustic phonon contribution can be obtained from Brillouin scattering, since it probes thermally excited acoustic phonon modes. The relative contributions of the acoustic and optical phonons can also be probed by measuring the clamped and unclamped electrooptic coefficient.

In order to assess the relative contributions of the electrons and phonons to the electrooptic effect, the electrooptic and the optical parametric susceptibilities can be compared [40].

1.3.2. Nonlinear optical properties of organic compounds

Molecular polarizability

The dipole moment of an isolated molecule in an external field is given by the equation [46]

$$p_i = \mu_i + \alpha_{ij}E_j + \beta_{ijk}E_jE_k + \gamma_{ijkl}E_jE_kE_l + \ldots, \qquad (23)$$

where μ_i is the permanent dipole moment, α_{ij} is the polarizability

tensor, β_{ijk}, γ_{ijkl}, etc. are the hyperpolarizability tensors, and E_j is a component of the electric field acting on the molecule. All the tensors are frequency dependent and should be written as functions of the frequency of the fields and the polarization produced.

Molecular crystals are formed from individual molecules which interact through weak intermolecular forces (dispersion, dipole-dipole, etc.) and retain their individual identity to a high degree.

Molecules with low-lying charge-transfer states of appropriate symmetry are characterized by high β values. In general, these molecules have the structure D -⟨⬡⟩- A where D and A are electron donating and electron accepting substituents that provide a substantial C-T resonance interactions through the π-electron system of the aromatic ring. Oudar [47], using the perturbation calculation method, obtained an approximated expression for β, in which the dominant CT intramolecular component β_{CT} is given by

$$\beta_{CT} = \frac{3\, e^2\, \hbar^2\, W\, f\, \Delta\mu}{2\, m\, [W^2-(2\hbar\omega)^2][W^2-(\hbar\omega)^2]} \quad , \tag{24}$$

where β_{CT} is a function of the laser fundamental photon energy $\hbar\omega$, the electron charge e and the mass m, W is the energy gap between the lowest excited and ground electronic states of the molecule, f is the oscillator strength of the CT transition in the molecule, and $\Delta\mu = \mu_{excited} - \mu_{ground}$ is the change in the dipole moment involved in that transition.

Crystal structure considerations

The search for an efficient nonlinear crystal is, in fact, the search for a "polar crystal" in which the macroscopic properties reflect asymmetric molecular properties. Since $\chi^{(n)}$ are tensorial quantities, the unit cell characteristics and the orientations of the molecules within the crystal lattice are of great importance, if the molecular properties are to manifest themselves fully. Among 32 unique point groups, there are 18 useful for SHG, which are biaxial (triclinic 1;monoclinic 2, m; orthorhombic 222, mm2), uniaxial (trigonal 3, 32, 3m; tetragonal 4, 4mm, $\bar{4}$, $\bar{4}$2m; hexagonal 6, $\bar{6}$, 6mm, $\bar{6}$m2); and cubic 23, $\bar{4}$3m.

The important relationships between microscopic molecular hyperpolarizability and macroscopic crystal hyperpolarizability were neatly formalized by Zyss and Oudar [48] in a quantitative mode.

The other problem, the efficiency-transparency trade-off, occurs in conjugated and polar molecules possessing the CT characteristics needed for large hyperpolarizability (high β value means almost inevitable loss of transparency). For practical purposes the crystal should not absorb at

either fundamental or harmonic wavelengths, otherwise an optical damage is likely to occur.

Survey of extensively studied NLO organic materials

Organic compounds extensively studied for their nonlinear optical properties can be grouped according to their chemical formulae. An excellent review has been published by Nicoud and Twieg [49].

Among the best organics known until now there are: urea and its derivatives [50], [51], m-disubstituted benzene derivatives [52], [53], aromatic nitro-compounds [54]-[56], nitrobenzenes [49], nitropyridines [57], polar olefins [58] , carbohydrates and amino acids.

There is a large variety of novel compounds that have been studied by the SHG powder method and for which further efforts at molecular engineering should be attempted. The example is a class of organic salts. Although the organic salts are not formally molecular compounds in a structural sense, they bridge the covalent organics and fully ionic inorganic materials. The organic part of the salt may be an anion or a cation, and either of them may be optically active. Among the organic anions, simple carboxylic acids predominate (formate, propionate, oxalate, etc.) although more complicated (phthalate) and optically active (tartarate) anions have also been employed. The organic cations are more rare, but the amino acids (glutamic acid and arginine), in which the basic functionalities are protonated, are the examples. A few more recent examples of organic salts are of particular interest: racemic potassium malate [59], yttrium formate [60] and L-arginine phosphate monohydrate (LAP) [61].

For other reviews on studies of inorganic crystals exhibiting NLO properties the reader is referred to the comprehensive works of Bechmann and Kurtz [62], Kurtz et al. [63] and Jerphagnon et al. [64].

1.4. Experimental methods

As this work presents an experimental approach, various experimental techniques are quoted throughout the text. In this chapter we wish to describe briefly techniques (methods) used in our experiments with a particular emphasis put on methods employed in the author's laboratory.

The piezoelectricity can be probed by the method elaborated by the author in 1980 and called Thermally Induced Electric Oscillations method [65]-[68] as well as by the standard method based on piezoelectric resonance-antiresonance measurements of a plane-parallel sample [7],

[10].

The pyroelectric coefficient can be determined by two complementary techniques: a dynamical method of Chynoweth [69], [70] and a continuous current pyroelectric method [71].

In the former technique a HeNe (5mW) laser light chopped usually at 75 Hz frequency periodically heats a sample. The pyroelectric response is measured after a suitable amplification with a lock-in nanovoltmeter. The pyroelectric coefficient p can be calculated from

$$p = \frac{(2)^{3/2}\, V\, \varepsilon\, (\Omega\, K\, \rho\, c)^{1/2}}{I\, \eta\, d}\ , \tag{25}$$

where V is the measured pyroelectric voltage, Ω is the modulation frequency; K, ρ and c are the thermal conductivity, density and heat capacity of the sample, respectively; I is the incident intensity of light; η is the emissivity of the blacking layer and d is a sample thickness [70].

The continuous current method consists in the measurements of the pyroelectric current I_p flowing through a short-circuited sample while it is cooled or heated at a known rate. The pyroelectric coefficient p can be calculated using a formula

$$p = \frac{I_p}{A\, r}\ , \tag{26}$$

where A is the area of electrodes, and $r = (dT/d\tau)$ stands for the rate of temperature changes. The absolute values of spontaneous polarization $P_s(T)$ are evaluated by a graphic integration of pyroelectric coefficient p(T) curve.

For the investigations of the electrooptical properties of the crystals we have built a standard equipment to the Pockels effect measurements [72] and since 1989, an equipment to SHG measurements employing the pulsed YAG laser system.

The experimental determination of linear electrooptic coefficients r is based on the equation

$$\Delta n(E) = n^3\, r\, \frac{E}{2}\ , \tag{27}$$

where $\Delta n(E)$ is the change in the refractive index n induced by an electric field (E) (tensor subscripts have been omitted for clarity). The morphology and orientation of the sample as well as the crystal symmetry determine the tensor components that can be identified in a particular experiment. Small changes in the refractive index can be measured by

detecting the phase shift of light traversing the material (Γ)

$$\Gamma = \left(\frac{2\pi}{\lambda}\right) \Delta n \, l \, , \tag{28}$$

where l is the optical path length. In order to detect the phase retardation due to the electrooptic effect, the phase must be fixed or referenced. In general two methods can be employed. The first consists in fixing the phase by birefringent propagation in the crystal, i.e., the relative phase of the ordinary and extraordinary rays is fixed by the crystal boundary. The second method refers the phase to an external interfering beam. In both techniques either static or ac modulating electric fields can be applied.

The birefringent phase-retardation method (used in this work), is based on measurement of the material birefringence as a function of the applied modulating voltage. The relationship between the induced birefringence and the electrooptic coefficient is given by the equation [73]

$$\left[\left(\frac{1}{n^2} \right)_{ij} + \Delta \left(\frac{1}{n^2} \right)_{ij} \right] x_i x_j = 1 \, , \tag{29}$$

where the change in dielectric impermeability is related to the electrooptic coefficient r_{ijk} (cf. also equations (15) and (22))

$$\Delta \left(\frac{1}{n^2} \right)_{ij} = r_{ijk} \, E_k \, , \tag{30}$$

resulting in

$$\left[\left(\frac{1}{n^2} \right)_{ij} + r_{ijk} \, E_k \right] x_i x_j = 1 \, . \tag{31}$$

The phase retardation Γ can be measured employing a Sénarmont compensator [74] in which an incident polarizer, the crystal, a quarter-wave plate, and an analyzer are arranged for extinction of the transmitted light. The term Γ is related to the angle between the incident and analyzing polarizers. In another method, the phase modulation is converted to an amplitude modulation by means of fixed orthogonal polarizers at the input and output.

The determination of the electrooptic coefficients of a crystal in a birefringence phase-retardation experiment can be improved if the modulating field is applied at a nonzero frequency. Among the advantages of the ac techniques there are: high measurement sensitivity due to the use of optical detectors and heterodyning techniques, as well as the

ability to vary the modulating frequency into both clamped and unclamped regions of the material's frequency response, thereby probing the contributions of phonon structure to the electrooptic coefficient.In addition to direct methods described above, an indirect method has been reported [75] which consists in measurements of electroreflectance spectra ($\Delta R/R$) versus photon energy.

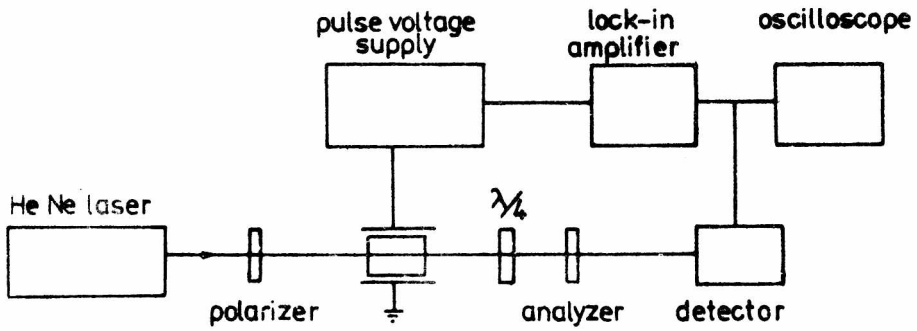

Fig. 2. Experimental setup for the measurements of the linear electrooptic coefficients

The experimental setup used by the author to measure the electrooptic effect is schematically shown in Fig. 2.

The 50 mW or 10 mW HeNe laser served as a linearly polarized light source (632.8 nm). Rectangular pulses of voltage were supplied from the modified high voltage supply (0 - 1000 V) at frequency 10 kHz, and a fast photodiode served as a light intensity detector. The signals were monitored on the oscilloscope screen or measured by a lock-in nanovoltmeter.

Measurements of dielectric properties presented in this monograph were mostly carried out by R. Jakubas at the Institute of Chemistry of the University of Wrocław. Measurements of the static electric permittivity were performed at 1 kHz (E = 500 V/m) with a Meratronic E 315A automatic capacitance bridge. Some experiments were performed at 300 Hz, 1 kHz and 10 kHz with a Tesla semi-automatic C bridge BM 484 (E = 300 V/m). Cooling (and/or heating) rates were kept constant in the vicinity of phase transitions and usually amounted to ± 0.05 K/min.

The auxiliary measurements presented in this work such as IR, Raman and Brillouin spectroscopy, calorimetry, as well as X-ray structure determination were done mostly in collaboration with two French groups: Groupe de Physique Cristalline, Université de Rennes I, and Laboratoire

de Dynamique de Cristaux Moléculaires, U.R.F. de Physique, Université de Lille I, though some FTIR experiments were also done at NRC Canada.

Raman spectra measured in Rennes were excited with a Coherent Radiation krypton or argon ion laser operating at 647.1 and 514.5 nm, respectively. The Stokes Raman scattering at 90° was analyzed in the frequency shift range of 0 - 3500 cm^{-1} with a Coderg LRDH 800 Raman spectrometer. Spectral resolution was maintained in the range of 0.8 - 2 cm^{-1} depending on the spectral region studied. Raman scattering measurements in the temperature range of 90 - 295 K were performed using a cryostat equipped with a temperature controller enabling one to maintain the temperature constant within ± 0.1 K. Measurements at temperatures higher than room temperature were performed in a laboratory-made furnace consisting of a copper block inserted into a circular heater with appropriate glass windows. The temperature stability in this case was ± 0.4 K. The Raman spectra measured in Lille excited using Spectra Physics 165 argon laser light (488.0 nm), were analyzed by means of a Coderg T880 triple monochromator. A Dilor data acquisition system coupled with an Apple IIe microcomputer and MicroVax II computer enabled recording and numerical fitting of experimental data. The crystals were mounted into a goniometer head, enabling a precise sample orientation with respect to the incident and scattered directions. In order to perform low temperature measurements the sample was cooled by the stream of gaseous nitrogen.

The Brillouin spectra measured in Rennes were taken using a Coherent laser operating at 514.5 nm and a piezoelectrically scanned multipass Fabry-Perrot interferometer (RC-22).

The Fourier transform infrared (FTIR) technique (NRC Canada) has been used to study the IR spectra of C-TNB complex within the range 700 - 3800 cm^{-1}. The spectra were recorded with a Digilab FTS-11 spectrometer equipped with a high sensitivity narrow range mercury cadmium telluride detector. Typically 100 interferograms were recorded, apodized with a triangular function and Fourier-transformed to give a spectral resolution of 0.9 cm^{-1}.

Calorimetric experiments were made with Perkin-Elmer DSC-2 and Setaram DSC-111 differential scanning calorimeters coupled with HP86 microcomputers for data acquisition and processing.

The X-ray diffraction measurements were performed with an automatic Diffractometer Enraf-Nonius CAD-4 in Rennes and Lille.

2. ORGANIC-INORGANIC HALIDES

2.1. Introduction

Organic-inorganic materials are the compounds in which crystal engineering can be approached through systematic modification of both types of constituents. Such an approach has been successfully realized by the team from the Institute of Chemistry of the Wrocław University headed by Professor L. Sobczyk. Jakubas [76] has found an interesting family of ferroelectric crystals which can be described by a general formula $[(CH_3)_nNH_{4-n}]_3X_2Y_9$ where X = Sb, Bi, and Y = Cl, Br and I [77]-[82].

This newly discovered group of materials is a branch of a large family of organic salts known as organic-inorganic double halides widely studied in the last two decades. A short but excellent review on organic-inorganic halides has been published by Arend [83] in which a classification based on structural aspects has been proposed. The compounds of this type crystallize in perovskite-type layer structures [83]-[88] consisting of nearly isolated layers formed by octa- or tetrahedra of metal coordinated by halide atoms. The cavities between them contain various organic groups, whose amine heads form NH...Y type hydrogen bonds with the halide atoms.

The group of $(C_nH_{2n+1}NH_3)_2MCl_4$ compounds, where M = Mn, Cd, Fe, Cu, ... is among the most intensively studied; when $1 \leq n \leq 4$, the alkyl chains are arranged almost perpendicularly up and down apart from the octahedra layers, the interlayer distance varying regularly with n [89].

A well known subgroup is formed by the compounds of general formula $[(CH_3)_4N]_2MX_4$ with X = Cl, Br. Within this group, a number of interesting sequences of phase transitions and in particular the occurrence of incommensurate phases and ferroelectricity were found [90]-[94]. $[(CH_3)_4N]_2ZnCl_4$ and $[(CH_3)_4N]_2CoCl_4$ crystals show ferroelectricity [90], [95], $[(CH_3)_4N]_2CuCl_4$ crystal undergoes a ferroelastic phase transition at about 291 K [96], [97] and possesses an intermediate phase with an incommensurate structure [98]. $[(CH_3)_4N]_2CuBr_4$ crystal was also found to be ferroelectric [92]. Zinc tetrachlorides containing primary alkyl ammonium ions with aliphatic chains are of interest because of their phase transition behaviour which is strongly dominated by the dynamics of the organic parts. Long chain compounds (n = 10 - 16) form intercalated structures bearing some resemblance to biomembranes.

AMX_3 compounds with X = Cl, Br, I, whose structure consists of columns formed by face sharing octahedra, can form linear magnetic systems [99], with large organic ammonium ions acting as suitable spacers

between these columns. In these materials structural phase transitions are linked to order-disorder phenomena of the organic ammonium ions. A particular case of a complex phase sequence could be found in $(CH_3)_3NHCdCl_3$ crystal, where the hydrogen bond can switch between columns of octahedra [100]. Ferroelectricity was also observed in $(CH_3)_4NHHgI_3$ crystal [101] which is a rare example of one-dimensional compound with the polar direction perpendicular to the column axis.

Halide perovskites with aromatic rings, for example $(C_6H_5CH_2NH_3)_2CdCl_4$, are piezoelectric in contrast to all studied aliphatic chain compounds. However, their physical properties have not been studied yet [83]. What is interesting and promising within this particular class is that nonsaturated hydrogen chains can be introduced with a parallel equidistant arrangement via amine heads into the perovskite matrix. Distances between neighbouring chains can be adjusted by the size of metal cations and halogen anions. Cross-linking of neighbouring chains can be induced by the γ or UV irradiation. Polymerization of this type has been performed with diacetylenes and trans,trans-butadienes [83]. The polymers obtained have an extremely high thermal stability.

3-dimensional corner sharing compounds of the type $(CH_3)_{4-n}NH_nGeCl_3$ with n = 0...3 crystallize in a Pm3m high temperature structure. All of them have different phase sequences, the majority of which leads towards phases allowing for ferroelectricity. A striking feature of their high temperature phases is, however, a high ionic conductivity (10^{-4} -10^{-2} $\Omega^{-1}m^{-1}$) and activation energies between 0.29 and 0.6 eV [83].

Hybrid structures, when the columnar arrangement AMX_3 is interpenetrated by A_2MX_4 isolated tetrahedra, lead to a total composition of $A_3M_2X_7$. This is only possible at present, if A = $(CH_3)_3NH^+$ and M = Mn, Cu or Cd. Such compounds were first described in 1976 [102], and it was found that they are polar and exhibit triboluminescence.

Our interest in the described class of materials started in 1986 when the first papers concerning ferroelectricity in crystals of $[(CH_3)_nNH_{4-n}]_3X_2Y_9$ compounds were published [79], [80], [103]. Having in mind also the NLO properties we have been particularly interested in establishing whether polar materials or phases exist in this group.

The subsequent chapters will contain description of numerous experimental results obtained on some of the compounds from the group mentioned above. The crystals for these studies were kindly supplied by Dr. R. Jakubas form the Institute of Chemistry of Wrocław University. All of the experiments aimed at understanding the specific nature of the compounds by comparing the results obtained within the group with those obtained for other compounds of a similar type.

2.2 Tris(trimethylammonium)nonachlorodiantimonate III (TMACA)

2.2.1. Structure description of TMACA and other early studies

The synthesis of $[(CH_3)_3NH]_3Sb_2Cl_9$ and its preliminary X-ray structure was described by Kruger et al. [104]. The full structure of TMACA has been subsequently established by Kallel and Bats [105]. In this compound the metal shows a tendency towards distorted octahedral coordination with some relatively long Sb-Cl bonds, which is attributed to the aspherical distribution of lone-pair electrons at Sb(III). The structure of TMACA contains $SbCl_3$ pyramids with Sb-Cl bonds ranging from 2.401 to 2.473 Å . The Cl^- anions interconnect the $SbCl_3$ groups into a two-dimensional network by forming bridges with Sb-Cl of lengths ranging from 2.883 to 3.316 Å [105]. Then the distorted octahedra of $SbCl_6^{3-}$ are formed. The cavities between the octahedra contain three nonequivalent $(CH_3)_3NH^+$ cations, two of them forming N-H...Cl hydrogen bonds of intermediate strength with the bridge chlorine atoms (N...Cl distances being 3.220 and 3.254 Å). The third cation which occupies a free space inside a twelve-membered $(-Sb-Cl-)_6$ ring in the (bc) plane (cf. Fig. 3) is reportedly linked to the chlorine atoms with a very weak bifurcated hydrogen bond (the N...Cl distances being equal to 3.455 and 3.588 Å in that case). Large thermal parameters show this cation to be disordered.

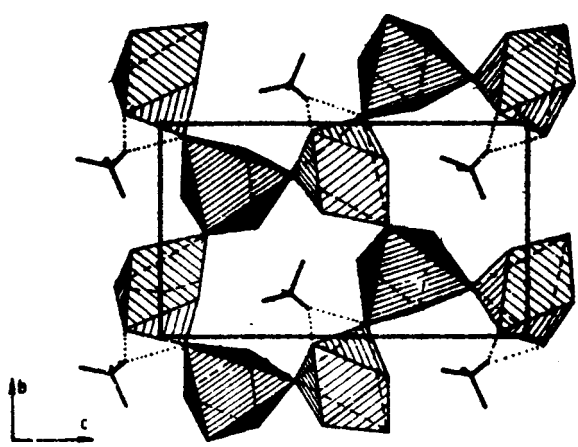

Fig. 3. Schematic view of the structure along a-axis, showing the two-dimensional network. The $SbCl_6$ octahedra are represented by their surfaces, the $(CH_3)_3NH$ tetrahedra by their bonds (after [105])

A coordination of Sb atom similar to that in TMACA was found in the crystal structure of α-$Cs_3Sb_2Cl_9$ [106] and β-$Cs_3Sb_2Cl_9$ [107].

At room temperature (T = 296 K) TMACA crystallizes in the monoclinic system, within Pc space group [104], [105]. Lattice parameters are: a = 10.085 Å, b = 9.072 Å, c = 15.495 Å, β = 90.17°, Z =2, the density being D_c = 1.744 Mg/m^3.

Single crystals of TMACA were obtained by isothermal evaporation, at 293 K, of aqueous solutions of a stoichiometric mixture of $(CH_3)_3NHCl$ and $SbCl_3$ with an excess of HCl. Thick hexagonal shaped crystals of TMACA with a perfect cleavage plane (perpendicular to the a-axis) are transparent and colourless.

In the m point group, to which TMACA belongs, the occurrence of pyroelectricity, ferroelectricity as well as NLO properties is possible. Ferroelectricity of TMACA has been found by Jakubas et al. [80] who observed a ferroelectric hysteresis loop. The spontaneous polarization measurements by the Sawyer-Tower method gave $P_s = 1.3 \times 10^{-2}$ C/m^2 at 330 K, and revealed the transition to the paraelectric phase at about 367 K [80].

Preliminary differential scanning calorimetry measurements (hereafter abbreviated as DSC) revealed an anomaly at about 364 K with the transition entropy change of about 4 J/(mol K) [80].

The dielectric permittivity measurements reported in the same paper clearly indicated an existence of a first order phase transition at 367 K of a ferroelectric character with a ε_c' value (measured along the c-axis) reaching 750. An existence of a metastable phase between the ferroelectric and paraelectric phases was also pointed out.

Mrózz et al. reported in [103] on the pyroelectric coefficient measurements in TMACA over a much wider temperature range. The temperature dependence of spontaneous polarization gave the value of about 1.6 C/m^2 at 330 K, but also indicated some broad anomaly of P_s around 200 K. In the temperature range of 200 - 220 K a dielectric relaxation process has been found basing on $\varepsilon_c'(T)$ and tan $\delta(T)$ measurements [103].

Proton magnetic resonance (NMR) studies of TMACA [108] revealed that the $(CH_3)_3NH^+$ ions are relatively free exhibiting a rotation of methyl groups (C_3) as well as a rotation of the whole cation (C_3') around respective three-fold molecular axes.

2.2.2. Calorimetric measurements of TMACA [109], [110]*

Specific heat (c_p) measurements performed on heating single crystalline samples of TMACA in the range of 355 - 375 K revealed two distinct endotherms with the maxima at 365.6 K and 364.9 K (cf. Fig. 4).

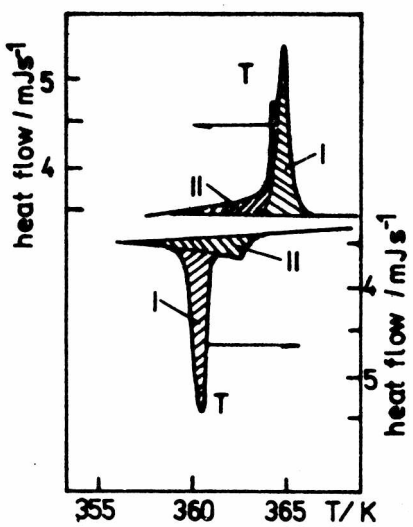

Fig.4. Heat flow curves measured in TMACA single crystals upon heating (upper curve) and cooling (lower curve). Scanning rate ± 2.5 K/min. Separation of the contributions due to the first and the second order phase transitions is schematically shown [109], [110]

The existence of two peaks around the temperature of 365 K pointed out that there might occur two phase transitions in this region, and not a single one as reported earlier [80]. In order to check this hypothesis, several DSC experiments were performed on heating and cooling the samples, using various scanning rates (1 - 10 K/min). The exotherms recorded in the cooling runs showed two neatly separated peaks. One of them, rather narrow, shows characteristic features of a first order phase transition, the other, much broader, resembles a peak due to a second order transition (cf. Fig. 4). The apparent orders of the transitions were also deduced from the magnitudes of thermal hystereses measured for

*The literature citations given in titles of sections refer the Reader to the present author's work on the topic described in the respective section.

both of them. From the DSC measurements performed at different scanning rates and then extrapolated to the zero scanning rate, the temperature of second order transition was determined to amount to T_{II} = 363.7 K and the thermal hysteresis to 0 K. The temperature of the other phase transition extrapolated to the zero scanning rate was found equal to T_I^c = 363.0 K or T_I^h = 364.2 K depending on whether it was determined from cooling or heating runs, respectively [110]. It is interesting to note that on heating, the first order transition is observed above the second order one, whereas on cooling an inverse sequence is observed: the first order transition appears at lower temperature than the second order one.

The enthalpy of the first order phase transition amounts to 1.02 kJ/mol, thus the entropy of the transition (ΔS_T^I) equals to 2.97 J/(mol K). The entropy of the second order phase transition (ΔS_T^{II}) was found to be equal to 1.67 J/(mol K). These values are likely to be charged with an error as large as 15%. The large values of ΔS for the two transitions suggest that both of them are of the order-disorder character. The entropy change assigned to the first order transition ΔS_T^I comes very close to the value $\frac{1}{2}$ R ln 2 (= 2.88 J/(mol K)) which can be understood as a conformational entropy change of two entities in the unit cell, ordered below the phase transition point and disordered above it. A possible candidate might be reorientation of one among three nonequivalent $(CH_3)_3NH^+$ cations. The value of transition assigned to the second order transition indicates that most probably we do not deal with a pure order-disorder case, but, on the other hand, ΔS_T^{II} value is too large to be connected with a pure transition of displacive type. The existence of these facts raises the question on the nature of the considered transition, which seems to have a rather complex character.

The DSC measurements performed in the low temperature region (170 - 260 K) on a virgin TMACA sample, showed also a thermal anomaly in the region 197 - 204 K, with enthalpy amounting to ΔH = 42.3 J/mol. Another measurement, when repeated immediately after the first one, showed no sign of any anomaly around 200 K. However, the samples were found to recover: the effect for the sample stored at ambient temperature over 30 min amounted to about 30% of that observed on the virgin sample. Thus DSC measurements confirmed existence of anomalies in this region in TMACA reported earlier by Mróz et al. [103].

2.2.3. Dielectric and pyroelectric measurements of TMACA [109], [110]

The temperature dependences of the electric permittivity measured quasi-statically along the c-axis (ε_c') both upon heating and cooling are

shown in Fig.5.

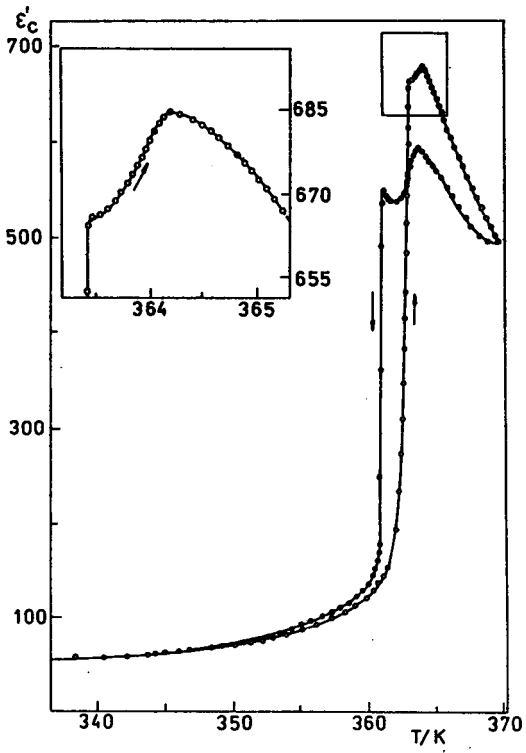

Fig.5. Temperature dependence of static electric permittivity ε_c' for a TMACA single crystal along the c-axis (heating and cooling runs are indicated by the arrows). Insert: the phase transition region (after [110])

The c-axis is the one for which the highest values of the electric permittivity were observed. One can notice two anomalies at 363.4 and 364.2 K on heating, and at 363.8 and 361.7 K on cooling the sample. The peak at 364 ± 0.2 K remains at a practically constant position irrespective of the direction of temperature changes. On the contrary, the other anomaly exhibits an appreciable thermal hysteresis. The large jump of dielectric constant for c-axis, ε_c' corresponds to the first order transition, whereas the subsequent maximum to the second order transition. The precise measurements of the electric permittivity along the a crystallographic direction also confirmed the existence of two types of anomalies, observed in all series of measurements [109].

The Chynoweth method [69], [70] employed in studies of pyroelectric properties allowed us to measure pyroelectric response of materials under

influence of externally applied electric field and at arbitrarily low rates of temperature changes (the latter condition cannot be realized using the continuous current pyroelectric method). Neither a measurable effect on the behaviour and magnitude of the pyroelectric coefficient nor any shift of phase transition temperature under the influence of externally applied electric field were found up to the field strength 7×10^5 V/m. An example of pyroelectric response obtained in TMACA on heating and cooling is shown in Fig.6.

The thermal hysteresis observed at the rate of about 1 K/min amounted to 2.4 K. It is unusual that the pyroelectric response depends on the direction of temperature changes. The measurements of pyroelectric properties point out that the raise of the spontaneous polarization in TMACA is entirely associated with the first order transition, because $P_s(T)$ follows the same thermal hysteresis on heating or cooling as the first order transition does. The pyroelectric response in the intermediary polar phase (on heating) can be influenced by the occurrence of the second order transition within this temperature range.

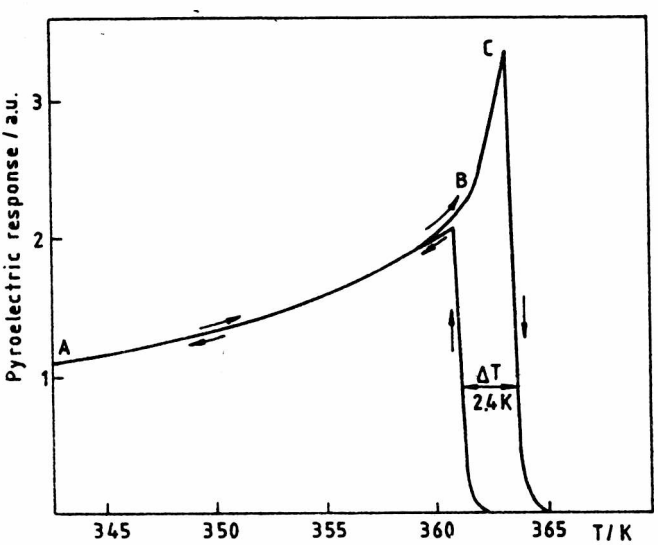

Fig. 6. Pyroelectric response obtained for TMACA along the c direction using the Chynoweth technique. The rate of temperature changes amounted to ± 1 K/min. Heating and cooling runs are indicated by the arrows

Measurements of electric permittivity performed in the range of 170 - 260 K at several frequencies clearly enabled to establish the relaxational mechanism of the low-temperature anomaly (cf. Fig.7). The ε''

maxima exhibit a distinct temperature shift towards lower temperatures on decreasing the measurement frequency. The activation energy determined from the ln ω versus 1/T plot amounts to ca. 30.6 kJ/mol. This value falls within the range of energies of weak hydrogen bonds [111]. Such a character of dielectric anomalies suggests that the process responsible for the observed features is most probably a freezing of motions of some molecular entities when decreasing the temperature.

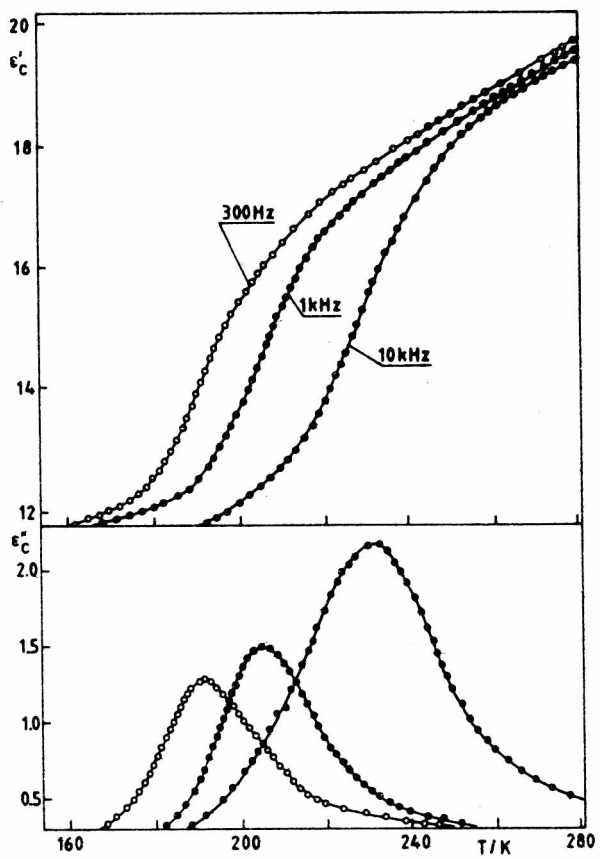

Fig.7. ε'(T) and ε''(T) dependences in TMACA in the low temperature region (after [110])

2.2.4. Raman and Brillouin scattering in TMACA [112], [113]

Light scattering techniques have been extensively used to study

lattice dynamics and structural phase transitions in perovskite layer-type compounds, and in particular in compounds belonging to the groups of $(C_nH_{2n+1}NH_3)_2MCl_4$ [84], [114]-[116], $(CH_3)_4NMCl_3$ [117] or $(NH_3(CH_2)_3NH_3)MnCl_4$ [118] where interesting sequences of phase transitions were observed.

Until now, no Raman scattering studies in the group of $[(CH_3)_nNH_{4-n}]_3Y_2X_9$ have been published, except for those co-authored by the present author [112], [113].

As mentioned in Section 1.2.1. the crystal structure of TMACA consists of two $[(CH_3)_3NH]_3Sb_2Cl_9$ formula units in a unit cell, and thus 318 normal modes of vibration are predicted. A large difference between intramolecular (C-N, C-H, N-H, Sb-Cl) and intermolecular N-H...Cl force constants allows for the separation of the internal vibrations of $(CH_3)_3NH^+$ and $SbCl_6^{3-}$ ions from their external motions (librations and translations; R_x, R_y, R_z and T_x, T_y, T_z, respectively). In the rigid-body approximation, one can assume that the corner-sharing $SbCl_6$ octahedra form an infinite two-dimensional layer, whereas the three $(CH_3)_3NH^+$ cations located at C_1 symmetry sites can be treated as separate entities. With this simplification, one should expect 39 modes of lattice vibrations, decomposed into 18 A' and 18 A'' irreducible representations of the m (C_{1h}) symmetry point group. The lattice modes should appear in the low-frequency region (0 - 300 cm^{-1}).

To assign the Raman modes the low temperature spectra have been analyzed [113]. Typical spectra of TMACA at 90 K within the spectral range of 5 - 340 cm^{-1} are shown in Fig. 8. About 20 Raman bands can be observed for any Raman tensor component in this range. The large number and mixing of vibrational modes in the considered region make the band assignment difficult. Focusing attention on the most pronounced features of the spectra at 90 K, we assigned the Raman lines by comparing the spectra of TMACA with the spectra of other compounds with identical molecular (organic and inorganic) subgroups [104], [119]-[121]. The bands observed in TMACA at 90 K are listed and accompanied by their tentative assignments in [113].

It is worth noting that careful comparison of the two spectra belonging to the same Raman tensor element, but taken in different configurations (for example z(y,z)y and x(y,z)y) show many minor differences. The shifts of band positions by 1 - 2 cm^{-1} can probably be connected with LO-TO differences. According to Kaminow and Johnston [122] high values of electrooptic coefficients might be expected in ionic crystals having large LO-TO splittings .

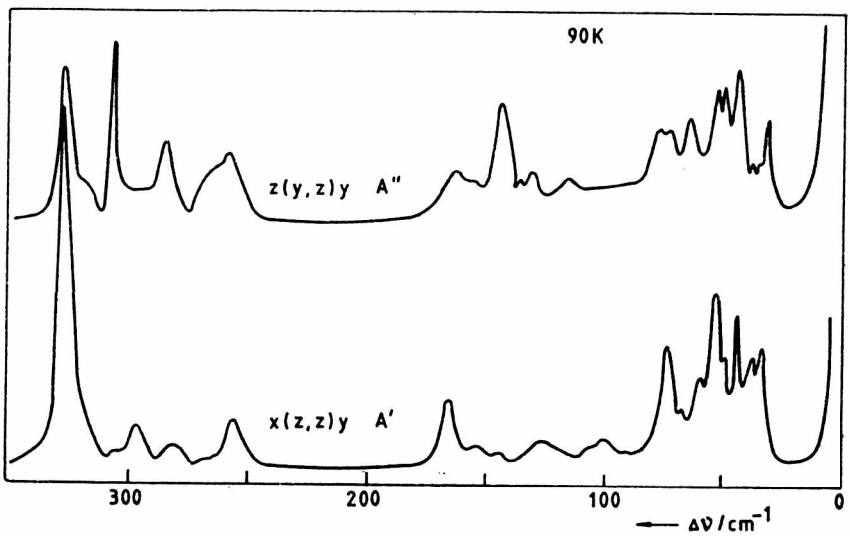

Fig. 8. Low-frequency polarized Raman spectra (10 - 350 cm^{-1}) of $[(CH_3)_3NH]_3Sb_2Cl_9$ at 90 K [113]

On increasing temperature the main feature of the evolution of Raman scattering spectra of TMACA is a considerable line broadening accompanied by shifts of the bands. A typical example of such behaviour is shown in Fig.9. No dramatic changes in the spectra were observed while passing through temperatures 206 K and 364 K, where anomalies of other physical properties were reported. However, a single (well separated) band of frequency 305 cm^{-1} at 90 K changed its intensity considerably between 90 and 300 K. We performed careful measurements of its peak intensity, half-width and frequency (cf. Fig. 10). A considerable broadening of the band at 305 cm^{-1} and characteristic temperature changes of the peak intensity and frequency (with angular points around 200 K) can be seen.

The band at 305 cm^{-1} has been assigned to the torsion of methyl group, and thus it represents an internal, non-dispersive mode. The variations of half-width of a non-dispersive phonon associated with an order-disorder mechanism, as we assumed in our work [113], were derived from the Langevin formalism by Andrade et al. [123]-[125]. Over a wide temperature range, the temperature dependence of the linewidth of a phonon associated with a self diffusion process is a function of the correlation time τ_c, and is given by

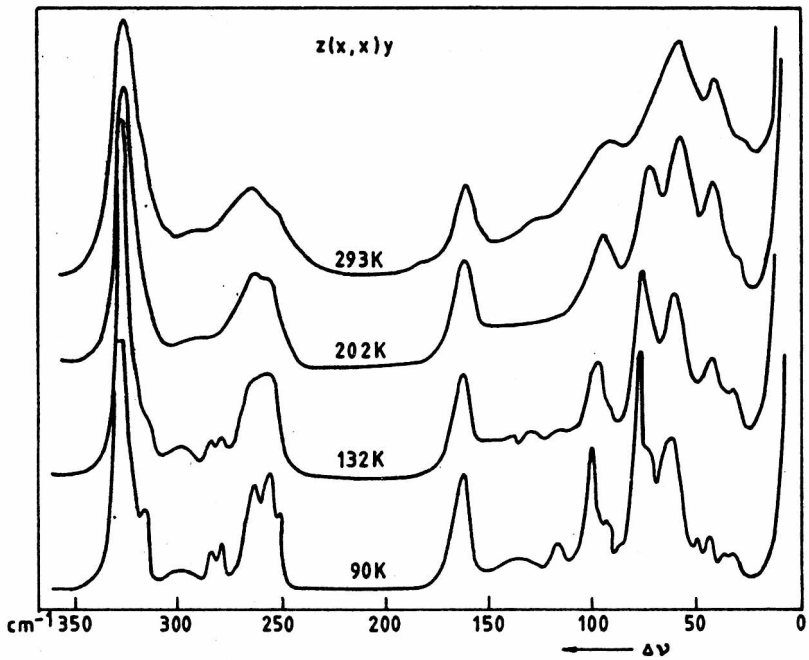

Fig.9. Evolution of the α_{xx} Raman spectra with temperature increase for TMACA (90 - 293 K) (after [113])

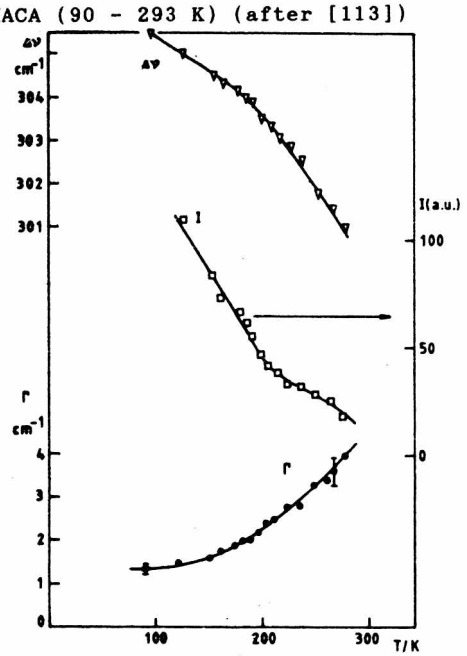

Fig. 10. Half-width (Γ), peak intensity (I) and frequency (Δν) variations of torsional vibrations of methyl group as a function of temperature [113]

$$\Gamma = (a + b\,T) + \left[\frac{\tau_c}{1 + \omega^2 \tau_c^2}\right], \qquad (32)$$

where ω is the phonon pulsation. The time-dependent statistical behaviour of the disorder mechanism is described by a correlation time which usually is assumed to be of the form

$$\tau_c = \tau_o \exp(E_a/kT), \qquad (33)$$

where E_a is an activation energy corresponding approximately to the height of the potential barrier between equivalent molecular positions governing the disorder mechanism. By fitting the equation (32) to experimental $\Gamma(T)$ dependence we obtained activation energy E_a = 10.0 ± 0.9 kJ/mol which is close to that estimated by Idziak et al. [108] (E_a = 11.2 ± 1.7 kJ/mol) and linked with the rotation of a whole $(CH_3)_3NH^+$ cation around its C_3' axis. An assumption of the existence of a cooperative local motion of molecules or their parts with a coherence lengths of a few lattice periods is necessary to rationalize the collected data. This local ordering may concern only one among the three nonequivalent $(CH_3)_3NH^+$ cations.

The evolution of the α_{yx} Raman spectrum in the temperature range of 294 - 400 K is shown in Fig. 11. One of the most characteristic features seen in the spectra is the raise of the background close to the Rayleigh line on approaching the transition temperature (T_o = 364 K). In order to visualize the character of this phenomenon more clearly, we plotted the ratio of the scattered light intensity measured at 20 cm^{-1}, where there is no Raman band, and the peak intensity of the 140 cm^{-1} band against temperature (see Fig. 12). A similar behaviour has already been observed for many compounds in which transitions of an order-disorder type occur [126], [127]. A small kink (the dotted line) seen at the transition temperature, T_o, may come from the first-order transition. Again, no dramatic changes occurred in the low-frequency region in the Raman spectra close to 364 K. However, a spectacular evidence of the existence of the phase transition has been found in the internal vibrations region, 2800 - 3050 cm^{-1} (see Fig. 13).

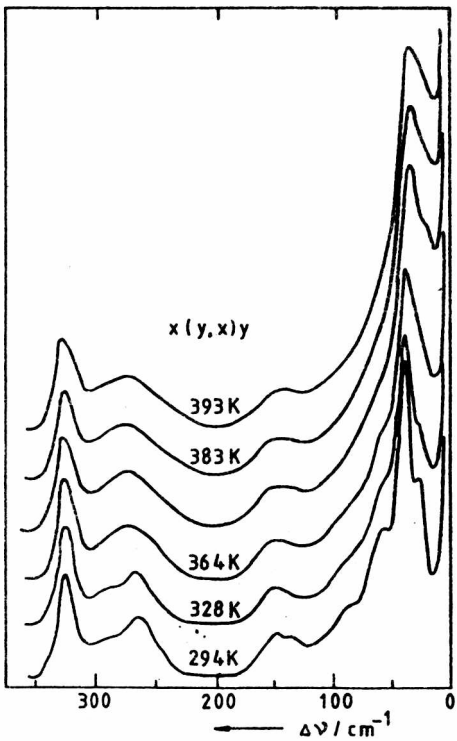

Fig. 11. Temperature evolution of the α_{yx} spectrum of TMACA in the vicinity of 364 K phase transition [113]

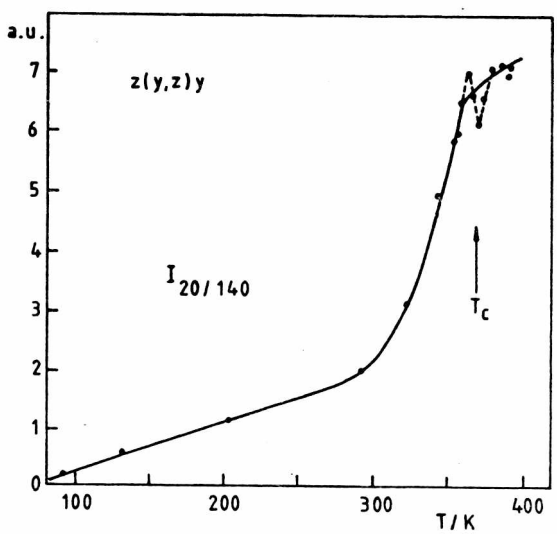

Fig. 12. Changes in background intensity at 20 cm^{-1} normalized to intensity of 140 cm^{-1} Raman band as a function of temperature in the range of 290 - 400 K [113]

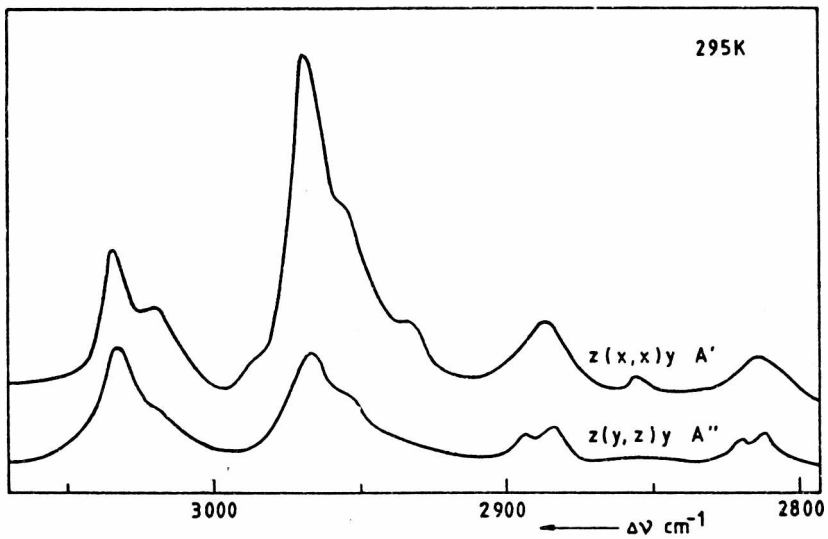

Fig. 13. Raman spectra in the region of symmetric and antisymmetric stretchings of CH_3 at 295 K

One can observe evolution (convergence) of two bands at 3020 and 3034 cm^{-1} (cf. Fig. 14) while other bands in this region do not change.

Above the transition temperature, there is a single band of frequency of 3035 cm^{-1} which splits into two bands below T_c. Intensity and frequency variations for these two lines are plotted as a function of temperature in Fig. 15a . The plot of logarithm of the magnitude of the splitting, $\ln [\Delta(\Delta\nu)]$ versus $\ln(T_c-T)$, is a straight line of the slope of 0.47 (see Fig. 15b). This value is close to that expected for mean field type transitions and we believe the observed splitting be indirectly connected with an order parameter governing the second-order phase transition in TMACA.

Auxiliary Brillouin scattering measurements were performed in the high temperature region [112]. However, close to the temperature of the transition (367 K) only minor deviations of LA phonon propagation were observed (cf. Fig. 16). Moreover, no soft-mode like behaviour of propagation of acoustic phonons has been found.

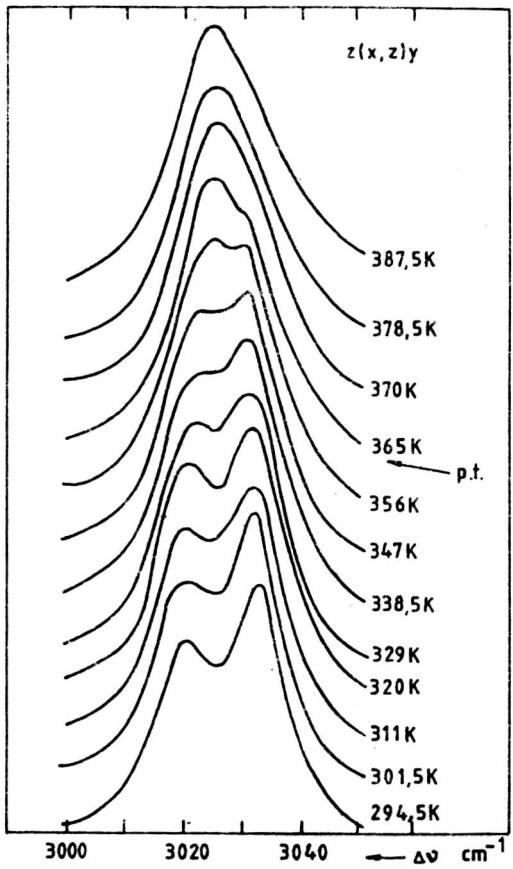

Fig. 14. Evolution of the α_{xz} Raman spectra in the 3000 - 3050 cm^{-1} region in the vicinity of 364 K phase transition region

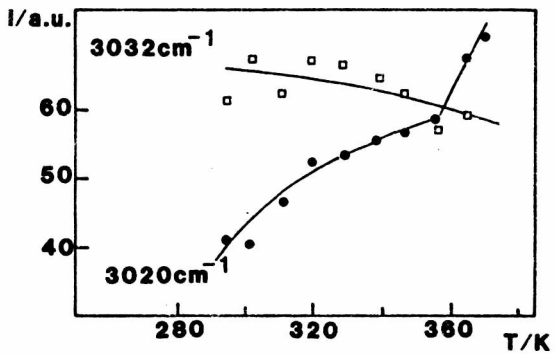

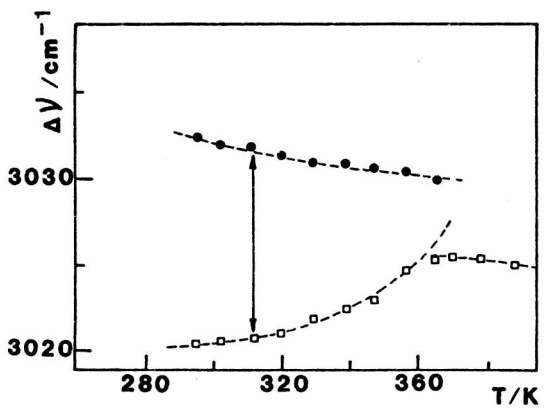

Fig. 15. a) Intensity (I) and frequency ($\Delta\nu$) variations of CH_3 stretching bands in the proximity of the phase transition in TMACA at 364 K. b) Temperature dependence of the splitting

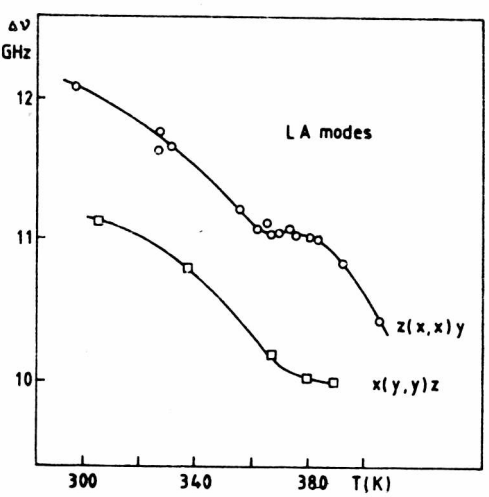

Fig. 16. Brillouin shifts of the two longitudinal acoustic modes in the region of the phase transition in TMACA

2.2.5. On the phase transitions in TMACA

Basing on the experimental data presented above, one can establish a schematic sequence of phases in TMACA [109]:

Second order (?)		First order		Second order	
203 K		363 K		364 K	
Polar	Ferroelectric		Intermediate		Paraelectric
phase IV	phase III		phase II		phase I

The lack of crystallographic data (except for the room temperature structure) makes the analysis of the phase transitions difficult, especially of that around 203 K, whose nature still remains unclear. An open question is the nature of the intermediate phase II. It is known from the literature data that in compounds of similar type the disorder of the organic parts is involved in phase transitions [128]-[130], moreover some ferroelectric type transitions are followed by appearance of the commensurate or incommensurate structures, e.g., in $[(CH_3)_4N]_2CuBr_4$ [131], [132] or in $[(CH_3)_4N]_2ZnCl_4$ crystals [133]. Some features of calorimetric and dielectric measurements data for TMACA resemble those found for $RbLiSO_4$ where an incommensurate phase has been found between two closely lying phase transitions at 475 and 477 K [134]. One may only speculate that also in the case of TMACA the intermediate phase is of an incommensurate character.

When describing the nature of transitions in TMACA one should realize that it is a system consisting of two sublattices: organic and inorganic ones, linked together by ionic and H-bond interactions. Then, for example, a disorder among $(CH_3)_3NH^+$ cations can coexist with an ordered state of $SbCl_6$ octahedra.

We tried to rationalize the ferroelectricity in TMACA by assuming that one among three nonequivalent $(CH_3)_3NH^+$ cations is responsible for occurrence of the spontaneous polarization. It is possible that the cation reportedly linked to the two chlorine atoms, Cl(2) and Cl(4), by a bifurcated H-bond [105] at room temperature occupies, in reality, one of the two possible positions with proton situated along the directions of N(3)-H-Cl(2) or N(3)-H-Cl(4). The disorder seen by X-ray analysis can be only statistical and not dynamical one. Following this hypothesis we tried to calculate by a semiempirical quantum mechanical (INDO) method [135], [136] the total electronic energy of the TMACA molecule during rotation of its disordered cation around the N(3) atom in the N(3)-Cl(2)-Cl(4) plane. This rotation ($\pm$ 50° from the crystallographically determined position) simulated the proton movement in the

disordered cation. We have found an energy curve with two minima corresponding to the two linear H-bonds N(3)-H-Cl(2) and N(3)-H-Cl(4) [137], as is shown in Fig. 17.

This result obtained for an isolated molecule shows that the favourable energetically states are those with linear H-bonds and the energetic barrier between them is of the order of a few kT at 364 K. We think that this barrier can be easily overcome (due to its apparent lowering) if the rotation of $(CH_3)_3NH^+$ cations proceeds via coherent movements (domain wall movement) of its neighbours. Furthermore, we have tried to calculate the total electronic energy dependence on position of H-atom on the lines of N(3)-Cl(2) and N(3)-Cl(4). The result of these calculations is shown in Fig. 18 [137].

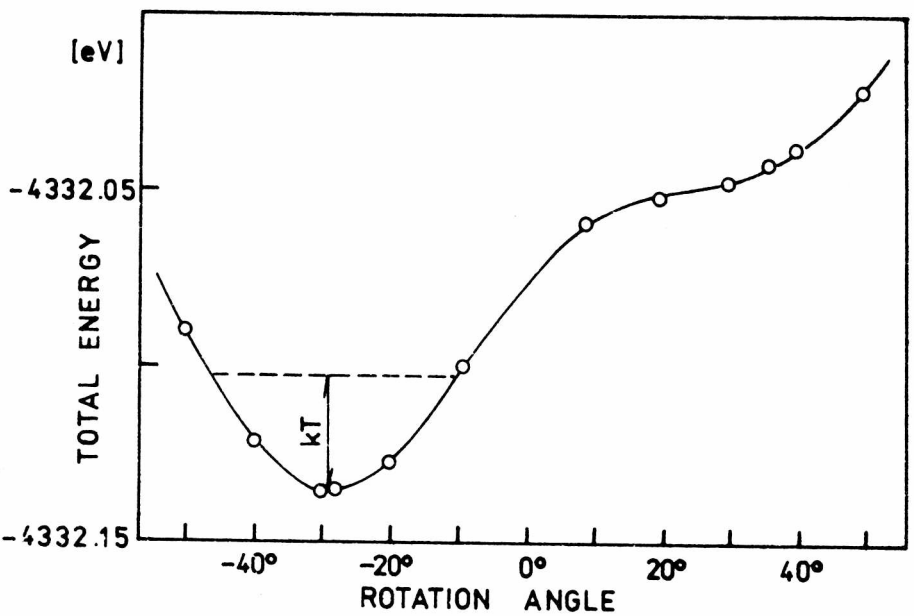

Fig. 17. INDO calculations of total electronic energy of $[(CH_3)_3NH]_3Sb_2Cl_9$ molecule; one of the $NH(CH_3)_3$ groups rotate in plane of the bifurcated H-bond. N-H distance is assumed to be equal to 1.1 Å

What is interesting, these calculations locate the proton closer to the Cl atoms than to the N atom as the absolute minima occur for the distance N(3)-H equal to 2.2 Å. However, this highly unexpected result, cannot be considered as a final one because in the course of the calculations the influence of the crystalline lattice has not been taken into account, as well as, all the molecular groups remained rigid and were described by structural parameters established at 294 K [105].

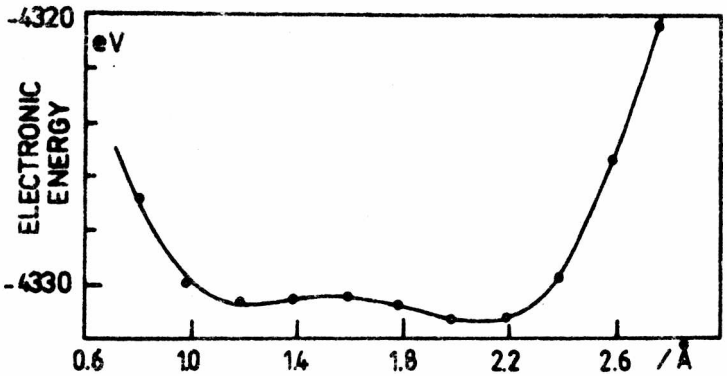

Fig. 18. Total electronic energy of an isolated TMACA molecule with straight H-bonds vs proton position along N(3)-Cl(4) direction

Basing on the above remarks we do not claim that the results presented in Fig. 18 are not false. Nevertheless, the calculations do not contradict the possibility that the ferroelectricity of TMACA is governed by the coherent movements of $(CH_3)_3NH^+$ cations with the proton localized in one or another H-bond. This model will be confirmed if the temperature of the ferroelectric-paraelectric phase transition changes on deuteration (i.e., $(CH_3)_3ND^+$). It is obvious that disorder in the inorganic sublattice will influence the dynamics of the $(CH_3)_3NH^+$ cations via the H-bonds and thus it is highly probable that both transitions are mutually dependent.

The low temperature dielectric anomalies observed at about 203 K when combined with the Raman scattering investigations can be understood on the basis of a relaxation process of one of three nonequivalent cations which gradually looses some of its degree of motions. The presently available data seem to point out that it can be either freezing of the hindered rotation of the $(CH_3)_3NH$ group around the C_3' axis or its localization in one of the several possible positions in the high temperature phase III. The low temperature phase can represent a kind of glass ordered only in a microscale but disordered in a macroscale. Then the observed anomalies not necessarily must indicate the presence of a structural phase transition.

2.2.6. Electrooptic measurements [138]

As the Kleinman symmetry does not apply to the linear electrooptic effect, one should expect for the m point group 10 nonzero Pockels

coefficients. In the case when the b-axis is a unique one i.e., it is perpendicular to the symmetry plane m, these coefficients are: r_{11}, r_{13}, r_{21}, r_{23}, r_{31}, r_{33}, r_{42}, r_{51}, r_{53} and r_{62}.

Because of low crystal symmetry, finding out all of the coefficients is a difficult task. We restricted ourselves to determination of effective coefficients only, important for application of this material as a light modulator. Two different transverse electrooptic modulators were prepared:

(i) in the 1st configuration the laser light propagates along the a-axis and the modulating electric field is applied along the c-axis,

(ii) in the 2nd configuration the optical beam path is parallel to the c-axis and the field is applied along the a-axis.

In the 1st configuration we attained 100% modulation of the light intensity under influence of an electric field. Considering the equation (31) and neglecting second order terms connected with the components r_{51} and r_{53}, one can derive a formula describing the field induced phase retardation in this case

$$\Gamma = \frac{2\pi}{\lambda} \left[\frac{1}{2} \left(r_{23}(n_2^\circ)^3 - r_{33}(n_3^\circ)^3 \right) \frac{l}{d} \right] V \quad , \tag{34}$$

where V is the applied voltage, d is the distance between electrodes, l is the length of crystal traversed by the light of the wavelength λ. The magnitude of the voltage necessary to obtain 100% intensity modulation (under the condition l = d), corrected for the dimensions of the crystal, is called the reduced half-wave voltage V_π. For the geometry described above V_π = 1.2 kV for TMACA [138], which is much lower than that for ADP (14.8 kV) and KDP (8.5 kV) [72] or even $LiNbO_3$ (3 kV) [73]. The half-wave voltage obtained for TMACA is one of the lowest reported so far, although recently a crystal with lower V_π was described: 3-(1,1-dicyano-ethenyl)-1-phenyl-4,5-dihydro-1H-pyrazole [139] (V_π = 370 V).

Nevertheless, one can safely state that the electrooptic properties of TMACA are promising for applications. For the second configuration, the effective electrooptic coefficient of TMACA is lower than that for the first configuration by about two orders of magnitude, which, in our opinion reflects the anisotropy of the crystal along and perpendicularly to the ferroelectric axis c.

Other electrooptic figure of merit for this material, an effective coefficient $r_c = (r_{23}n_2^3 - r_{33}n_3^3)/ n_3^3$, is equal to 122×10^{-12} m/V. The refractive indices necessary to estimate its value were measured using the prism method: n_{22} = 1.63 ± 0.01 and n_{33} = 1.64 ± 0.01 [138].

The origin of such high nonlinearities in TMACA is still an open question and needs further measurements using a sophisticated

experimental setup.

2.3 Tris(dimethylammonium)nonachlorodiantimonate (DMACA) and tris(dimethylammonium)nonabromodiantimonate (DMABA)

2.3.1. Structure descriptions and phase transitions.

$[(CH_3)_2NH_2]_3Sb_2Cl_9$ (DMACA) and $[(CH_3)_2NH_2]_3Sb_2Br_9$ (DMABA) will be presented together because, as the X-ray crystallographic studies have shown, the both compounds are isomorphous at room temperature [81], [140] and crystallize in the monoclinic system. The details of their structures at room temperature are given below:

DMACA: space group $P2_1/a$, a = 14.045(4), b = 9.018(3), c = 9.670(2) Å, β = 95.47(2)°, Z = 2, D_m = 1.89 Mg/m^3, [142].

DMABA: space group $P2_1/a$, a = 14.612(8), b = 9.228(4), c = 10.005(8) Å, β = 94.91(6)°, Z = 2, D_m = 2.72 Mg/m^3 [81].

The crystals usually take the form of hexagonal plates and possess a perfect cleavage plane nearly perpendicular to the c-axis. DMACA is colourless and DMABA is yellow. The methods of their syntheses are described by Whealy and Yeakley [141].

The projection of the structure of DMACA along the c-axis is shown in Fig. 19.

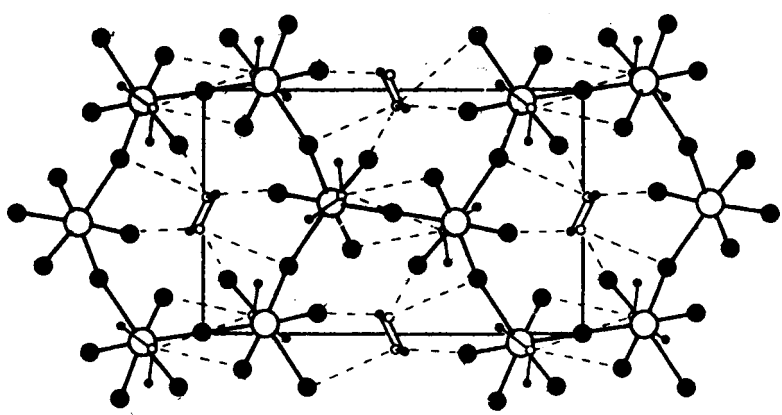

Fig. 19. Projection of the structure of DMACA (DMABA) along the c-axis [142]

As is seen in Fig.19 polyanions $[(Sb_2Cl_9)^{3-}]_n$ form a two-dimensional network. The N-H...X hydrogen bonds connect the cations to the inorganic layers.

Jakubas [79] discovered that DMACA undergoes a second order phase transition at 242 K with a high dielectric anomaly along the a-axis (ε'_a reached the value of 10^3). It has been established that this phase transition is of paraelectric-to-ferroelectric type. The hysteresis loops could be observed down to 186 K though at low temperatures electric fields as high as 1×10^6 V/m were necessary. Despite the similarity of DMACA and DMABA, it has been established [81] that DMABA undergoes two phase transitions at 228 K and 164 K. The transition at 228 K having a character of a second order transition and that at 164 K being of ferroelectric type with the Curie-Weiss law obeyed in a narrow temperature range, with the Curie constant C_{para} (as paraelectric) equal to 1.28×10^2 K. A continuous increase of the spontaneous polarization P_s below 164 K was observed but due to an abrupt increase of the coercive field could be traced to only 161.5 K.

2.3.2. Pyroelectric properties [142], [143]

The results of measurements of the temperature dependences of pyroelectric coefficient p and spontaneous polarization P_s along the a and c^* directions in DMACA are presented in Fig. 20.

As it is shown in the Fig. 20 a distinct anomaly occur at 243 K, confirming the existence of a ferroelectric type transition. The maximum value of P_s^a at 210 K amounts to about $6.8\times10^{-3}C/m^2$. The pyroelectric coefficient measured along the a-axis in the temperature range of 135 - 200 K is approximately constant and amounts to $1.8\times10^{-5}C/(Km^2)$. The pyroelectric coefficient measured along the c^* direction was found to be 16 times lower than that observed for the a direction. In the b direction there is no pyroelectric response.

In order to correlate the temperature behaviour of $P_s(T)$ with the known phenomenological theories we have plotted the results in the log P_s^a vs. $\log(T_c-T)$ coordinates. The result shown in Fig. 21 yields a straight line with a slope of 0.5 in the region of 0.5 to 10 K below T_c = 243 K. Such a result suggests a Landau type second order phase transition. The symmetry considerations for equitranslational, non-ferroelastic transitions from the paraelectric class 2/m predict only two possible classes of symmetry of the low-temperature phase: m and 2 [144], [145]. However, the orientation of the spontaneous polarization vector suggests that the low-temperature phase of DMACA belongs to the m class.

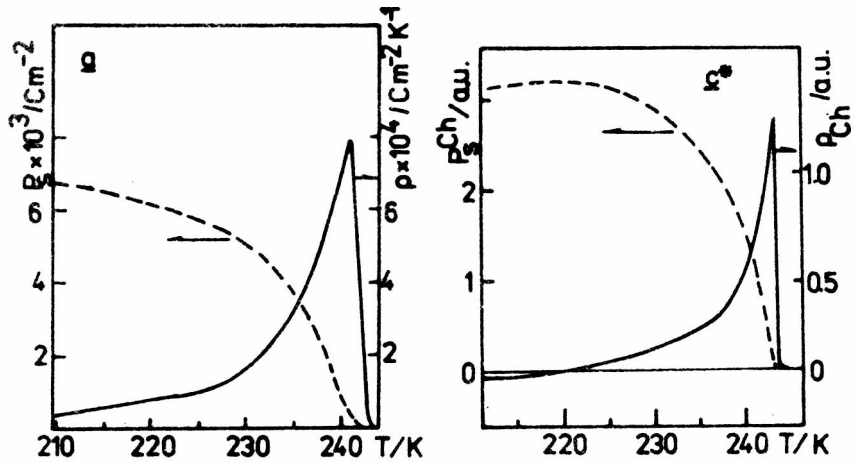

Fig. 20. Temperature dependences of the pyroelectric coefficient p and the spontaneous polarization P_s in the DMACA single crystal. The results were obtained: a) along the a crystallographic direction by the continuous pyroelectric method and b) along the c^* direction by the Chynoweth technique [142]

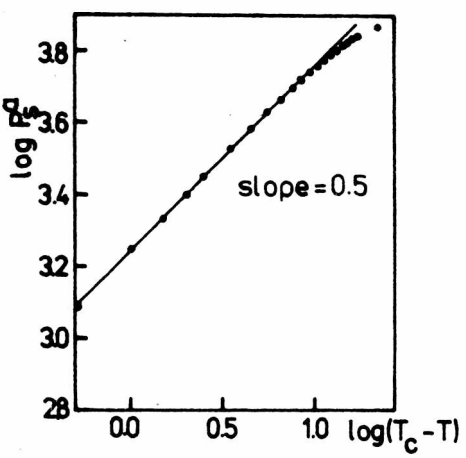

Fig. 21. Temperature dependence of the spontaneous polarization for the DMACA single crystal plotted in the coordinates log P_s^a vs. log(T_c-T) , T_c = 243 K, biasing electric field E = 2×10^5 V/m [142]

Very interesting and different pyroelectric properties have been found in DMABA single crystal [143]. The pyroelectric responses were measured along three principal directions of the room temperature structure. No pyroelectric response was detected above the temperature of the paraelectric-ferroelectric phase transition at 164 K, but considerable signal was measured below it. Results of these measurements carried out in DMABA are presented in Fig. 22.

A large thermal hysteresis is an evidence of the first order character of the observed transition. As is shown in Fig. 23, the pyroelectric anomalies along the c axis show an interesting behaviour: as temperature is lowered, P_s^c rises steeply at T_c and then slowly decreases with an approximately constant slope, becoming zero about 15 K below T_c and negative afterwards. Such a behaviour of P_s is quite unusual but a similar one was observed for $(NH_4)_2SO_4$ [146] and $Rb_2Cd_2(SO_4)_3$ [147]. An absolute determination of $P_s(T)$ using the current method revealed that the saturation value of P_s along the a-axis amounts to 4×10^{-5} C/m^2, the maximum positive values along the c and b-axes amount to 8×10^{-4} C/m^2 and 5×10^{-6}C/m^2, respectively. It should be noted (cf.Fig.23) that along the c-axis the negative value of P_s is as high as 3.5×10^{-3} C/m^2 at 110 K.

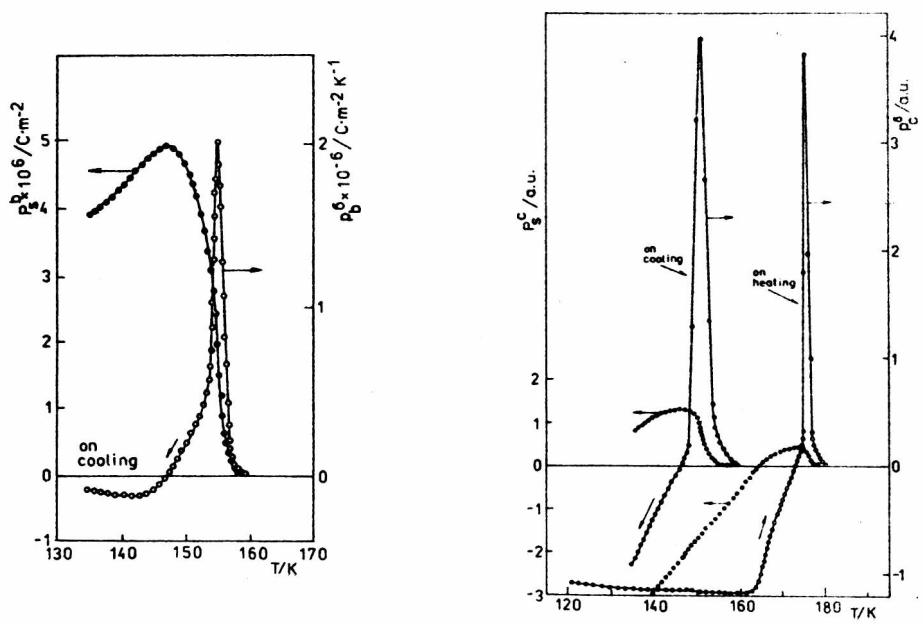

Fig. 22. Temperature dependences of the pyroelectric coefficients and spontaneous polarizations P_s measured along the b and c directions of DMABA crystal using the Chynoweth technique. Scanning rate amounted to 1.5 K/min, biasing electric field equal to 1×10^5 V/m [143]

We separated the observed $P_s^c(T)$ dependence into two parts as shown in Fig. 23 by the dashed lines. On the positive side of the vertical coordinate we observe a step-like rise of $P_s^c(T)$ on decreasing temperature. This, we believe, is a manifestation of the first order phase transition. This part of P_s^c was most probably seen by Jakubas et al. [81] in his

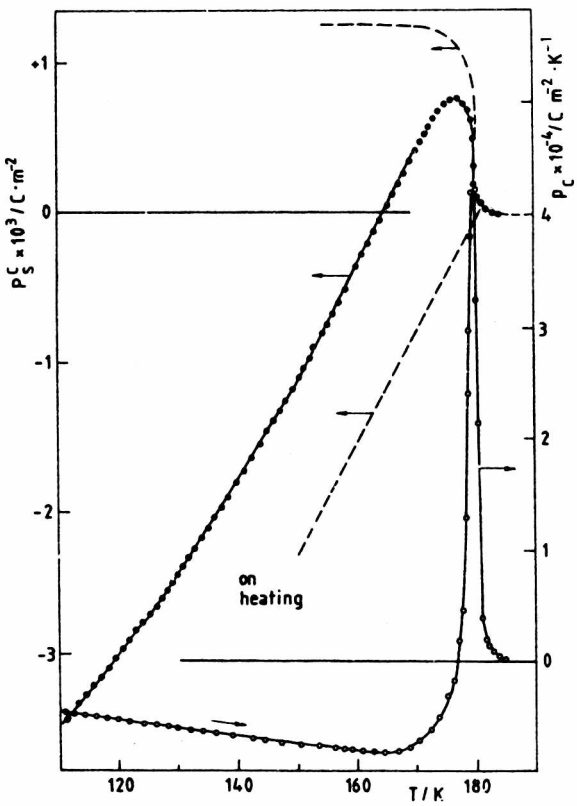

Fig. 23. Temperature dependences of the pyroelectric coefficient p_c and spontaneous polarization P_s^c measured along the c direction in DMABA using the continuous current technique [143]. For further explanations see the text

measurements of ferroelectric hysteresis loops. The saturation values of P_s^c established by these two techniques are close to each other (1.3×10^{-3} C/m^2 [143] and 2×10^{-3} C/m^2)[81]. The other part of P_s^c linearly depending on temperature, cannot probably be switched by the 50 Hz ac electric field but it can be switched by a constant electric field. Its temperature dependence can be understood on the basis of a detailed

discussion put forward for the CdS by Minkus [148], where the linear $P_s(T)$ dependence is the result of dipole reorientations. The $(CH_3)_2NH_2^+$ cations might be the species which undergo such reorientation, as they are located between the inorganic layers. Contraction along the c-axis can be the reason for their movement.

It should be mentioned that a model of a ferroelectric phase transition in DMABA has been postulated basing on the ^1H NMR spin-lattice relaxation studies [149]. In this model a 180° flips of the $(CH_3)_2NH_2^+$ play an essential role, however, this hypothesis needs further experimental verification.

2.3.3. Light scattering experiments in DMABA and DMACA [150], [151]

Brillouin scattering in DMABA

The Brillouin light scattering experiment using a backscattering geometry [152] was employed to study temperature dependences of longitudinal acoustic (LA) phonon modes in DMABA [150], though using of the other geometries was also tried out. Sound velocities v were computed from the formula

$$\Delta\nu = \pm \left(\frac{v}{\lambda}\right) \left(n_i^2 + n_s^2 - n_i n_s \cos\theta \right)^{1/2} \quad , \tag{35}$$

where $\Delta\nu$ is the Brillouin shift, λ is the laser wavelength, n_i and n_s are the refraction indices for the incident and scattered light.

The refractive indices were measured at room temperature using small angle Brillouin scattering technique; at 647.1 nm they are as follows: $n_a = 1.83$, $n_b = 1.85$ and $n_c = 1.80$ with an error of ± 0.02.

The results of the measurements of the Brillouin frequency shifts $\Delta\nu$ corresponding to LA phonon phase velocities in the range of 100 - 300 K are shown in Fig. 24.

In the direction perpendicular to the cleavage plane ($\| \underline{c}^*$) one can observe a characteristic inverted S-like shape of the $v_c^L(T)$ curve with the very large (of about 46%) change in the sound velocity between room temperature and 100 K (v_c^L(294 K) = 2.752 km/s and v_c^L(100 K) = 4.031 km/s). Such a pronounced anomaly can be due to either an important thermal expansion of the crystal along the $\underline{c}^*$ direction or to the effect of dispersion of an acoustic wave in crystalline solid. One can distinguish between these two processes by measuring the Brillouin natural-phonon linewidth (Γ/π) (Full Width at Half Maximum - FWHM).

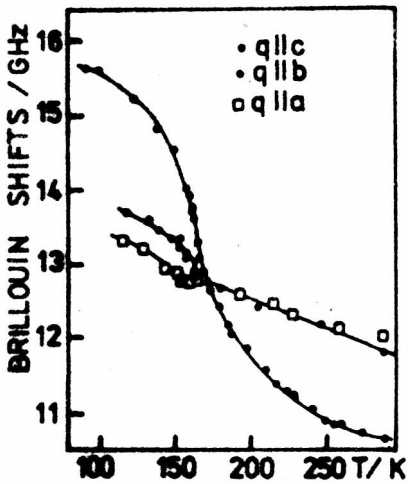

Fig. 24. Temperature dependence of the Brillouin shifts of longitudinal phonon modes in DMABA. The solid lines serve as the guide for an eye [150]

Assuming that the phonon velocity dispersion is connected with the mechanism of attenuation due to a molecular relaxation, one can derive a formula for Γ/π

$$\frac{\Gamma}{\pi} = \frac{\alpha v}{\pi} = \frac{\omega^2 \tau}{1 + \omega^2\tau^2} \cdot \frac{v^2(\infty) - v^2(0)}{2\pi^2 v(\omega)} , \tag{36}$$

where $\omega = 2\pi\Delta\nu$, $v(0)$ and $v(\infty)$ are the low- and high-frequency limiting velocities, τ is the molecular relaxation time and α - the attenuation coefficient. As can be derived from equation (36), the maximal value of the theoretical linewidth (FWHM), (i.e., the linewidth at the temperature T_m, for which $\omega\tau(T_m) = 1$), is given by

$$\left[\frac{\Gamma}{\pi}\right]_{max} = \frac{1}{2} \cdot \frac{(\Delta\nu_\infty)^2 - (\Delta\nu_o)^2}{\Delta\nu(T_m)} . \tag{37}$$

Then one can calculate the maximal natural-phonon linewidth $(\Gamma/\pi)_{max}$ which amounts to 4.85 GHz. The experimental value of linewidth as a function of temperature, after deconvolution with an instrumental function, is presented in Fig. 25.

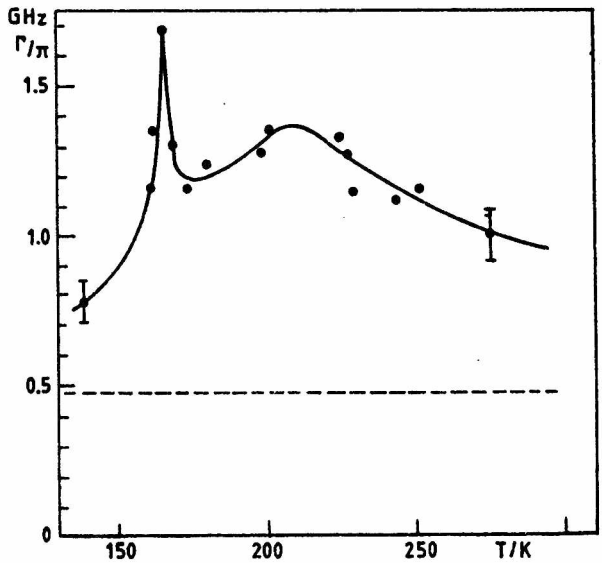

Fig. 25. Temperature dependences of the Brillouin linewidths Γ/π. The circles represent experimentally observed Brillouin line widths deconvoluted from the apparatus function, the solid line serves as a guide for an eye. Instrumental linewidth (dashed line) has to be subtracted from the observed linewidth in order to obtain the natural-phonon linewidth [150]

The natural-phonon linewidth is considerably lower than that resulting from a dispersion process at any temperature of interest. This clearly indicates that the origin of the S-like shape of the sound velocity curve along the $\underline{c}^*$-axis in DMABA is not connected with any dispersion process but it is rather a consequence of significant changes of crystal dimensions due to the thermal expansion in this particular direction.

The data presented in Fig. 25 suggest the presence of two anomalies on the curve of temperature dependence of the Brillouin linewidth. It is clear that a sharp peak of $\Gamma(T)$ at T_c =164 K is due to a coupling of a phonon with critical fluctuations of the order parameter [153]. The broad peak with maximum at ca. 210 K looks like the one due to a phonon dispersion process. The relaxing entities able to couple with the longitudinal phonons propagating perpendicular to the inorganic layers could be $(CH_3)_2NH_2^+$ cations. The movements of these cations have recently been studied by Idziak et al. [149] in H^1 NMR spin-lattice relaxation

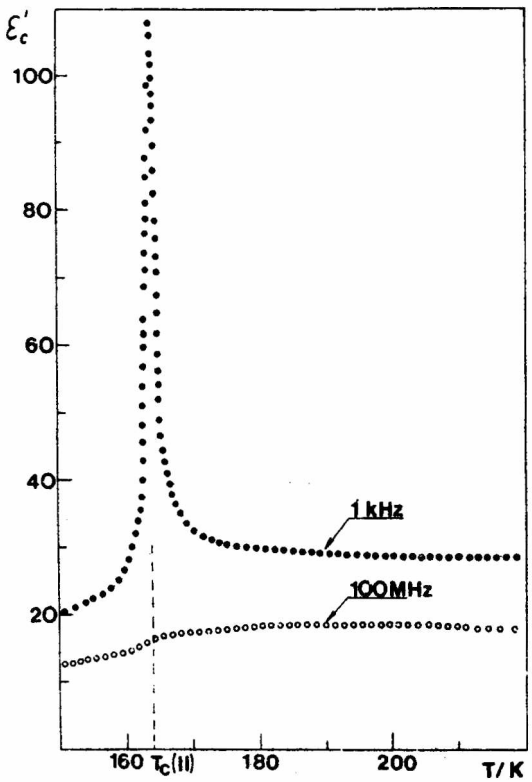

Fig. 26. Real part of electric permittivity along the c*- direction measured at 1 kHz and 100 MHz in the region of the phase transitions in DMABA [150]

experiments . Two different relaxation times measured for DMABA have been attributed to rotations of CH_3 groups situated at two nonequivalent cations in the unit cell. The correlation times and activation energies quoted in [149] are: $\tau_o^{(1)} = 1.9\times10^{-12}$ s, $E_a^{(1)} = 7.1$ kJ/mol and $\tau_o^{(2)} = 1.9\times10^{-13}$ s, $E_a^{(2)} = 7.1$ kJ/mol for the two processes, respectively. Using the E_a values reported in [119] and employing our Brillouin data one can calculate the elementary relaxation times from the relation $2\pi\Delta\nu(T_m)\tau_o\exp(E_a/RT) = 1$, obtaining $\tau_o = 2.1\times10^{-13}$ s and $\tau_o = 1.9\times10^{-13}$ s for the first and second process, respectively. The latter value of τ_o is the same as the value of elementary relaxation time $\tau_o^{(2)}$ determined in NMR experiment, suggesting the same origin of the dispersion process. The parameters of this process are close to those observed for $(C_2H_5NH_3)_2MnCl_4$ by Brillouin scattering technique [154]. One can then

conclude that the anomaly of $\Gamma(T)$ around 210 K is connected with the internal rotations of CH_3 groups.

Supplementary dielectric measurements performed for DMABA along the c^*- direction reveal a pronounced effect of the measuring frequency on ε_c' , i.e., one observes a sharp peak on the curve of temperature dependence of ε_c' measured at 1 kHz and only a weak anomaly of ε_c' at 100 MHz (cf. Fig. 26). This suggests the "order-disorder" character of the ferro-paraelectric phase transition at 164 K. These results are consistent with the ones obtained by the Brillouin scattering method which also point out lack of any dispersion process at still higher frequencies of an order of 10 GHz.

The LA phonons propagating within the (a b) layer are affected by the transition at 164 K (see Fig. 24). Below 164 K the temperature dependences of the sound velocities of these phonons change in a way which can be described as being due to a biquadratic coupling between proper strain components e_α and components of the order parameter $\eta(\eta_1, \eta_2)$ i.e., $e_\alpha{}^2\eta^2$.

Raman scattering in DMACA [151]

DMACA is the second compound of the group for which preliminary Raman scattering results are available [151].

Room temperature structure of DMACA is $P2_1/a$ with $Z = 2$, hence one should expect only A_g and B_g symmetry modes active in Raman scattering. Typical polarized spectra observed above and below the transition temperature 242 K are shown in Fig. 27. One can easily distinguish a group of bands at about 310 - 340 cm^{-1} assigned to symmetric and asymmetric stretchings of $SbCl_6$ octahedra, the bands being present also in TMACA [113]. At about 300 cm^{-1}, a CH_3 torsional vibrations can be distinguished and a group of bands at about 160 cm^{-1} can be assigned to asymmetric stretching deformations of $SbCl_6$ octahedra. However, these assignments are only tentative.

The main goal of our Raman scattering investigations of DMACA was observation of changes in the spectra induced by a structural phase transition. A review concerning this subject has been published by Petzelt and Dvořák [155], [156] for various types of phase transitions.

No soft mode type behaviour has been noticed, suggesting that the transition is not of a displacive character.

A numerical fitting of the observed spectra to a proper set of oscillator functions proved to be necessary for the studies of temperature dependences of Raman bands. The results obtained for DMACA are presented in Fig. 28.

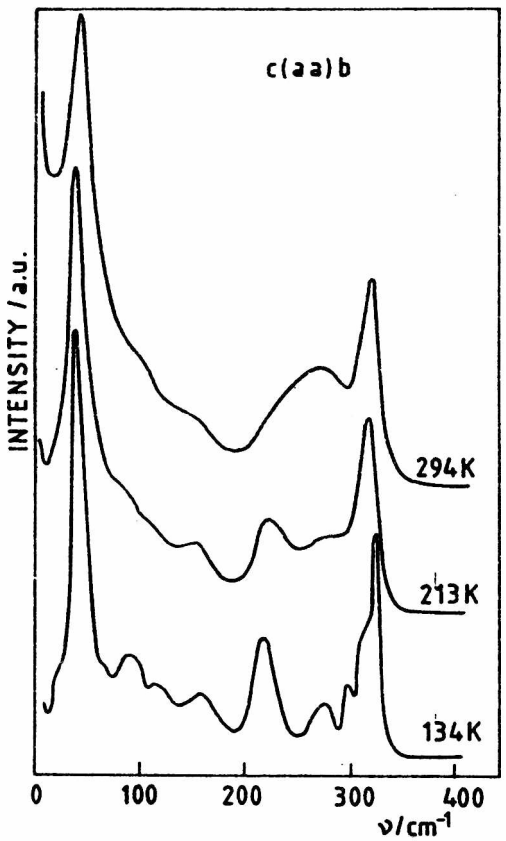

Fig. 27. Polarized $\underline{c}^{*}(\underline{a},\underline{a})\underline{b}$ (A_g) Raman scattering spectra of DMACA in the range of 0 -420 cm^{-1} at temperatures above and below the phase transition temperature (T_c = 242 K) [151]

According to their dependence on temperature two types of Raman bands can be distinguished in the spectra:

(i) lines of frequency slowly decreasing with increasing temperature. This behaviour is due to anharmonic effects (lattice expansion)

(ii) lines which frequency shows strong temperature dependence below the T_c temperature, and remains almost constant above it.

Similar dependences were also observed for ferroelectric TGS and TGSe crystals [157], and explained on the basis of the Mean Field Approximation and pseudospin-phonon interactions of the type other than the well known bilinear ones.

An analysis of temperature dependences of well separated bands

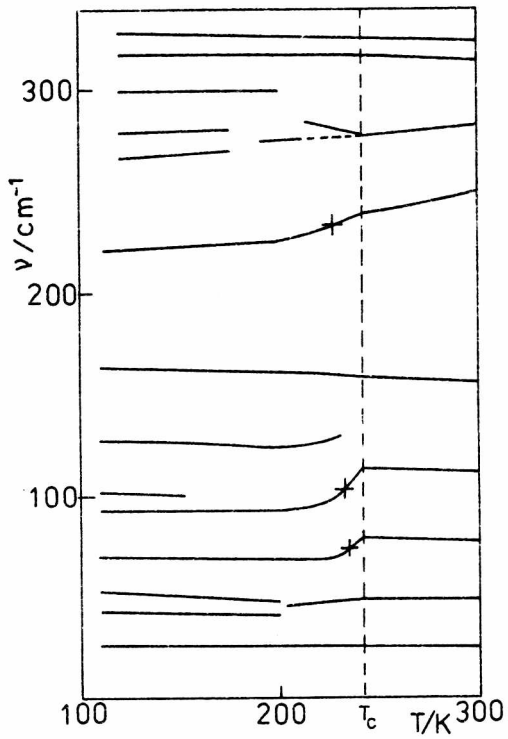

Fig. 28. Temperature dependence of the positions of maxima of the Raman bands observed in DMACA [151]

located at 70, 93 and 222 cm^{-1} (at 110 K), which exhibit a "hardening" on approaching the temperature T_c from below, shows that they change the frequency in a manner similar to that observed in Brillouin experiments and explained on a basis of Landau and Khalatnikow theory [158]. O'Brien and Litowitz [159] applied this theory to derive the temperature dependence of relaxation time τ (associated with the approach of long-range order to equilibrium) in TGS basing on the sound velocity dispersion measurements. The relaxation time is given by the equation

$$\tau = \frac{\beta}{T_c - T} \qquad (38)$$

Then, assuming that the temperature dependence of the frequencies of the optical phonons are rounded upward below T_c due to their interaction with fluctuations of an order parameter, one can derive a temperature dependence of τ by determining the temperature and frequency at which the condition $\omega \cdot \tau = 1$ is fulfilled for each curve [160], i.e., where $\Delta\nu$ passes through the midpoint of the dispersion curve. Taking our three experimental points (cf. Fig. 29) one can obtain the relaxation time of the order parameter depending on temperature as was predicted by Equation (38) with $\beta = 5.0 \times 10^{-12}$ s K. The relaxation time dependence on temperature obtained by this way is not dramatically different from that obtained for TGS ($\beta = 2.25 \times 10^{-10}$ s K [191] or $\beta = 2.9 \times 10^{-11}$ s K [160]).

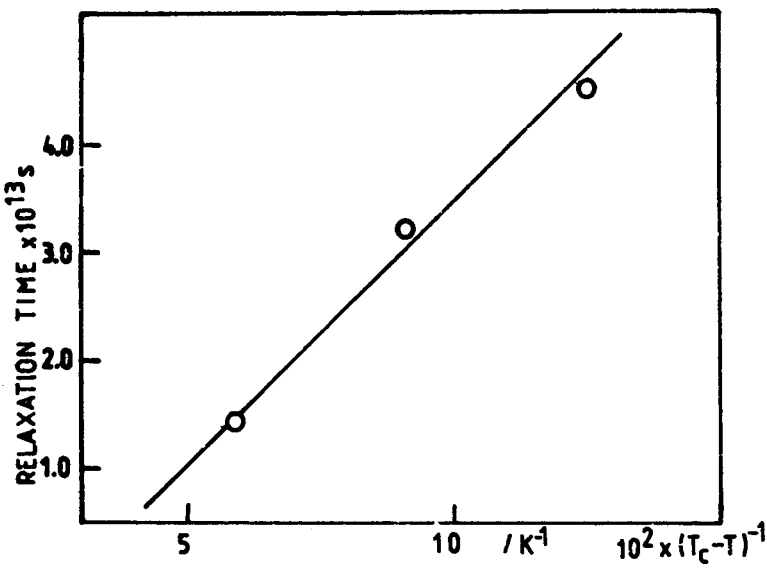

Fig. 29. The temperature dependence of the relaxation time τ of order parameter fluctuations in DMACA as obtained from Raman scattering experiment [151]

2.3.4. Ferroelasticity in DMABA [161], [162]

Ferroelasticity in DMABA has been discovered recently [161], [162]. This is the first report on the ferroelasticity within the whole $[(CH_3)_nNH_{4-n}]_3Y_2X_9$ group of crystals.

The observations of ferroelastic domain patterns were performed using a polarizing microscope in the temperature range (294 - 430 K). At room temperature the ferroelastic domains can be seen on plates cleaved perpendicular to the c^*- direction. A properly applied (small) axial stress along some directions within the (ab)- plane can induce, change or reverse the domain pattern. The observed ferroelastic domain walls are sharp and they form several characteristic, repeatable angles (i.e., 53.5°, 26.4° etc.) which can be linked easily with the microscopic structure of deformed hexagonal ring of $(SbCl)_m$ units. 6 different wall directions were observed on the (ab)- plane. The ferroelastic nature of the crystal combined with the fact that the room temperature structure is monoclinic (2/m point group) suggest that in Aizu's terminology crystal

could be described either as a hexagonal 6/mF2/m or a trigonal $\bar{3}$mF2/m species. Only these two species are characterized, according to Sapriel [18], by three orientation states and six domain wall directions. The so called "permissible domain walls" are crystallographically prominent planes of fixed indices. Their orientation can be calculated on a basis of a strain tensor of the form

$$S = \begin{vmatrix} -a & 0 & c \\ & a & 0 \\ & & 0 \end{vmatrix}$$

with components a and c calculated on a basis of the monoclinic lattice parameters [66]. For DMABA a = 0.046 and c = 0.201 and for its analog DMACA a = 0.050 and c = 0.195. The characteristic domain pattern in DMABA observed along the c-axis is shown in Fig. 30.

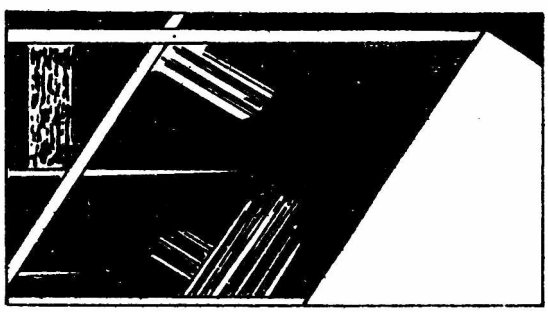

Fig. 30. The single crystal of DMABA placed between two crossed polarizers with its ferroelastic typical domain pattern [162]

The ferroelastic-paraelastic phase transition temperature has not been reached since any optical observation turned to be impossible above 398 K, due to the occurrence of another irreversible process (decomposition ?). It is highly probable that the isomorphous chlorine analog of DMABA also exhibits ferroelasticity, evidently connected with the existence of inorganic sublattice of deformed pseudohexagonal or pseudotrigonal structure.

2.4 Tris(methylamine)nonabromodiantimonate (MABA) [163]

Crystals of $(CH_3NH_3)_3Sb_2Br_9$ (MABA) are isomorphous with those of $(CH_3NH_3)_3Sb_2Cl_9$ (MACA) where the first order phase transition at 208 K

was found [78]. In the bromine derivative the existence of two reversible (presumably of first order) phase transitions has been evidenced at 168 and 131 K [77]. The room temperature phase of MABA belongs to the $P\bar{3}m1$ space group of trigonal symmetry.

The temperature dependence of electric permittivity measured along the a-axis at 100 MHz shows two distinct anomalies at the temperatures quoted above (cf. Fig. 31). Detailed studies in the range 0.3 kHz-100 MHz revealed the relaxational character of the dielectric dispersion in the vicinity of the 131 K transition with the macroscopic relaxation time of 0.5×10^{-3} s at 130 K [163].

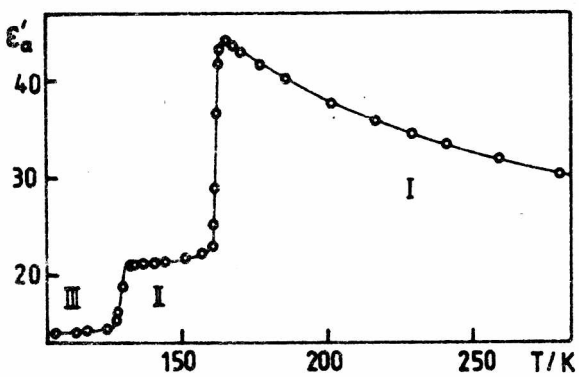

Fig. 31. Temperature dependence of electric permittivity ε'_a measured at 100 MHz for $(CH_3NH_3)_3Sb_2Br_9$ single crystal [163]

The results of pyroelectric measurements performed on plates cut perpendicularly to the c-axis are shown in Fig. 32. No response was obtained for measurements on plates cut perpendicularly to the a-axis except noise-like currents in the region of 110-125 K.

The pronounced anomalies of pyroelectric coefficient p_c (cf. Fig. 32) with the maxima values of 2.4 $\mu C/(m^2K)$ at 148 K and 11.8 $\mu C/(m^2K)$ at 116 K are correlated with the temperatures of the reported transitions, though they occur at lower temperatures due to thermal hysteresis effect. The polarization changes $\Delta P_s(T)$ were calculated by a graphic integration of the pyroelectric coefficient yielding the values $\Delta P_s = 1.4\times10^{-5}$ C/m^2 in the phase labelled as II and $\Delta P_s = 5.5\times10^{-5}$ C/m^2 in the phase labelled as III. We have also tried to check whether the constant field (5×10^5 V/m) applied parallelly to the c-axis is able to reverse the direction of polar axis. However, no change in sign or value of the pyroelectric coefficient has been noticed, pointing out that either both II and III phases of MABA are non-ferroelectric or the coercive field is much higher than 5×10^5 V/m. One should note that in the described experiment the

field was applied at ca. 100 K and 130 K but not at the temperatures of the transition where the lowest coercive fields could be expected.

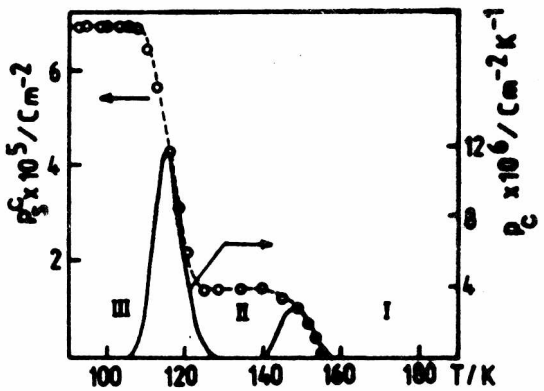

Fig. 32. Temperature dependences of the spontaneous polarization P_s^c and pyroelectric coefficient p_c measured along the c-axis in $(CH_3NH_3)_3Sb_2Br_9$ single crystals on cooling [163]

The relatively long macroscopic relaxation time τ measured in the vicinity of the II - III phase transition suggests an "order-disorder" mechanism, which is also supported by results of calorimetric studies [77]. The tentative models of the phase transition put forward in [163] take into account changes of rotational freedom of $CH_3NH_3^+$ cations as well as a formation of weak N-H...Br hydrogen bonds.

2.5 Non-layered type compound $(CH_3NH_3)_5Bi_2Br_{11}$

2.5.1. Structure description

The search for new crystals within the group of alkylammonium halogenoantimonates has recently led Jakubas [164] and Jakubas et al. [165] to the discovery of a new type compound of the formula $(CH_3NH_3)_5Bi_2Br_{11}$. The obtained new and rare stoichiometry of halogenobismuthates points to the existence of the novel type of bonding and coordination number of the bismuth atom. Moreover, it opens a great variety of paths in search for new materials of practical importance. As follows from [165], $(CH_3NH_3)_5Bi_2Br_{11}$ crystallizes in the orthorhombic

symmetry: space group $Pca2_1$, a = 13.43(5) Å, b = 14.468(9) Å, c = 16.033(7) Å, Z = 4, D_c = 3.11 Mg/m^3. Structural analysis shows that the $Bi_2Br_{11}^{5-}$ anions form bioctahedra joined via one bromine bridge. The $CH_3NH_3^+$ cations are embedded between them and linked to the Br atoms by a weak H-bond system. A projection of the inorganic sublattice structure of $(CH_3NH_3)_5Bi_2Br_{11}$ along the b-axis is shown in Fig. 33. The $(CH_3NH_3)_5Bi_2Cl_{11}$ crystal has the structure isomorphous to its bromine analogue.

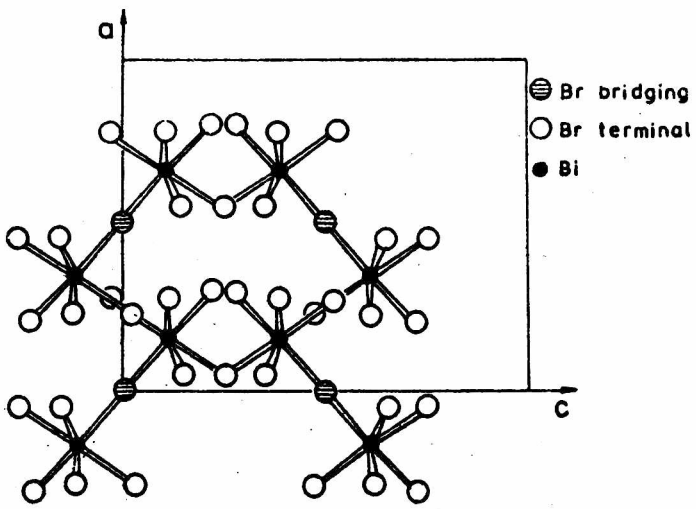

Fig. 33. Projection of the inorganic sublattice structure of $(CH_3NH_3)_5Bi_2Br_{11}$ along the b-axis [165]

2.5.2. Pyroelectric properties of $(CH_3NH_3)_5Bi_2Br_{11}$ [166]

The space group of $(CH_3NH_3)_5Bi_2Br_{11}$ is the polar ($Pca2_1$) one, hence the crystal can possess polar properties. It was found by measurements of electric permittivities that this crystal is ferroelectric at room temperature and undergoes a second order ferroelectric phase transition at 312 K with maximum of electric permittivity reaching the value of 5×10^3 along the polar c-axis [165]. In Fig. 34 results of $\varepsilon'(T)$ measurements in $(CH_3NH_3)_5Bi_2Br_{11}$ crystal along the c-axis are presented.

As it is shown in Fig. 34 the temperature dependence of dielectric susceptibility $\chi(T) = (\varepsilon' - 1)^{-1}$ obeys the Curie-Weiss law, the constants being C_{ferro} = 750 K and C_{para} = 3880 K in the ferroelectric and paraelectric phases, respectively. The ratio of these two constants

$C_{para}/C_{ferro} \cong 5$ is too high as compared with the ratio predicted by the Landau-Devonshire theory for the second order phase transition equal to ca. 2.

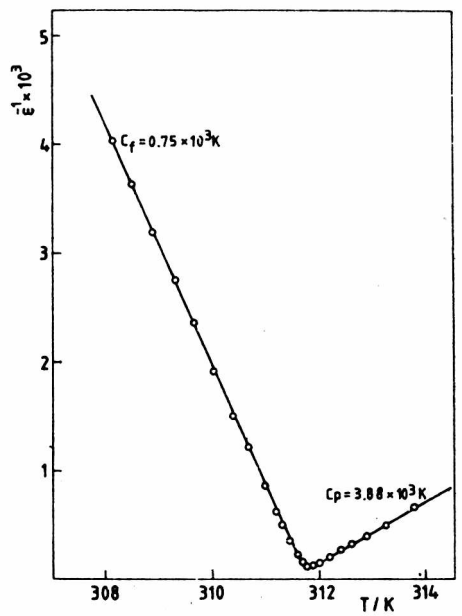

Fig. 34. The plot of $(\varepsilon')^{-1}$ vs temperature for $(CH_3NH_3)_5Bi_2Br_{11}$ crystal, ε' was measured along the c-direction at frequency of 1 kHz. The calculated Curie-Weiss constants ($C_f = C_{ferro}$ and $C_p = C_{para}$) are quoted in the figure [165]

Pyroelectric properties of the crystals were studied by the author employing both the dynamical Chynoweth method and the continuous current method [166]. The pyroelectric coefficient $p^{\sigma}(T)$ and the spontaneous polarization $P_s^c(T)$ determined on cooling by the continuous current technique are presented in Fig. 35.

The experimentally obtained value of spontaneous polarization amounts to 1.46×10^{-2} C/m^2 at 294 K. The fitting of $P_s(T)$ curve in the temperature interval 310 K - 311.3 K according to formula (11) is shown in Fig. 35. The obvious discrepancy between calculated and measured $P_s(T)$ values in the region below 309 K may be due to:

(i) non-pure second order character of the transition;

(ii) formation of the antiparallel domains in the absence of dc electric field;

(iii) other effects.

In order to resolve this problem we have employed the complementary pyroelectric method (Chynoweth) in which the sample during the measurements can be biased by externally applied electric field

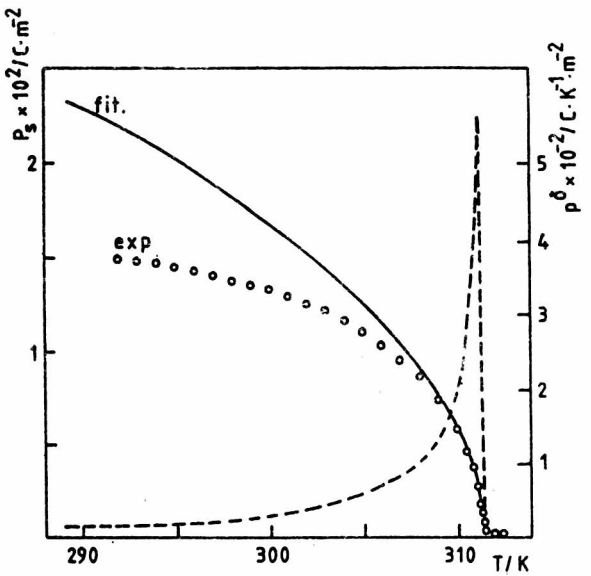

Fig. 35. The temperature dependences of the pyroelectric coefficient $p^{\sigma}(T)$ (dashed line) and the spontaneous polarization $P_s(T)$ (circles), measured for $(CH_3NH_3)_5Bi_2Br_{11}$ crystal along the c direction. The solid line represents the fit of the experimental data to the equation: $P_s(T) = \left[\frac{a}{2B}(T_c - T)\right]^{1/2}$ in the region of 2 K below the transition temperature T_c = 311.3 K. The fitting yielded the following parameters $a = 1.29 \times 10^{-4}$ Vm/(KC) and $B = 2.58$ m^5 V/C^3 [166]

(cf. Fig. 36 where the results are presented). From these results, as well as from the reasoning put forward in [166], it follows that the crystal is susceptible to form antiparallel domains able to change (diminish) the value of P_s measured by the continuous current method (under short-circuited conditions). The temperature dependence of $P_s^2(T)$ basing on the results presented in Fig. 36 (curve 1) is shown in Fig. 37. The obtained linear dependence suggests the second order phase transition.

The ratio of the Curie-Weiss constant, C_{para} to T_c for $(CH_3NH_3)_5Bi_2Br_{11}$ crystal is equal to $\simeq$ 12.5, then according to the Nakamura's classification [167] this phase transition belongs to the II group of ferroelectric transitions. To this group belong also the well known order-disorder transitions in TGS and $NaNO_2$ crystals.

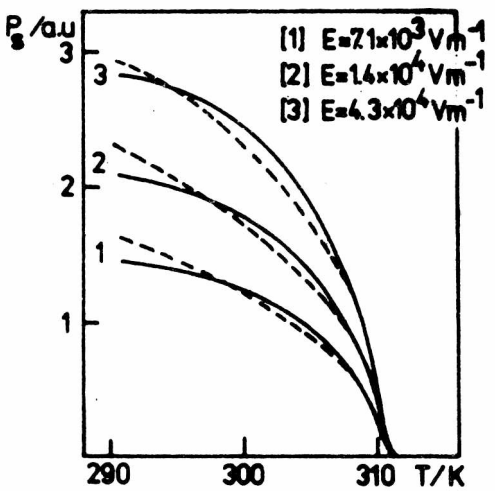

Fig. 36. The dependences of spontaneous polarizations on temperature $P_s(T)$ (solid lines) as obtained from the measurements of the pyroelectric responses by the dynamic Chynoweth method at various biasing fields, indicated in the figure. The dashed lines represent the fit of the experimental data according to the equation (11) within the region of 2 K below T_c [166]

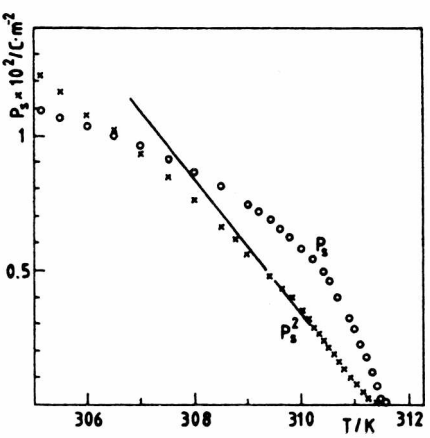

Fig. 37. The temperature dependence of $P_s^2(T)$ in the vicinity of the phase transition in the $(CH_3NH_3)_5Bi_2Br_{11}$ crystal [166]

The value of the molar entropy of the second order transition $\Delta S^{II} \cong 2.9$ J/(mol K) evaluated from the results of calorimetric measurements [165] is close to the values of molar entropies observed in $NaNO_2$, TGS, NH_4HSO_4 and $(NH_2CH_2COOH_2)HNO_3$ crystals [167] as well as to the value of $\frac{1}{2}$ R ln2 $\cong$ 2.88 J/(mol K) of an order-disorder process. The possible candidates for disordered dipoles can be organic cations or protons in the H-bond system. From this point of view the most probable prototypic (high temperature) point group symmetry should be mmm .

Being ferroelectric at room temperature, $(CH_3NH_3)_5Bi_2Br_{11}$ crystals may be used in pyroelectric devices. In order to evaluate their ability to serve as a pyroelectric detector we calculated the figures of merit $p_i/(c_p\varepsilon')$, p_i/c_p and $p_i/[c_p(\varepsilon'')^{1/2}]$ which yield information about voltage, current and detection of light sensitivities [168], and compared them with the values for commercially used pyroelectric active materials at room temperature (cf. Table 1).

Table 1

The merit factors for some commercially employed materials in pyroelectric devices [35]

Material	p_i	$\varepsilon'/\varepsilon_o$	c_p	$\varepsilon''/\varepsilon_o$	p_i/c_p	$p_i/c_p\varepsilon'$	$p_i/c_p(\varepsilon'')^{1/2}$
	$\mu C/m^2K$		$MJ/(m^3K)$		$\mu Am/W$	Vm^2/kJ	$(m^3/MJ)^{1/2}$
TGS + alanine	360	27	2.1	0.08	171	710	0.203
TGS	300	50	1.7	0.16	178	400	0.149
$LiTaO_3$	190	46	3.19	0.16	60	147	0.050
PVF_2	30	11	2.4	0.25	13	129	0.009
$(CH_3NH_3)_5Bi_2Br_{11}$	200	60	0.67*	1.2	299	563	0.07

* the value of c_p has been assumed to be equal to the mean value of c_p determined for other compounds of similar type [166].

As follows from the analysis of the presented data the $(CH_3NH_3)_5Bi_2Br_{11}$ crystals competes well with other well known materials.

2.5.3. Electrooptic properties of $(CH_3NH_3)_5Bi_2Br_{11}$ crystals [169]

Since the compound crystallizes under the mm2 point group there are five nonzero Pockels coefficients: r_{13}, r_{23}, r_{33}, r_{42} and r_{51}. Solving the Equation (30) and Equation (31) for a given geometry, one can find explicit formulae for the Pockels coefficients.

For the light beam propagating along the a crystallographic direction and the electric field applied parallel to the c-axis one finds for the change of index of refraction a following formula

$$\Delta n = \Delta n_3 - \Delta n_2 = -\frac{1}{2}\,(n_3^{\,3} r_{33} - n_2^{\,3} r_{23})\,E_3 \,. \tag{39}$$

For a wave propagating along the b-axis with the field applied along the c-axis one gets

$$\Delta n = \Delta n_3 - \Delta n_1 = -\frac{1}{2}\,(n_3^{\,3} r_{33} - n_1^{\,3} r_{13})\,E_3 \,. \tag{40}$$

For a wave propagating along the a-axis and the field $E_2 \parallel b$ one obtains

$$\tan 2\Theta = \frac{2\, r_{42}\, E_2}{\frac{1}{n_2^{\,2}} - \frac{1}{n_3^{\,2}}} \,, \tag{41}$$

where the compensation angle Θ can be measured using the Sénarmont compensator [168].
For a wave propagating along the b-axis and the field $E_1 \parallel a$

$$\tan 2\Theta = \frac{2\, r_{51}\, E_2}{\frac{1}{n_1^{\,2}} - \frac{1}{n_3^{\,2}}} \,. \tag{42}$$

By measurements of modulation of light $\Delta I/I_o$ and employing the formula derived in [169]

$$\frac{\Delta I}{I_o} = \sin^2\left[\frac{\Delta\Gamma(E)}{2}\right] - \sin^2\left[\frac{\Delta\Gamma(0)}{2}\right] \,, \tag{43}$$

in which ΔI stands as modulation depth, I_o - the total signal intensity transmitted through the crystal in the absence of an electric field and $\Delta\Gamma$ - phase retardation, one obtains the information about the nonlinear properties of the material

$$\Delta\Gamma(E) = \frac{2\pi}{\lambda}\,\Delta n(E)\,l + \Gamma_o \,, \tag{44}$$

where Γ_o is the zero voltage phase retardation due to intrinsic crystal birefringence.

Electrooptic measurements in $(CH_3NH_3)_5Bi_2Br_{11}$ [169]

The indices of refraction were measured using the prism method, and they are summarized below [169]:

	n_1	n_2	n_3	λ
$(CH_3NH_3)_5Bi_2Br_{11}$	1.91	1.93	1.96 ±0.07	632.8 nm.

The crystals of $(CH_3NH_3)_5Bi_2Br_{11}$ grown from solution appear yellow in colour. Their transparency region as well as short wavelength absorption edge have been determined using a sample-in sample-out technique using a Carl Zeiss Jena monochromator. The absorption edge is located at about 483 nm.

The electrooptic measurements were performed in the transverse configuration. The electric field was applied along the polar c-axis while the 45° polarized light (with respect to the c-axis) propagated along either the a- or b-axes. The measurements of a phase retardation $\Delta\Gamma(V)$ for the two configurations (cf. Fig. 38) allowed us to determine two figures of merit: $\frac{1}{2}(n_3^3 r_{33} - n_1^3 r_{13})$ and $\frac{1}{2}(n_3^3 r_{33} - n_2^3 r_{23})$. These figures of merit describe the crystal ability to serve as an electrooptic light modulator. From these measurements one can also calculate the reduced half-wave voltage, V_π.

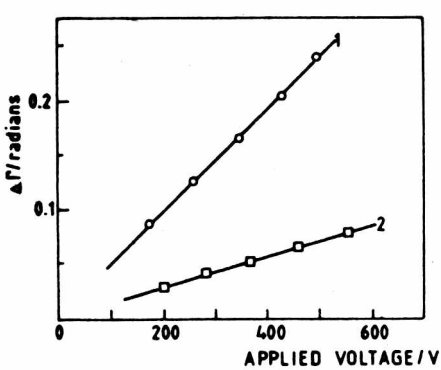

Fig. 38. Field induced phase retardation $\Delta\Gamma(E)$ versus voltage for two transverse electrooptic modulators made of $(CH_3NH_3)_5Bi_2Br_{11}$ crystal [169]

The results obtained for $(CH_3NH_3)_5Bi_2Br_{11}$ crystal at the wavelength λ = 632.8 nm are summarized below [169]:

$$\frac{1}{2}(n_3^3 r_{33} - n_1^3 r_{13}) = 13.3\times10^{-12}\,\text{m/V} \pm 1 \quad \text{and} \quad V_\pi \cong 23.8\ \text{kV}$$

$$\frac{1}{2}(n_3^3 r_{33} - n_2^3 r_{23}) = 21.9\times10^{-12}\,\text{m/V} \pm 2 \quad \text{and} \quad V_\pi \cong 14.4\ \text{kV}$$

for light propagating along the b-axis and the a-axis, respectively.

The reported above V_π values are considerably higher than those obtained for TMACA [138], nevertheless the electrooptic properties of this compound are relatively good even when compared with the best known materials [40], [139], [170]. In applications, however, besides high values of electrooptic coefficients, the material must fulfill other requirements: transparency in visible light, mechanical and chemical stability etc. Many of these requirements are met in the described substance, although the chemical stability is not satisfactory.

The important question concerns the origin of such high nonlinearities, whether they are of electronic or lattice origin. The discovery of this type of organic-inorganic salts as the new optoelectronic materials is regarded by the author as one of the most valuable results reported in this monograph.

3. ACID PHTHALATES

3.1. Introduction and structure considerations

The crystals of acid phthalates can be described by the general formula $(C_8H_5O_4^-)_n Me^{n+} \cdot m\ H_2O$ where Me^{n+} is a cation.

The presence of ionic and weak Van der Waals interactions, as well as a network of relatively strong hydrogen O-H...O bonds in a compound creates an interesting field for molecular engineering. The phthalates are widely used in investigations of X-ray spectra of the Sun, where they serve as gratings for diffraction of high-energy electromagnetic radiation due to their optical perfectness and transparency. Moreover, some of the compounds crystallize in a polar symmetry group mm2 of orthorhombic system. We restrict our interest only to polar crystals of monovalent cations i.e., potassium acid phthalate (abbreviated as KAP), sodium acid phthalate (NaAP), and rubidium acid phthalate (RbAP).

The most thoroughly studied is potassium acid phthalate whose structure was determined by Okaya [171]. The crystal belongs to the orthorhombic system with the space group of $P2_1ab$, with a = 6.46 Å, b =

9.60 Å and c = 13.85 Å , and four chemical units $K^+(C_6H_4 \cdot COOH \cdot COO^-)$ in a unit cell. The ionic structure consists of K^+ cations and the infinite network of $C_6H_4COO \cdot HCOO^-$ anions linked by short O-H...O hydrogen bonds. There exists a perfect cleavage plane perpendicular to the c-axis.

The structure of rubidium acid phthalate [172] is isomorphous with that of KAP, whereas the structure of NaAP [173] is slightly different. The sodium acid phthalate crystallizes under the Aba2 (C_{2v}^{17}) space group. The orthorhombic cell, with lattice parameters: a = 9.308 Å, b = 26.424 Å and c = 6.770 Å contains eight chemical units of formula $Na^+(C_6H_4COO \cdot HCOO^-)$ and four water molecules.

The physical properties of this group are almost unknown, except for KAP. Piezoelectric, optical, dielectric and elastic properties of KAP were reported by Belyaev et al. [174]. Its electrooptical properties have been measured by Shaldin et al. [175], and elastooptic coefficients by Belikova et al. [176] and Shahabuddin Khan et al. [177]. Pyroelectric properties of KAP were studied down to 4 K by Poprawski et al. [178]. Raman scattering in the region of lattice modes has been investigated by Krishnamurthy et al. [179] and in the internal vibration region by Orel et al. [180].

Much less is known about NaAP and RbAP for which only temperature dependences of the pyroelectric coefficients have been recently measured [178], [181].

Our interest in this particular group of compounds arises from the possibility of obtaining large single crystals of excellent optical quality by growth from solution. Their polar properties along with chemical stability may lead to a much wider application of this group of materials.

3.2. Raman and Brillouin scattering studies of NaAP and KAP [182], [183], [185]

Raman scattering studies

The Raman scattering studies in NaAP were aimed at understanding the lattice dynamics in the whole group of acid phthalates and to allow for deeper explanation of their polar properties. Single crystals of NaAP were obtained due to kindness of Dr. R. Poprawski (Institute of Physics, Technical University of Wroclaw).

Normal mode analysis of NaAP in the lattice region [182] predicts 15 external optic modes. Their distribution among the four irreducible representations of the mm2 point group (the two-fold symmetry axis is

along z-direction) is as follows:

$$\Gamma_{\text{lattice modes}} = (4A_1 + 4A_2 + 5B_1 + 5B_2)_{\text{libr. modes}} + (6A_1 + 7A_2 + 7B_1 + 7B_2)_{\text{trans. modes}} \quad (45)$$

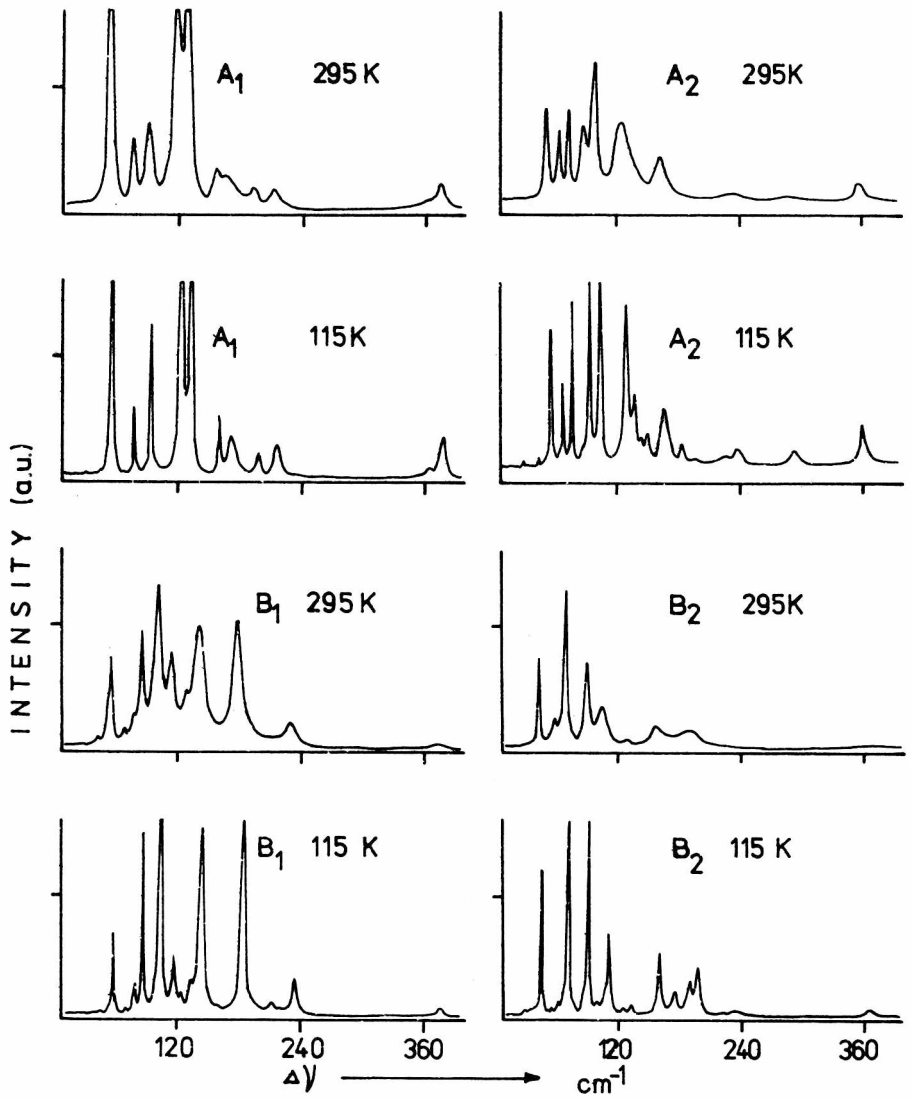

Fig. 39. Polarized Raman spectra of NaAP measured at 115 K and at room temperature [182]

All the lattice modes are Raman active and A_1, B_1 and B_2 ones are polar along z, x and y directions, respectively. The polarized Raman spectra of NaAP, measured in the region 5 - 400 cm^{-1} at 115 and 295 K are shown in Fig. 39.

The full characteristics of the observed Raman bands were obtained using simultaneous numerical fitting of all lines to a set of an appropriate number of oscillator functions. Iterative minimization procedures using least-squares method have been employed.

In Fig. 40 we present Fourier Transform Infrared (FTIR) spectra of NaAP obtained at 295 K by the reflection technique with an electric field vector parallel to z direction (A_1 modes) and x direction (B_1 modes).

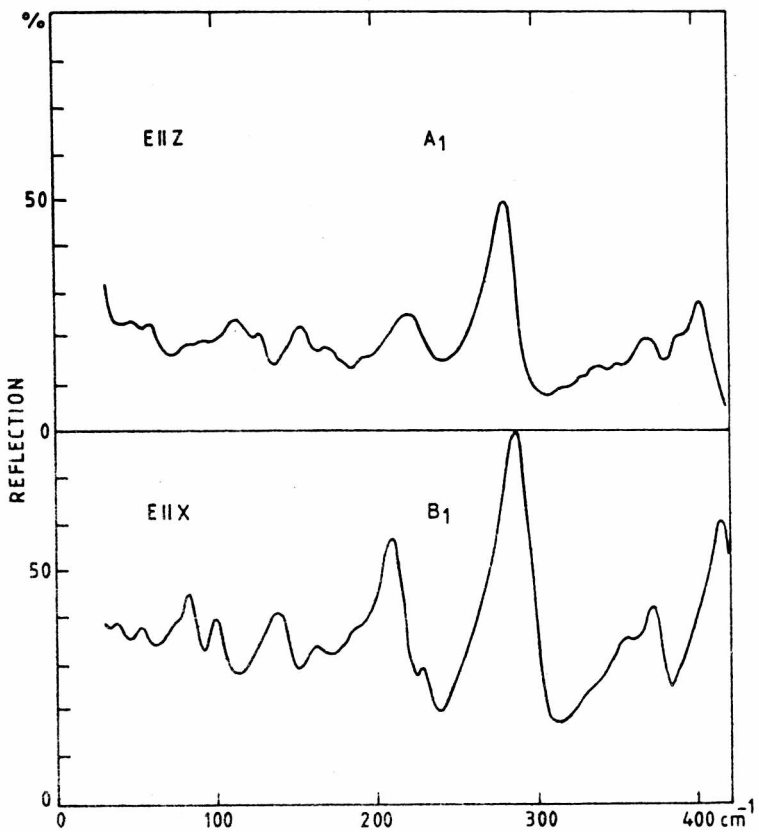

Fig. 40. Polarized infrared spectra of NaAP obtained by reflection method (T = 295 K) [182]

The assignment of the modes given in detail in [182] has been elaborated on a basis of comparison of the spectra of NaAP with those

measured for pure phthalic acid and KAP [179], [180]. We observed 9 A_1, 11 A_2, 9 B_1 and 9 B_2 lattice Raman bands.

Measurements of Raman spectra for different scattering geometries revealed considerable intensity changes of Raman bands belonging to a given representation. These changes were interpreted as arising from the crystal anisotropy. Significant intensity variations were found for vibrations of A_1 symmetry, i.e., for the three α_{xx}, α_{yy} and α_{zz} Raman tensor elements. These spectra taken at room temperature are shown in Fig. 41. The largest and the most spectacular peak intensity changes were observed for the 52 cm^{-1} phonon which dominates both the y(x,x)z and z(y,y)x spectra, and is of a medium intensity for the y(z,z)x configuration. Similar anisotropy effects have been also noticed for the 156 cm^{-1} and 213 cm^{-1} bands. However, an opposite situation takes place for the 61 cm^{-1} band which is well seen in y(z,z)x but absent in y(x,x)z and z(y,y)x configurations.

NaAP belongs to a noncentrosymmetric point group, then for the polar modes either the TO component or a "quasi-longitudinal" or a "quasi-transverse" mode can be observed by right angle Raman scattering. Only a small number of bands exhibits a significant dispersion. For the A_1 modes, there are two bands (at 88.4 cm^{-1} and 116.7 cm^{-1}) with dispersion greater than 2 cm^{-1} Generally, one can say that the LO-TO splittings in NaAP are of the same order as those for KAP [179]. The low frequency polarized Raman and infrared spectra of NaAP show some similarities to the spectra of KAP, although there are many differences, also due to the presence of a water molecules in the NaAP structure.

On the basis of Raman scattering experiment one can reveal that molecules of both acid phthalate and water are ordered in the crystal in the temperature range of 115 - 295 K.

KAP crystals of excellent quality (grown in this laboratory) made it possible to measure polariton dispersion [183], an experiment rarely performed due to experimental difficulties. The forward Raman scattering technique, is the technique in which small angles between the wave vectors of the incident photons k_i and the scattered photons k_s are employed, in order to obtain small wave vectors k_p of the polaritons. The beam divergence of the exciting laser must be lower than 0.7 mrad.

The polariton dispersion of polar modes in any insulating biaxial crystal near the center of the first Brillouin zone can be completely described by the generalized Fresnel equation [184]. The measurements of polariton dispersion in KAP were made for the scattering in xy plane (for the axes convention applied cf. Ref. [218]), for which the Fresnel equation is simplified to the form

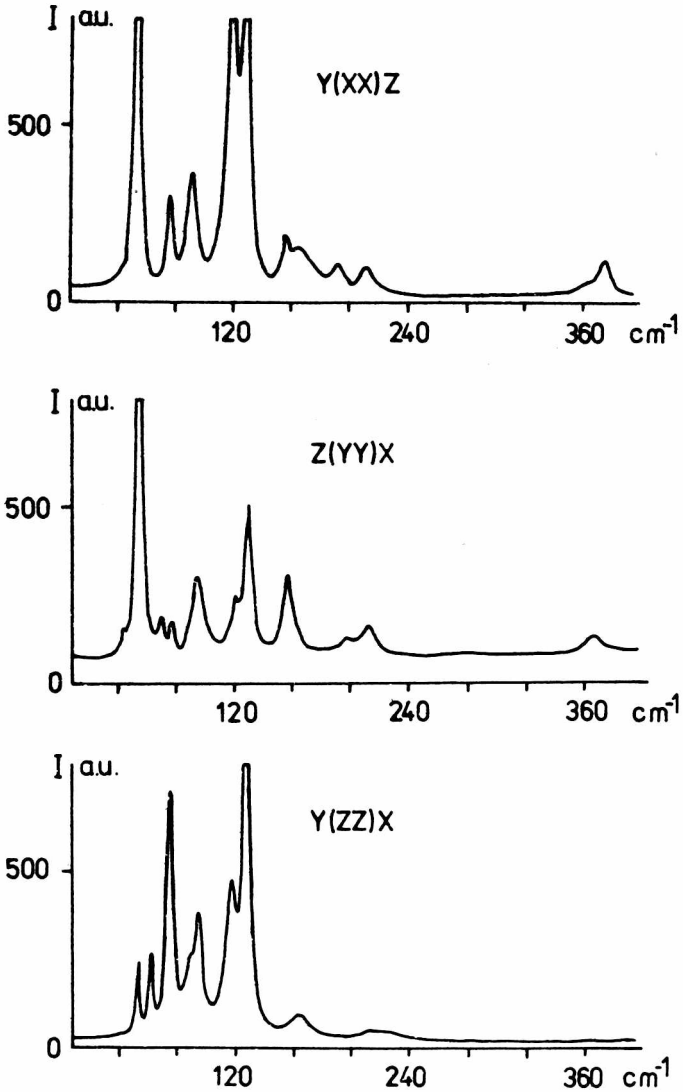

Fig. 41. A_1 symmetry Raman spectra of NaAP single crystal at 295 K for different polarization states [182]

$$(n^2 - \varepsilon_z(\omega))\{\varepsilon_x(\omega)(n^2 - \varepsilon_y(\omega))s_x^2 + \varepsilon_y(\omega)(n^2 - \varepsilon_x(\omega))s_y^2\} = 0. \qquad (46)$$

The s_α are the components of the wave normal vector and the dielectric functions for the three principal directions $\alpha = x, y, z$ are given by the

Kurosawa relations [184]

$$\varepsilon_\alpha(\omega) = \varepsilon_\alpha^\infty \prod_{i=1}^{m_\alpha} \frac{\omega_{\alpha Li}^2 - \omega^2}{\omega_{\alpha Ti}^2 - \omega^2} \quad , \tag{47}$$

$\omega_{\alpha Li}$ and $\omega_{\alpha Ti}$ are the frequencies of a m-th longitudinal and transverse optic modes along the α-axis, respectively, and the $(\varepsilon_\alpha^\infty)^{1/2} = n_\alpha$ denotes the high frequency refractive index of the material.

The solutions of Equation (46) are as follows: $n^2 = \varepsilon_z(\omega)$ describes the dispersion of purely transverse A_1 modes, whereas the zeros of the second bracket containing ε_x and ε_y describe mixed modes of the type $B_1 + B_2$ as well as TO + LO. Thus A_1(TO) modes can be observed for arbitrary wavevector directions in the xy-plane, e.g., by the (z,z) - Raman tensor element. A pure polariton dispersion causes, for a decreasing magnitude of the wavevector, a lowering of the frequency of the excitation from $\omega_{\alpha Li}$ to the next longitudinal frequency $\omega_{\alpha Li-1}$. The polariton branch of the lowest frequency reaches $\omega = 0$ for $k = 0$. The shift of the lowest A_1(TO) polariton, of frequency $\omega_o = 69.5\ cm^{-1}$, was as large as about 20% of ω_o for internal scattering angles ranging from $\Phi = 2.13°$ to $0.76°$ (cf. Fig. 42).

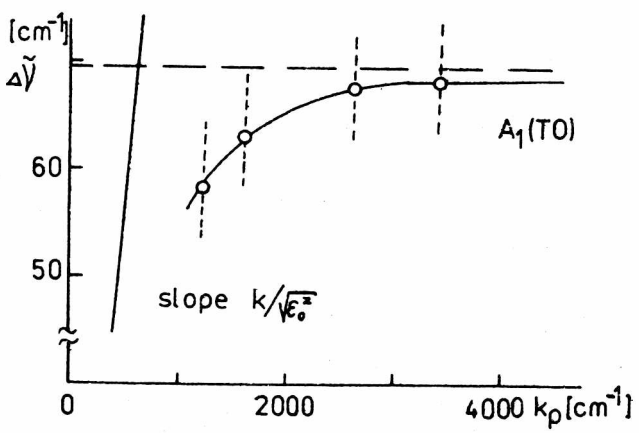

Fig. 42. Polariton dispersion curve for A_1(TO) mode in KAP (y(z,z)y, scattering plane - xy, $\omega_i = 19438\ cm^{-1}$). The dashed curves are calculated from the kinematic condition $k_p^2c^2 = |k_i - k_s|^2c^2 = n_i^2\omega_i^2 + n_s^2\omega_s^2 - 2n_in_s\omega_i\omega_s\cos\Phi$ [183]

The polariton observed in Raman experiment is also well seen as a strong band at 69 cm^{-1} in infrared absorption spectrum of KAP (cf. Fig. 43).

Large LO-TO splittings and a considerable polariton dispersion observed in KAP may suggest, according to Kaminow et al. [122], that the contribution from lattice polar modes to the overall electrooptic effect in KAP is considerable. Attempts to measure the polariton dispersion in NaAP were unsuccessful, mainly due to inferior sample quality.

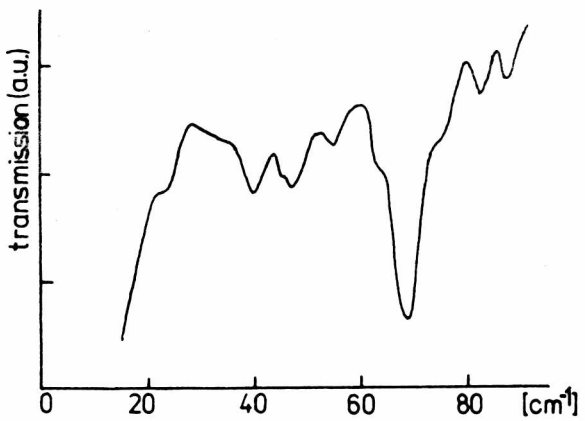

Fig. 43. z-polarized FTIR absorption spectrum of KAP single crystal, measured on xz-cut plate in the lattice region at room temperature [183]

Brillouin scattering studies [185]

In order to enlarge the knowledge about elastic properties of NaAP and KAP, necessary for evaluation of electrooptic coefficient, we have undertaken the Brillouin scattering studies of the mentioned crystals at room temperature. Right-angle, back and small-angle scattering techniques have been used in order to measure all necessary and some supplementary sound velocities. These measurements allowed us to calculate all the nonzero components of elastic stiffness tensor. As KAP and NaAP both belong to the mm2 point group, the elastic stiffness matrix $c_{\alpha\beta}$ (α,β = 1, ... 6) contains only nine nonzero independent components: c_{11}, c_{22}, c_{33}, c_{44}, c_{55}, c_{66}, c_{12}, c_{13} and c_{23}. The elastic constants measured by us [185] at frequency about 15 GHz were calculated from sound velocity values, measured for various crystallographic directions, using a least-square fitting procedure. They are listed for both of the compounds in Table 2.

Table 2

Values of elastic constants $c^{D}_{\alpha\beta}$ (10^9 N/m^2) for KAP and NaAP single crystals at 295 K measured by Brillouin scattering technique [185]

	c_{11}	c_{22}	c_{33}	c_{44}	c_{55}	c_{66}	c_{12}	c_{13}	c_{23}
KAP	19.32	18.40	13.65	6.40	5.11	6.82	12.45	7.66	8.26
NaAP	22.19	18.37	15.73	7.95	8.06	10.56	12.94	10.19	5.50

Measurements of this type are very important for the description of the material behaviour at very high frequencies. Generally they can be slightly different from the elastic constants obtained by ultrasonic techniques due to dispersion effects.

3.3. Electrooptic Pockels effect in KAP and NaAP [186], [187]

It was already stated that acid phthalate crystals can be easily grown in the form of optical quality boules. The materials are thus well suited to be model ionic-molecular electrooptic crystals.

Our studies of electrooptic properties of KAP at room temperature and some dielectric, piezoelectric and elastic properties in the temperature range of 100 - 400 K [186] were undertaken having in mind the fact that KAP seemed to be a promising material for application as nonlinear electrooptic crystal. These studies have shown that the crystal does not undergo any phase transition in the temperature range mentioned above.

We also measured the transverse Pockels effect in KAP [186] by determining the phase retardation of light propagating along the c-direction and with the electric field applied parallel to the a polar axis. As a result of the measurements a 5% modulation of 632.8 nm laser light at moderate fields and a linear dependence of the modulation on applied voltage has been established (cf. Fig. 44).

The merit factor for the geometry of transverse electrooptic shutter $\frac{1}{2}(n_1^3 r_{11} - n_2^3 r_{21})$ amounts to ca. 3×10^{-11} m/V. Then one can state that KAP crystals may be used as electrooptic modulators with an efficiency comparable to that of KDP crystals but without the necessity of protecting their surfaces.

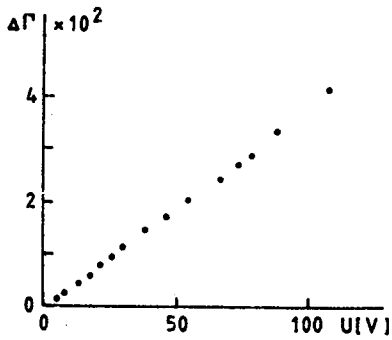

Fig. 44. The dependence of the phase retardation on voltage for KAP crystal. The ratio of crystal length to width was approximately equal to unity [186]

The electrooptic effect in KAP may arise from the contribution of both ionic and molecular mechanisms. The presence of well defined molecular moieties (a benzene ring) can contribute to the nonlinear susceptibilities in a manner similar to that found in π-electron system molecular materials. However, the weak efficiency of the powder SHG and large polariton dispersion observed in this material suggest that the optical nonlinearity of KAP is mainly of ionic (lattice) origin.

Similar experiments were recently carried out for NaAP [187]. Preliminary results obtained so far, indicate that the merit factor for the transverse modulation of light in NaAP is lower than that of KAP by more than one order of magnitude. The lower value of the merit factor in this case can be rationalized by taking into account the influence of water molecules present in the structure of NaAP and different orientation of phthalic acid molecules.

4. ORGANIC CHARGE TRANSFER (CT) COMPLEXES

The molecular charge transfer (CT) complexes form an interesting class of materials. Among numerous charge transfer complexes there is a group of weak π-electron donor-acceptor complexes. Usually, aromatic donors and acceptors make either parallel linear stacks of each individual component (segregated stack complexes) or stacks in which the individual molecules alternate (mixed stack complexes).

The author's interest in this group of materials, since 1980, has

been due to their interesting photoconduction properties [188]-[191] (which will not be described here) and a discovery of a noncentrosymmetric crystal, CT complex between carbazole and trinitrobenzene [65]. This raised a hope, that within this group of materials one can search for other polar crystals which can be good NLO active materials due to presence of intermolecular charge transfer with a large dipole change between ground and first excited electronic states leading to considerable molecular hyperpolarizability β_{ijk}. As the whole effect of intermolecular charge transfer is of electronic nature, such crystals, in principle, could compete with known one-component organic electrooptic crystals whose activity results from intramolecular charge transfer.

4.1. Carbazole - 1,3,5-trinitrobenzene (C-TNB)

4.1.1. Review of early studies

The group of sym-trinitrobenzene (TNB) complexes with various donor molecules has been extensively studied since the pioneering spectroscopic work of Briegleb et al. [192] and McGlynn et al. [193] on anthracene-TNB complex. Further structural studies of many TNB complexes were mostly devoted to investigations of the relationship between molecular conformation and electronic properties and structure [194]-[198].

The rare example, the noncentrosymmetric CT complex of TNB with carbazole has been investigated by Bechtel et al. [199] who established its structure at room temperature as being orthorhombic with the space group $P2_12_12_1$. The complex consists of molecular stacks of alternating donor and acceptor molecules parallel to the c-axis. The neighbouring stacks are linked to each other by weak hydrogen bonds (O...H-N) formed between the carbazole and trinitrobenzene molecules.

Since C-TNB is one of the most chemically stable complex among aromatic hydrocarbon-trinitrobenzene series, we undertook the study of its physical properties. In the early work [200] we have established its piezoelectric, elastic and thermal expansion properties. The temperature dependence of principal components of the tensor of thermal expansion (cf. Fig. 45) in C-TNB pointed out to the existence of a phase transition around 300 K.

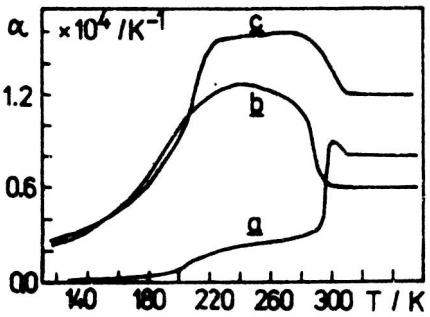

Fig. 45. Temperature dependence of principal components of the tensor of thermal expansion in C-TNB crystal [200]

Less pronounced anomalies were also found in the course of measurements of effective elastic coefficients [200], [201] which indicated the second order character of the observed transition. The existence of anomalies have been subsequently confirmed by the dielectric permittivity measurements and calorimetric measurements of C-TNB [202]. It has been found that the thermal anomaly extends over region of 10 K with a maximum located around 304 K (cf. Fig. 46).

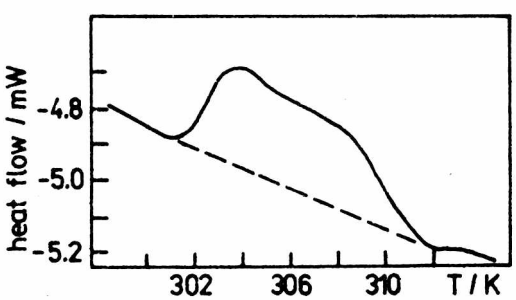

Fig. 46. The DSC measurements of C-TNB made on heating around the phase transition temperature [202]

The overall transition enthalpy ΔH was determined to amount to 135.1 J/mol and the transition entropy ΔS = 0.44 J/(K mol), respectively. A small value of ΔS for C-TNB may suggests that the transition should not be regarded as an order-disorder type.

In order to better understand the nature of this transition, the electric permittivity ε' and loss factor tan δ were measured at frequencies from 1 to 100 kHz [202], [203]. Around 300 K $\varepsilon'(T)$ changes

smoothly from 2.8 at 270 K to 3.6 at 320 K, whereas the dielectric losses rise slightly at the same temperature region.

Moreover, the thermally stimulated depolarization (TSD) currents were also measured for C-TNB crystals. The TSD spectra taken for main crystallographic directions of the complex show maxima of current near 300 K, their magnitude being proportional to the polarizing field. The results were interpreted [202] as originating from reorientation of molecular dipoles within the crystal.

4.1.2. Infrared spectroscopic measurements of C-TNB complex [204]

The room temperature infrared absorption spectra of C-TNB are shown in Fig. 47 together with the spectra of both constituents [204].

In order to check whether the spectrum of the complex is a sum of the spectra of the individual components, we performed a computer summation of the spectra of carbazole and TNB, from which we found that the effect of complex formation on the IR spectra is small (cf. Fig. 3 in Ref. [204]). Such a procedure allows us for assignment of the fundamentals in the complex spectrum. The largest observed shift of the IR band due to complex formation takes place for the N-H stretching of carbazole (3418.5 cm^{-1}; A_1). This shift, amounting to 18.5 cm^{-1}, supports the crystallographic data pointing out the existence of a weak hydrogen bond in the C-TNB crystal.

The main subject of the presented investigation concerned the question whether there are some evidences of a phase transition around 300 K. Precisely measured temperature dependences of the position, height and halfwidth of several IR bands revealed clear anomalies around this temperature (see Fig. 48).

It should be noted here that some bands are not influenced or weakly influenced by the existence of the transition. Thus these investigations did not supply conclusive information about the nature of the observed transition but confirmed its existence.

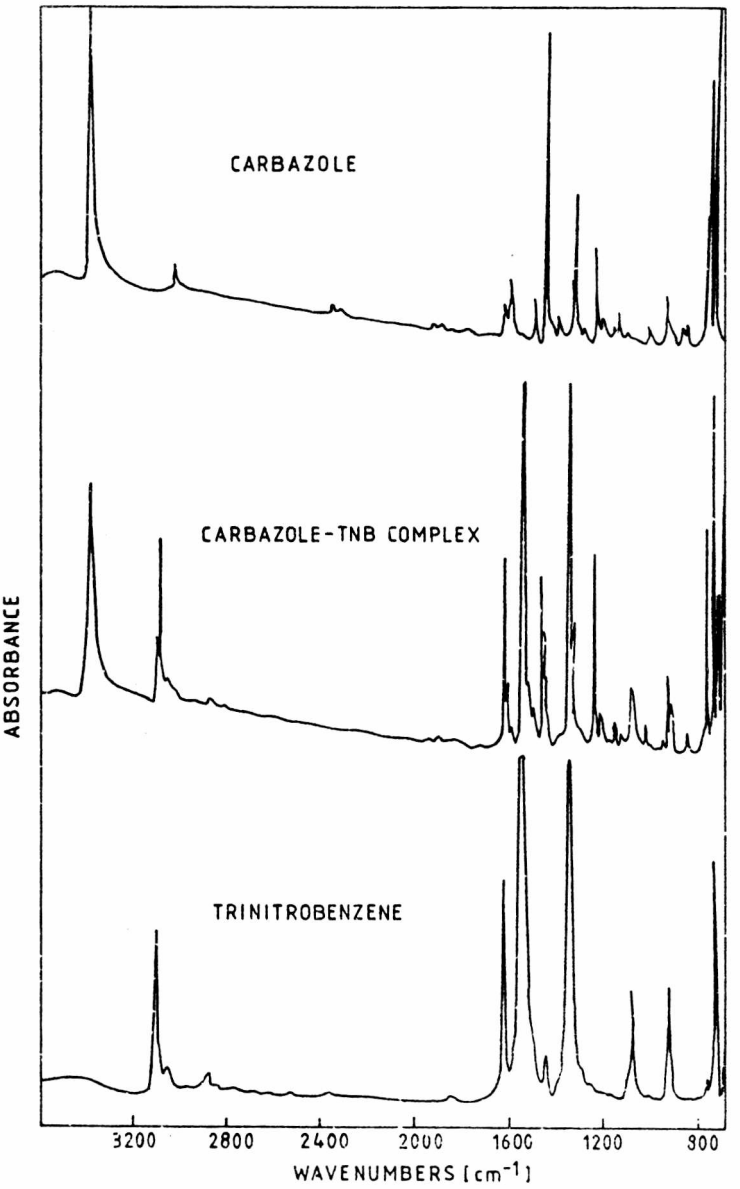

Fig. 47. Room temperature FTIR spectra (KBr pellets) of the C-TNB complex and its constituents [204]

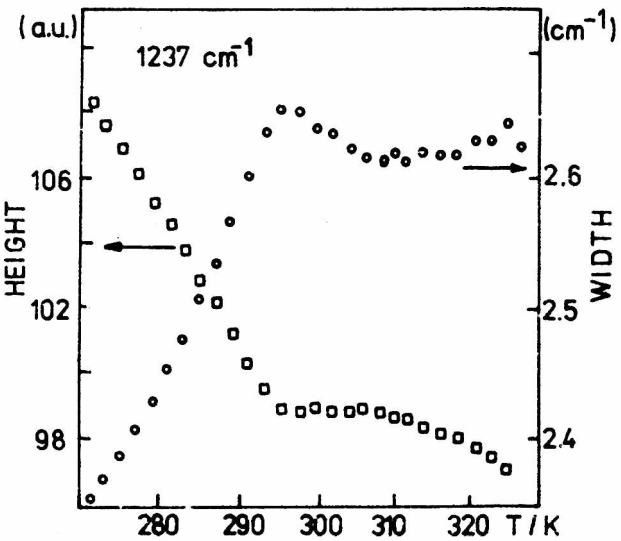

Fig. 48. Temperature dependences of the height and the width at 0.75 of maximum absorbance of the 1237 cm^{-1} band of C-TNB [204]

4.1.3. Crystallographic characterization of C-TNB at 123, 293 and 323 K [205]

In order to resolve the nature of the anomalies observed in C-TNB around 300 K we performed detailed structural investigations of the complex far below and above the phase transition temperature. The results of these investigations are reported in [205] together with all experimental details. The main finding is that the structure is essentially the same at all studied temperatures (123, 293 and 323 K) :

$C_{12}H_9N \cdot C_6H_3(NO_2)_3$ is orthorhombic, space group $P2_12_12_1$ (D_2^4), Z = 4, M_r = 380.32, lattice parameters:

	T = 123 K	T = 293 K	T = 323 K
a (Å)	6.833(5)	6.941(4)	6.935(2)
b (Å)	8.612(4)	8.729(4)	8.734(2)
c (Å)	27.951(9)	28.053(9)	28.075(5)
V (Å^3)	1644.8	1699.7	1700.4
D_{cal} (Mg/m^3)	1.536	1.486	1.486
R	0.060	0.057	0.074
R_w	0.066	0.049	0.067

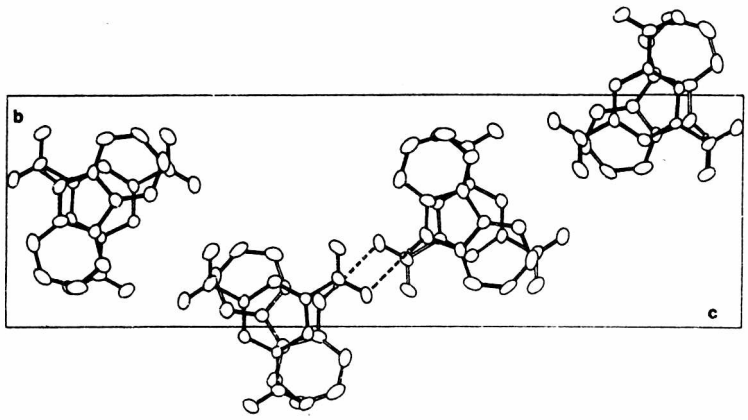

Fig. 49. Projection of a unit cell of C-TNB complex along the a-axis at 123 K. The hydrogen bonds are marked by dashed lines. H atoms are omitted [205]

The unit cell projection along the donor-acceptor stack axis (a-axis) is shown in Fig. 49. The analysis of temperature changes of some structural parameters such as unit cell dimensions, thermal ellipsoids (cf. Fig. 50) and O-H and N-H bond length (cf. Fig. 51) reveal noticeable deviations from linear behaviour around 300 K (for atom enumeration see [205]). The distribution of the thermal factors in carbazole molecule suggests that the molecule librates as a rigid body, similarly the TNB molecule librates slightly around normal to its benzene ring. Looking at the temperature behaviour of the angle between H(N4)- N(4) bond and C(7)-N(4) or C(10)-N(4) bonds one can notice that only at 323 K the H(N4) hydrogen atom approaches its non distorted position ($\simeq 120^{\circ}$). It is interesting to note that at 323 K both O(6)-H(N4) and O(5)-H(N4) distances decrease with respect to their room temperature values. It seems evident that all these effects are connected with changes of N(4)-H(N4)...O(5) hydrogen bond. This bond can be considered as a strong one at low temperatures but only of weak strength at 293 K. One can suppose that at 323 K this hydrogen bond does not exist at all.

The considerable loosening of a N(4)-H(N4)...O(5) hydrogen bond around the temperature of 300 K allows the carbazole molecule to maximize its CT interaction with TNB (it turns slightly and approaches the acceptor molecule). This effect produces a slight contraction along the donor-acceptor stack direction manifesting itself macroscopically in thermal expansion measurements [200] (one can observe a 0.1% contraction along the donor-acceptor stack direction).

Both calorimetric and dielectric anomalies observed in C-TNB complex around the temperature of 300 K can be explained, in our opinion, by the loosening of the H-bond and slight changes of orientation of NO_2 groups. This slight rearrangements are possible within the $P2_12_12_1$ space group because all the molecules occupy sites of C_1 symmetry. However, it is difficult to regard these rearrangements as a structural phase transition.

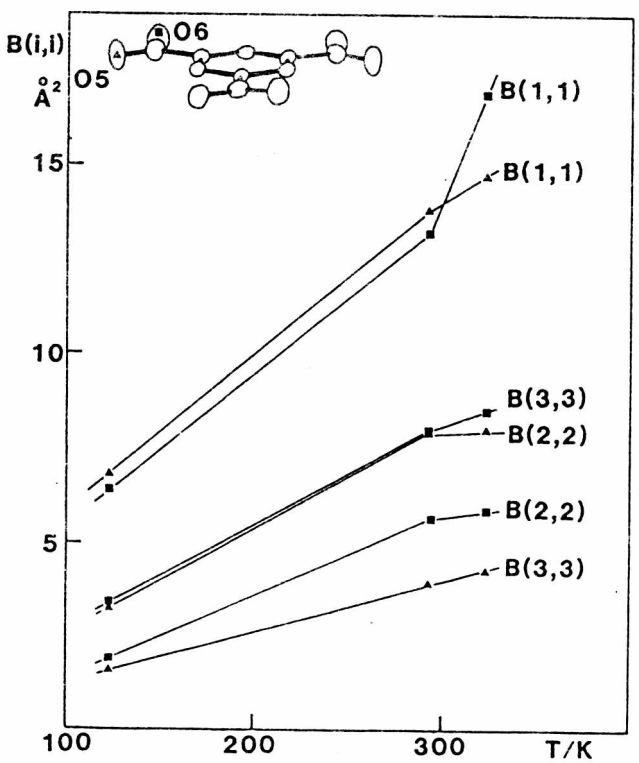

Fig. 50. Anisotropic thermal factors B(i,i) for O(5) and O(6) atoms of TNB crystal as a function of temperature. Insert: an ORTEP projection of TNB molecule at 323 K [205]

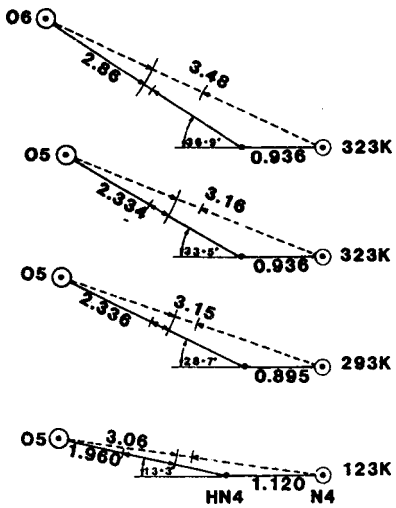

Fig. 51. Characteristics of N(4)-H(N4)...O(5) interactions in C-TNB complex, together with the N(4)-H(N4)-O(6) one given for comparison. (Distances are given in Å.)

4.1.4. Determination of elastic constants in C-TNB crystals [206]

The Brillouin scattering technique was used to study the elastic properties of the C-TNB complex [206]. Right-angle, back and small-angle scattering geometries were used.

The matrix of elastic stiffness coefficients $c_{\alpha\beta}$ contains only nine nonzero, independent components for orthorhombic symmetry .

Acoustic wave propagation in a piezoelectric solid is described by the modified Christoffel equation [9]

$$\rho v^2 u_i = \left(\Gamma_{il} + \frac{\gamma_i \gamma_l}{\epsilon} \right) u_l , \qquad i,j,k,l = 1,2,3 \qquad (48)$$

where ρ is the density of material, v is sound velocity, u_i stands for a component of the wave polarization vector, $\Gamma_{il} = c^E_{ijkl} l_j l_k$, with c^E_{ijkl} being elastic tensor component under constant electric field, l_j component of the unitary propagation vector, $\gamma_j = e_{kij} l_j l_k$, where e_{kij} - component of piezoelectric tensor and $\epsilon = \epsilon^s_{jk}$ being a component of dielectric tensor under constant deformation. Principal refractive indices, necessary for calculation, were measured for C-TNB at 647.1 nm and are as follows: $n_1 = 1.52$, $n_2 = 1.79$ and $n_3 = 1.78$ (± 0.01).

The measurements of pure longitudinal and pure transverse sound wave

velocities along the principal crystallographic axes can give directly the c^E_{11}, c^E_{22} and c^E_{33} (in this case $v^L_i = (c^E_{ii}/\rho)^{1/2}$) and c^E_{44}, c^E_{55}, c^E_{66} ($v^T_\alpha = (c^E_{\alpha\alpha}/\rho)^{1/2}$) values. The latter components can be slightly influenced by the piezoelectric coupling (usually the effect is less than a few percent of the value of a determined coefficient).

From the sound velocity measurements for various directions and polarizations of acoustic phonons for C-TNB single crystals, final values of tensor of elastic constants were calculated using a least square fitting procedure [206]. They are listed in the Table 3.

Using the presented values of elastic constants one can draw the diagrams of sound velocities in C-TNB (cf. Fig. 52).

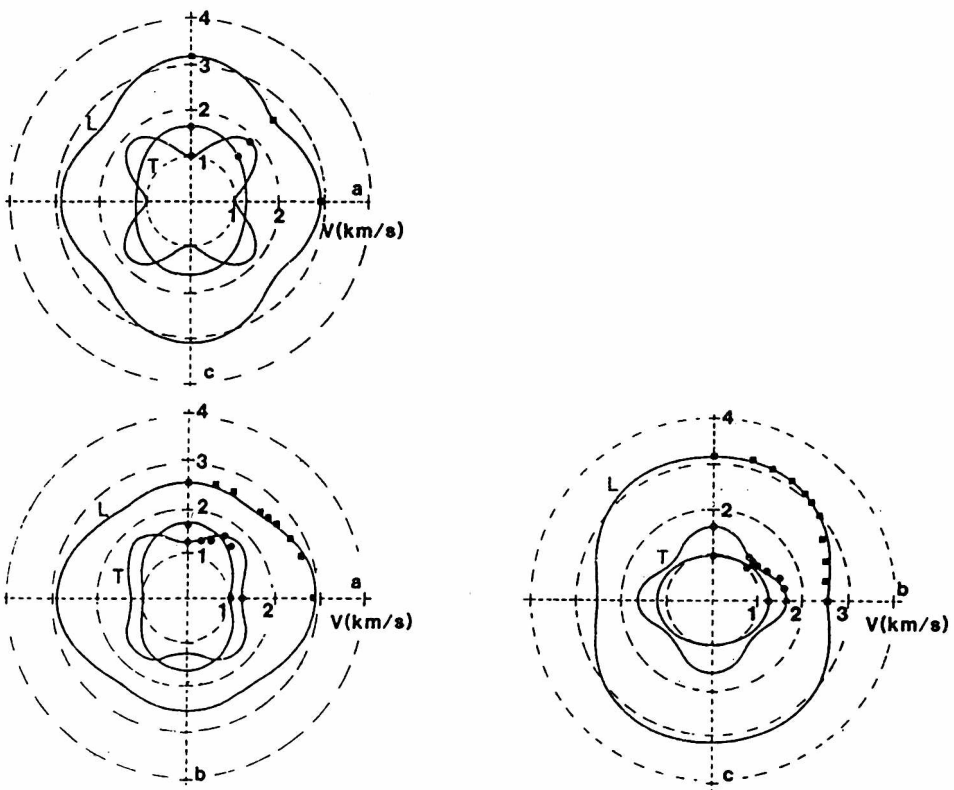

Fig. 52. Sound velocity diagrams for C-TNB single crystal at 293 K as viewed along the three principal crystallographic directions. v^L - velocity of longitudinal acoustic phonons, v^T - velocity of transverse acoustic phonons [206]

Table 3

Values of elastic stiffness $c^D_{\alpha\beta}$ and elastic compliance $s^D_{\alpha\beta}$ for C-TNB single crystal at 293 K and at ≈ 15 GHz [206]

$c^D_{\alpha\beta}$	c_{11}	c_{22}	c_{33}	c_{44}	c_{55}	c_{66}	c_{12}	c_{13}	c_{23}
(10^9 N/m^2)	12.13	9.52	14.67	3.92	1.40	2.16	2.58	2.97	7.41
$s^D_{\alpha\beta}$	s_{11}	s_{22}	s_{33}	s_{44}	s_{55}	s_{66}	s_{12}	s_{13}	s_{23}
(10^{-11}m^2/N)	8.83	17.63	11.13	25.53	71.33	46.30	-1.66	-0.95	-8.56

In the Fig. 52 the solid lines represent the calculated angular dependence of sound velocities whereas the points mark the experimentally obtained values. The longitudinal sound wave velocity does not show any pronounced anisotropy (v^l_1 = 2.78 km/s, v^l_2 = 2.484 km/s and v^l_3 = 3.048 km/s).

4.2. CT complexes of 1,2,4,5-tetracyanobenzene (TCNB)

Among the charge transfer complexes of 1,2,4,5-tetracyanobenzene (hereafter referred to as TCNB) the most extensively studied were those with anthracene [207]-[209] and naphthalene [209], [210], though many other structures were established as well: biphenylene-TCNB [211], α- and β-naphthol-TCNB [212], fluorene-TCNB [213], pyrene-TCNB [214] and phenanthrene-TCNB [215]. All those crystal structures exhibit quasi-one-dimensional stacking of alternating D-A-D-A molecules. In many structural studies an evidence of large anisotropic thermal motions and/or disorder has been found. The experimental and theoretical effort devoted to the complexes of TCNB [216]-[220] allowed for conclusion that the presence and nature of the disorder depends on size and symmetry of the donors embedded in the orientationally ordered TCNB sublattice. The character of observed disorder may be dynamical (anthracene-TCNB) [216], [217] or static (naphthalene-TCNB) [218].

Our recent interest in this type of complexes is connected with the search of noncentrosymmetric structures. The structures can be formed when a noncentrosymmetric donor molecule substitutes the centrosymmetric molecule (such as anthracene or naphthalene) in the TCNB complex. Then if

this donor molecule can arrange itself in an ordered fashion, a polar structure may arise, and consequently NLO properties could be expected. The molecules of enough similar structure and size to replace anthracene or naphthalene in the crystal lattice can be their nitrogen analogues: acridine ($C_{13}H_9N$) and quinoline (C_9H_7N).

4.2.1. Structure of the 1:1 complex of acridine with TCNB [221]

Single crystals of acridine-TCNB complex, 1×2×3 mm^3 in size, were obtained by a slow evaporation of equimolar acetone solutions of donor and acceptor. TCNB was prepared by the method described by Lawton et al. [222], whereas commercially available acridine was purified by multiple vacuum sublimation and zone melting.

The obtained structure can be characterized as follows: $C_{13}H_9N \cdot C_{10}H_2N_4$, triclinic, P1, Z = 1, M_r = 367.4, a = 7.447(4) Å, b = 7.885(5) Å, c = 8.072(9) Å , α = 73.93(9), β = 84.59(9), γ = 85.85(6)°, D_c = 1.31 Mg/m^3, R_w = 0.042 for 1241 measured independent reflections [221].

As it is shown in Fig. 53 and Fig. 54 the crystal of acridine-TCNB is built up of mixed-stacks extending along the a-axis i.e., in a fashion characteristic of π-π^* electron donor-acceptor complexes. The mean interplanar spacing between acridine and TCNB (3.48 Å) is close to that encountered in other complexes of TCNB.

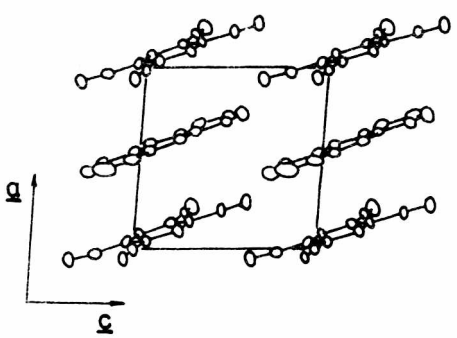

Fig. 53. Projection of the structure of acridine-TCNB complex along the b-axis [221]

Examination of the thermal ellipsoids for acridine, in the complex evidences a kind of disorder (cf. Fig. 54). Large anisotropic thermal parameters, especially for acridine might represent either an arrangement of statically disordered acridine molecules or an acridine molecule

executing large thermal librations. The "static" disorder corresponds to

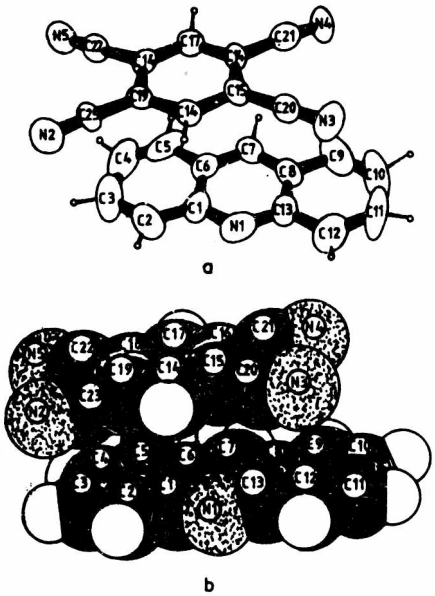

Fig. 54. a) Atom-numbering scheme and thermal ellipsoids for acridine and TCNB molecules. b) Perspective view of the complex with 80% van der Waals radii [221]

a W-shaped potential well with a barrier higher than kT value at room temperature and the librations ("dynamic disorder") to a flat-bottomed potential well. The third possibility, a W-shaped well with a barrier lower than kT at room temperature, would lead to a dynamic situation at high temperature, which could be frozen at low temperature (as was predicted and observed for anthracene-TCNB complex [216]).

As follows from the presented data, the structure of acridine-TCNB should be polar, however, no direct evidence of it has been found until now. Then one can suppose that we deal with the case similar to that described for fluorene-TCNB [213], whose space group is $P\bar{1}$ with Z = 1, i.e., the donor (fluorene) is disordered in either of two statistically possible sites related by a crystallographic centre of inversion.

In order to verify whether such a supposition can be true also for acridine-TCNB complex, and in order to establish the nature of the disorder in the crystal at room temperature, the calculations of the lattice interactions between acridine and its near neighbours were performed using semi-empirical atom-atom potentials, and introducing statically disordered arrangements into the lattice. For the purpose of these investigations, only in-plane librations of the acridine molecule were considered.

To a first approximation, the potential energy environment of a molecule in a nonionic lattice is described by intermolecular nonbonded Van der Waals interactions [223]. This can conveniently be modelled by summing all contributions from atomic pairs (i,j) at separation r_{ij}, interacting according to a Buckingham potential

$$V(r) = \frac{1}{2} \sum [a_{ij}\exp(-b_{ij}r_{ij}) - c_{ij}/r_{ij}^6] \ . \qquad (49)$$

The summation extended to 32 unit cells from the reference unit cell (and molecule) in all directions. The results of these calculations are shown in Fig.55.

The contributions to the overall potential (EA + ED) of librating acridine molecule from acceptors (EA) and donors (ED) are shown separately in Fig. 55. The calculations reflect the crystal packing and explain small angle (± 10°) of librations of acridine. Turning the acridine in the lattice of by ca. 180° and performing similar calculations of single-particle potential one finds that the energy difference between acridine at its normal (0°) position and that at 180° is less than kT value (within the limit of our approximate calculations).

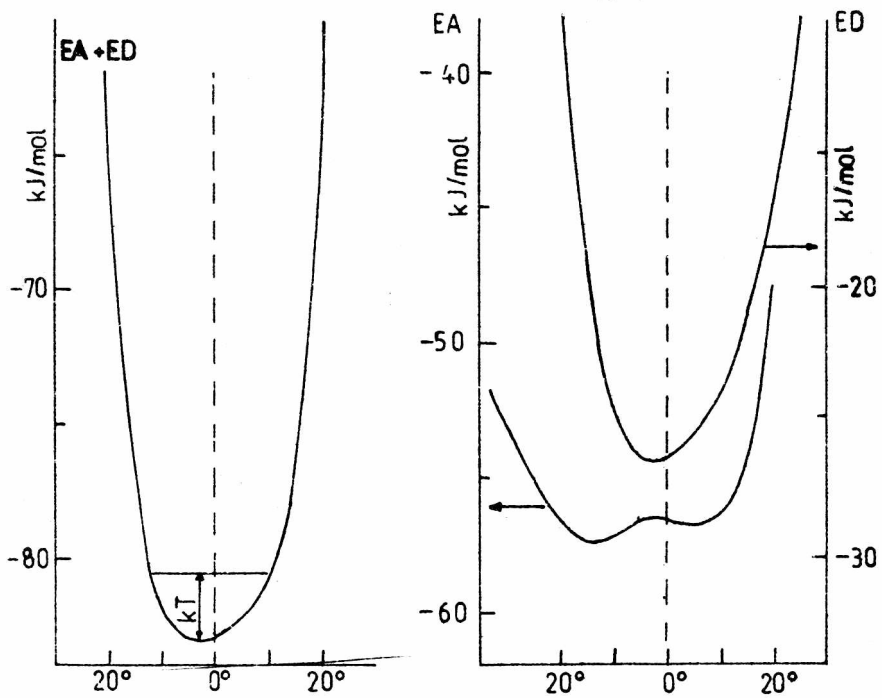

Fig. 55. Single-particle potential for acridine molecule rotating around the normal to its plane in the complex acridine-TCNB [224]

This allows us for conclusion that the structure $P\bar{1}$ with $Z = 1$ can also be true for acridine-TCNB complex (that means acridine is statically disordered). Indeed, the inversion center generated due to static disorder (0° and 180°) of acridine prevents observation of polar properties in this compound.

The structural investigations of the quinoline-TCNB complex [224] revealed that the quinoline is statically disordered in its site, then the solution of the structure needs difficult elaboration of a proper model of such a disorder.

Despite the difficulties encountered in our studies of the acridine and quinoline complexes of TCNB we attempted to determine the structure of durene-TCNB complex obtaining the following parameters [225]: $C_{10}H_{14}\cdot C_{10}H_2N_4$, $M_r = 312.4$, monoclinic, $P2_1/a$, $Z = 2$, $a = 15.249(6)$ Å, $b = 7.750(3)$ Å, $c = 7.520(2)$ Å, $\beta = 105.28^\circ$, $D_c = 1.21$ Mg/m^3.

The space group of durene-TCNB crystal $P2_1/a$, is the same as those of low-temperature phases of anthracene and naphthalene complexes of TCNB. The structure is ordered already at room temperature and no order-disorder librational type phase transition can be expected in this complex at higher temperatures. Though the structure is centrosymmetric, there is a chance that the substitution of one methyl group by a similar size atom or other group can lead to an ordered CT complex with the polar structure imposed by packing.

Concluding the data presented above, we can state that in the group of weak CT complexes of TCNB there is no, until now, suitable polar structure for observation of NLO properties, however the efforts in finding such a structure should be continued.

5. CONCLUSIONS

The investigations presented in this monograph were aimed to search for materials with interesting polar properties.

One of the most fundamental findings is that macroscopic properties of the materials can be tailored by proper substitutions. It has been shown that within any of the described groups crystals lacking a symmetry center have been found. Moreover, in the group of organic-inorganic halides a gentle substitution of atoms or organic groups led to materials being ferroelectric at different temperatures, undergoing one or more phase transitions, being ferroelastic or not. This is what one calls "molecular engineering".

Another important finding is that the delicate balance of the forces leading to such a diverse phenomenon as ferroelectricity can be relatively easily found in the group of crystals containing perovskite type structure, but extremely difficult within organics. We believe that the new ferroelectric groups of crystals should be searched within mixed organic-inorganic compounds where the ionic forces are supplemented by dipolar, H-bond and van der Waals interactions.

The purpose oriented search for new polar materials is always time-consuming, and the final result depends not only on the amount of effort devoted, but frequently it is a matter of luck. However, on the basis of presented above investigations, there is no doubt that further studies should be concentrated within the most fruitful group of organic-inorganic halides and not within organic charge transfer complexes. However, from the viewpoint of applications, the crystals belonging to the group of acid phthalates as being optically perfect, easy to grown, chemically and thermally stable are more suitable to be exploited in electrooptic devices than some of the representatives of other groups.

One should emphasize that the results of studies presented in this work do not close, but rather open a large field for other studies. It would be tempting, for instance, to try to prepare mixed compounds of the type $((CH_3)_3NH)_3Sb_2Cl_{9-n}Br_n$ or $(CH_3NH_3)_5Bi_2Br_{11-n}Cl_n$ for studying subtle changes of pyroelectric or electrooptic properties. There is a possibility to use other organic groups for preparation new materials on the basis of the perovskite inorganic sublattice. The electrooptic crystals of acid phthalates can be properly doped in order to obtain new materials showing photorefractive effect. Besides, there is a need for basic studies, both experimental and theoretical, of phase transitions of the double nature, such as that found in TMACA.

The most important from the practical point of view is the finding of good pyroelectric and electrooptic properties in $(CH_3NH_3)_5Bi_2Br_{11}$ and $((CH_3)_3NH)_3Sb_2Cl_9$ compounds with some perspectives for their applications in commercial devices. Also the studies of electrooptic and elastic properties of potassium, sodium and rubidium acid phthalates are of great importance as these crystals possess a potential value for application, too.

The most interesting from the point of view of fundamental research is the dynamics and interaction between two sublattices in the group of organic-inorganic halides. Our Raman, Brillouin and other studies in TMACA, DMACA, DMABA and similar crystals revealed the complex nature of phase transitions in these compounds due to dimensionality of the transitions. Interesting is also the effect of organic moieties on the

nature of observed properties, especially the electrooptic activity of the crystals.

We believe that the goal of this work formalised in the Introduction has been fulfilled.

Acknowledgements

This work was partially supported by the Programme of Polish Academy of Sciences CPBP 01.12.

The author is grateful to the University of Rennes I and University of Lille I for financial supports.

REFERENCES

[1] H. Kuhn, [in:] Proc. Int. Symposium on Future Electron Devices, Bioelectronic and Molecular Electronic Devices, R & D Association for Future Electron Devices, Tokyo 1985.

[2] D. Jerome, A. Mazaud, M. Ribault and K. Bechgaard, J. Physique Lett. 41, L95 (1980).

[3] T. Skotheim, The handbook of conducting polymers, Dekker, New York 1985.

[4] Nonlinear optical properties of organic and polymeric materials, D. Williams (ed.), Am. Chem. Soc., Washington 1983.

[5] A.L. Solomon, Phys. Rev. 104, 1191 (1956).

[6] D. Bordeaux, J. Bornarel, A. Capiomont, J. Lajzerowicz-Bonneteau, J. Lajzerowicz and J.F. Legrand, Phys. Rev. Lett. 31, 314 (1973).

[7] W.P. Mason, Piezolectric crystals and their application to ultrasonics, Van Nostrand, Princeton 1950.

[8] D.A. Berlincourt, D.R. Curnan and H. Jaffe, [in:] Physical acoustics, principles and methods, W.P. Mason (ed.), Academic Press, New York 1964.

[9] E. Dieulesaint and D. Royer, Ondes eastiques dans les solides, Masson, Paris 1974.

[10] W.G. Cady, Piezolectricity, McGraw-Hill, New York 1946.

[11] J.F. Nye, Physical properties of crystals, Oxford Univ. Press, London 1957.

[12] F. Jona and G. Shirane, Ferroelectric crystals, Pergamon Press, Oxford 1962.

[13] J.C. Burfoot, Ferroelectrics, an introduction to the physical principles, D. van Nostrand, London 1967.

[14] J. Grindlay, An introduction to the phenomenological theory of ferroelectricity, Pergamon Press, Oxford 1970.

[15] T. Mitsui, I. Tatsuzaki and E. Nakamura, An introduction to the physics of ferroelectrics, Gordon and Breach Science Publishers, New York 1976.

[16] K. Aizu, J. Phys. Soc. Jpn. 27, 387 (1969).

[17] S.C. Abrahams, Mater. Res. Bull. 6, 881 (1971).

[18] J. Sapriel, Phys. Rev. B, 12, 5128 (1975).

[19] H. Mueller, Phys. Rev. 58, 565 (1940).

[20] A.F. Devonshire, Adv. Phys. 3, 85 (1954).

[21] L.D. Landau, Phys. Z. Soviet. 11, 26 (1937).

[22] L. Tisza, On the general theory of phase transitions [in:] Phase transformations in solids, Wiley, New York 1951.
[23] M.E. Drougard and D.R. Young, Phys. Rev. 94, 1561 (1954).
[24] S. Hoshino, T. Mitsui, F. Jona and R. Pepinsky, Phys.Rev. 107, 1255 (1957).
[25] S. Nomura, J. Phys. Soc. Jpn. 16, 2440 (1961).
[26] K. Hamano, J. Phys. Soc. Jpn. 19, 945 (1964).
[27] H. Mueller, Phys. Rev. 57, 829 (1940).
[28] M. de Quervain, Helv. Phys. Acta 17, 509 (1944).
[29] H. Baumgartner, Helv. Phys. Acta 24, 326 (1951).
[30] A.F. Devonshire, Phil. Mag. 40, 1040 (1949).
[31] E.J. Huibregtse and D.R. Young, Phys. Rev. 103, 7705 (1956).
[32] J.-C. Toledano and P. Toledano, The Landau theory of phase transitions, World Scientific, Singapore 1987.
[33] J.C. Slater, Phys. Rev. 78, 748 (1950).
[34] R.A. Cowley, Adv. Phys. 29, 1 (1980).
[35] M.E. Lines and A.M. Glass, Principles and applications of ferroelectrics and related materials, Oxford University Press, Oxford 1977.
[36] L.D. Landau and E.M. Lifshitz, Statistical physics, Pergamon, London 1959.
[37] P.A. Franken, A.E. Hill, C.W. Peters and G. Weinreich, Phys. Rev. Lett. 7, 118 (1961).
[38] J. Kerr, Phil. Mag. 50, 337 (1875) (after [42]).
[39] F. Pockels, Lehrbuch der Kristalloptik, Teubner, Leipzig 1906 (after [42]).
[40] I.P. Kaminow, An introduction to electrooptic devices, Academic Press, New York 1974.
[41] D.A. Kleinman, Phys. Rev. 126, 1977 (1962).
[42] N. Bloembergen, Nonlinear optics, Benjamin, Massachusetts 1965.
[43] F. Zernike and J.E. Midwinter, Applied nonlinear optics, J. Wiley, New York 1973.
[44] I.P. Kaminow, IEEE J. Quantum Electron. QE-4, 23 (1968).
[45] D.S. Chemla and J. Zyss, Nonlinear optical properties of organic molecules and crystals, Academic Press, Orlando 1987.
[46] C. Flytzanis, Quantum electronics : a treatise, 1 (A), 19 (1975), Academic Press, New York 1975.
[47] J.L. Oudar, J.Chem.Phys. 67, 446 (1977).
[48] J. Zyss and J.L. Oudar, Phys. Rev. A26, 2028 (1982).
[49] J.F. Nicoud and R.J. Twieg [in:] Nonlinear optical properties of organic molecules, D.S. Chemla and J. Zyss (ed.), Vol. 1, Academic Press, London 1987.

[50] S.K. Kurtz and T.T. Perry, J. Appl. Phys. 39, 3798 (1968).
[51] J. Zyss and G. Berthier, J. Chem. Phys. 77, 3635 (1982).
[52] P.D. Southgate and D.S. Hall, J. Appl. Phys. 43, 2765 (1972).
[53] K. Kato, IEEE J. Quantum Electron. QE-16, 1288 (1980).
[54] B.F. Levine, C.G. Bethea, C.D. Thurmond, R.T. Lynch, J.L. Bernstein, J. Appl. Phys. 50, 2523 (1979).
[55] J.S. Zyss, D.S. Chemla, J.F. Nicoud, J. Chem. Phys. 74, 4800 (1981).
[56] J.L. Oudar and R. Hierle , J. Appl. Phys. 48, 2699 (1977).
[57] R.J. Twieg, A Azema, K. Jain and Y.Y. Cheng, Chem. Phys. Lett. 92, 208 (1982).
[58] D. Adhikesavalu and K. Venkatesan, Acta Crystallogr. C39, 589 (1983).
[59] L. Schuler, K. Betzler, H. Hesse and S. Kapphan, Opt. Commun. 43, 157 (1982).
[60] N.G. Furmanova, Z.P. Razmanova, L.V. Soboleva, I.A. Maslyanitsyn, H. Siegert, V.D. Shigorin and G.P. Shipulo, Sov. Phys. Crystallogr. 29, 285 (1984).
[61] D. Xu, M. Jiang and Z. Tan, Acta Chim. Sin. 2, 230 (1983).
[62] R. Bechmann and S.K. Kurtz, [in:] Landolt-Börnstein tables, Vol. III (2), p. 167 , Springer-Verlag, Berlin 1969.
[63] S.K. Kurtz, J. Jerphagnon and M.M. Choy, [in:] Landolt-Börnstein tables, Vol. III (11), p. 671, Springer-Verlag, Berlin 1979.
[64] J. Jerphagnon, S.K. Kurtz and J.L. Oudar, [in:] Landolt-Börnstein tables, Vol. 18, Springer-Verlag, Berlin 1984.
[65] A. Miniewicz, Thesis, Wrocław 1980 (in Polish).
[66] A. Miniewicz, M. Samoć, J. Sworakowski and B. Jakubowski, Conf. Proc. 9th Molecular Crystal Symposium, p. 175,Mittelberg, Kleinwersertal, Austria 1980.
[67] A. Miniewicz and J. Sworakowski, Ferroelectrics 34, 213 (1981).
[68] A. Miniewicz, M. Samoć, J. Sworakowski and Z. Zboiński, Materials Science 7, 441 (1981).
[69] A.G. Chynoweth, J. Appl. Phys. 27, 78 (1956).
[70] P. Christie, C.A. Jones, M.C. Petty and G.G. Roberts, J. Phys.. D: Appl. Phys. 19, L167 (1986).
[71] S.B. Lang and F. Steckel, Rev. Sci. Instr. 36, 929 (1965).
[72] T.S. Narasimhamurty, Photoelastic and electro-optic properties of crystals, Plenum Press, New York 1981.
[73] A. Yariv and P. Yeh, Optical Waves in Crystals, J. Wiley, New York 1984.
[74] R.W. Lee, J. Opt. Soc. Am. 59, 1574 (1969).
[75] Y. Tokura, A. Kurita and T. Koda, Phys. Rev. B31, 2588 (1985).
[76] R. Jakubas and L. Sobczyk, Phase Transitions (to be published)

[77] R. Jakubas, Z. Galewski, L. Sobczyk and J. Matuszewski, J. Phys. C. 18, L857 (1985).

[78] R. Jakubas, Z. Czapla, Z. Galewski, L. Sobczyk, O.J. Żogał and T. Lis, Phys. Stat. Solidi (a) 93, 449 (1986).

[79] R. Jakubas, Solid State Commun. 60, 389 (1986).

[80] R. Jakubas, Z. Czapla, Z. Galewski and L. Sobczyk, Ferroelectrics Lett. 5, 143 (1986).

[81] R. Jakubas, L. Sobczyk and J. Matuszewski, Ferroelectrics 74, 339 (1987).

[82] R. Jakubas, U. Krzewska, G. Bator and L. Sobczyk, Ferroelectrics 77, 129 (1988).

[83] H. Arend, [in:] Crystal Growth of Electronic Materials, E. Kaldis (ed.), p. 307, Elsevier Science Publishers, B.V. 1985.

[84] E.R. Peterson and R.D. Willet, J. Chem. Phys. 56, 1879 (1972).

[85] G. Chapuis, H. Arend and R. Kind, Phys. Stat. Solidi (a) 31, 449 (1975).

[86] G. Chapuis, R. Kind and H. Arend, Phys. Stat. Solidi (a) 36, 285 (1976).

[87] G. Heger, D. Mullen and K. Knorr, Phys. Stat. Solidi (a) 31, 455 (1975).

[88] W. Depmeier, Acta Crystallogr. B33, 3713 (1977).

[89] G. Chapuis, Acta Crystallogr. B44, 1506 (1978).

[90] S. Sawada, Y. Shiroishi, A. Yammamoto, M. Takashige and M. Matsuo, J. Phys. Soc. Jpn. 44, 687 (1978).

[91] R. Almairac, M. Ribet, J.L. Ribet and Bziouet, J. Physique Lett. 41, L315 (1980).

[92] K. Gesi, J. Phys. Soc. Jpn. 51, 2532 (1982).

[93] K. Gesi, J. Phys. Soc. Jpn. 51, 203 (1982).

[94] P. Muralt, H. Arend, D. Altermatt and G. Chapuis, Ferroelectrics 56, 7 (1984).

[95] S. Sawada, Y. Shiroishi, A. Yammamoto, M. Takashige and M. Matsuo, Phys.Lett. 67A, 56 (1978).

[96] A. Sawada, J. Sugiyama, M. Wada and Y. Ishibashi, J. Phys. Soc. Jpn. 48, 1773 (1980).

[97] K. Gesi and M. Izumi, J. Phys. Soc. Jpn. 48, 1775 (1980).

[98] H. Mashiyama and S. Tanisaki, Phys. Lett. 76A, 347 (1980).

[99] Landolt-Börnstein, Magnetic properties of transition metal compounds, New Series, Vol. II, Springer, Berlin 1979/1980.

[100] K. Walther, Solid State Commun. 27, 901 (1978).

[101] E. Fatuzo and R. Nitsche, Phys. Rev. 117, 939 (1960).

[102] R.E. Caputo, Inorg. Chem. 5, 820 (1976).

[103] J. Mróz, Z. Czapla and R. Jakubas, Acta Phys. Polonica A70, 705 (1986).

[104] F.-J. Kruger, F. Zettler and A. Schmidt, Z. Anorg. Allg. Chem. 449, 135 (1979).

[105] A. Kallel and J.W. Bats, Acta Crystallogr. C41, 1022 (1985).

[106] K. Kihara and T. Sudo, Z. Kristallogr. 134, 142 (1971).

[107] K. Kihara and T. Sudo, Acta Crystallogr. B30, 1088 (1974).

[108] S. Idziak and R. Jakubas, Solid State Commun. 62, 173 (1987).

[109] A. Miniewicz, J. Sworakowski, R. Jakubas, M. Bertault and C. Ecolivet, Ferroelectrics, 94, 323 (1989).

[110] R. Jakubas, A. Miniewicz, M. Bertault, J. Sworakowski and A. Collet, J. Physique France 50, 1483 (1989).

[111] G.C. Pimentel and A.L. McClellan, The hydrogen bond, Freeman, San Francisco 1960.

[112] A. Miniewicz, R. Jakubas and C. Ecolivet, Ferroelectrics 80, 153 (1988).

[113] A. Miniewicz, R. Jakubas, C. Ecolivet and A. Girard, J. Raman Spectrosc. 20, 381 (1989).

[114] R. Mokhlisse, M. Couzi and J. Lassegues, J. Phys. C 16, 1353 (1983).

[115] R. Mokhlisse, M. Couzi and P. Loyzance, J. Phys. C 16, 1367 (1983).

[116] M. Couzi, A. Daoud and R. Perret, Phys. Stat. Solidi (a) 41, 271 (1977).

[117] M. Couzi and Y. Milk, J. Raman Spectrosc. 17, 117 (1986).

[118] C. Sourisseau and G. Lucazeau, J. Raman Spectr. 8, 311 (1979).

[119] M. Schlaak, M. Couzi, J.C. Lassegues and W. Drexel, Chem. Phys. Lett. 45, 111 (1977).

[120] M. Mylrajam and T.K.K. Srinivasan, Spectrochimica Acta 44A, 485 (1988).

[121] M. Mylrajam and T.K.K. Srinivasan, J. Phys. C 21, 1673 (1988).

[122] I.P. Kaminow and W.D. Johnston Jr., Phys.Rev. 160, 519 (1967).

[123] P. da R. Andrade and S.P.S. Porto, Solid State Commun. 13, 1249 (1973).

[124] P. da R. Andrade and S.P.S. Porto, Solid State Commun. 14, 547 (1974).

[125] P. da R. Andrade, A.D. Prasad Rao, R.S. Katiyar and S.P.S. Porto, Solid State Commun. 12, 847 (1973).

[126] A. Girard, M. Sanquer and G.P. Charbonneau, Mol. Cryst. Liq. Cryst. 95, 237 (1983).

[127] W. Dultz, J. Chem. Phys. 65, 2812 (1976).

[128] H. Fuess, M. Korfer, H. Arend and R. Kind, Solid State Commun. 56, 137 (1985).
[129] S. Kashida and S. Sato, J. Phys. Soc. Jpn. 54. 2934 (1985).
[130] K. Gesi, J. Phys. Soc. Jpn. 51, 2031 (1982).
[131] K. Hasebe, T. Asahi, S. Tanisaki and K. Gesi, J. Phys. Soc. Jpn. 57, 1138 (1988).
[132] M. Wada, M. Suzuki, A. Sawada, Y. Ishibashi and K. Gesi, J. Phys. Soc. Jpn. 50, 1813 (1981).
[133] K. Hasebe, H. Mashiyama, N. Koshiji, S. Tanisaki, J. Phys. Soc. Jpn. 56, 3543 (1987).
[134] Y. Shiroishi and S. Sawada, J. Phys. Soc. Jpn. 46, 148 (1979).
[135] J.A. Pople, D.L. Beveridge, P.A. Dobosh, J. Chem. Phys. 47, 2026 (1967).
[136] J. Lipiński, Int. J. Quantum Chem. 34, 423 (1988).
[137] A. Miniewicz, M. Pyka and J. Lipiński, unpublished data
[138] A. Miniewicz and R. Jakubas, [in:] Proc. Third International Conf. on Unconventional Photoactive Solids, p. 138, Schloss Elmau, FRG 1987.
[139] S. Allen, T.D. McLean, P.F. Gordon, B.D. Bothwell, M.B. Hursthouse and S.A. Karaulov, J. Appl. Phys. 64, 2583 (1988).
[140] M. Gdaniec, Z. Kosturkiewicz, R. Jakubas and L. Sobczyk, Ferroelectrics 77, 31 (1988).
[141] R.D. Whealy and R.L. Yeakley, J. Inorg. Nucl. Chem. 25, 365 (1963).
[142] A. Miniewicz and R. Jakubas, Solid State Commun. 63, 933 (1987).
[143] A. Miniewicz and R. Jakubas, Solid State Commun. 67, 1079 (1988).
[144] V. Janovec, V. Dvorak and J. Petzelt, Czech. J. Phys. B25, 1362 (1975).
[145] P. Toledano and J.-C. Toledano, Phys. Rev. B14, 3079 (1976).
[146] H.G. Unruh and V. Rudiger, J.Physique France 33, C2-77 (1972).
[147] N.Yamada, J. Phys. Soc. Jpn. 46, 561 (1979).
[148] W.J. Minkus, Phys. Rev.A138, 1277 (1965).
[149] S. Idziak and R. Jakubas, Ferroelectrics 80, 75 (1988).
[150] C. Ecolivet, A. Miniewicz and R. Jakubas, Solid State Commun. 71, 143 (1989).
[151] A. Miniewicz, J.Lefebvre and R. Jakubas, [in:] Proc.VIth EMF, Saarbrücken, FRG 1989, Ferroelectrics (accepted).
[152] C. Ecolivet, M. Sanquer, J. Pellegrin and J. Dewitte, J. Chem. Phys. 78, 6317 (1983).
[153] W. Rehwald, Adv. Phys. 22, 721 (1973).
[154] E. Käräjämäki, R. Laiho, T. Levola, W. Kleemann and F.J. Schäfer, Physica 111B, 24 (1981).
[155] J. Petzelt and V. Dvorák, J. Phys. C 9, 1571 (1976).

[156] J. Petzelt and V. Dvorák, J. Phys. C 9, 1587 (1976).
[157] V. Winterfeld and G. Schaack, Ferroelectrics 15, 21 (1977).
[158] L.D. Landau and I.M. Khalatnikov, Dokl. Akad. Nauk SSSR 96, 469 (1954).
[159] E.J. O'Brien and T. Litovitz, J. Appl. Phys. 35, 180 (1964).
[160] H.Z. Cummins, Phil. Trans. R. Soc. London A293, 393 (1979).
[161] C. Ecolivet, A. Miniewicz, W. Kusto, P. Bourges, Reunion Française de Ferroelectricité, Orleans, France 1988 (abstract).
[162] A. Miniewicz, R. Jakubas and C. Ecolivet, [in:] Proc.VIth EMF, Saarbrücken, FRG 1989, Ferroelectrics (accepted).
[163] R. Jakubas and A. Miniewicz, Ferroelectrics 70, 145 (1986).
[164] R. Jakubas, Solid State Commun. 69, 267 (1988).
[165] R. Jakubas and L. Sobczyk, Ferroelectrics, 1989 (in press).
[166] A. Miniewicz and R. Jakubas, Ferroelectrics, 1989 (submitted).
[167] E. Nakamura, T. Mitsui and J. Furuichi, J. Phys. Soc. Jpn. 18, 1477 (1963).
[168] A. Shaulov, M.I. Bell and W.A. Smith, J. Appl. Phys. 50, 4913 (1979).
[169] A. Miniewicz and R. Jakubas, J. Mol. Electronics (accepted).
[170] G.F. Lipscomb, A.F. Garito and R.S. Narang, J. Chem. Phys. 75, 1509 (1981).
[171] Y. Okaya, Acta Crystallogr. 19, 879 (1965).
[172] R.A. Smith, Acta Crystallogr. B31, 2347 (1975).
[173] V.F. Bereznitskaya, V.I. Andrianov and V.I. Simonov, Sov. Phys. Crystallogr. 21, 528 (1976).
[174] L.M. Belyaev, G.S. Belikova, A.B. Gilvarg and I.M. Silvestrova, Sov. Phys. Crystallogr. 14, 544 (1970).
[175] Yu.V. Shaldin and T.M. Okhrimenko, Sov. Phys. Crystallogr. 20, 750 (1975).
[176] G.S. Belikova, L.M. Belyaev, M.P. Golovei, Yu.V. Pisarevskii, I.M. Silvestrova and T.I. Turskaya, Sov. Phys. Crystallogr. 19, 351 (1974).
[177] M.D. Shahabuddin Khan and T.S. Narasimhamurty, J. Mat. Sci. Lett. 1, 268 (1982).
[178] R. Poprawski, S. Matyjasik and Yu.V. Shaldin, Solid State Commun. 62, 257 (1987).
[179] N. Krishnamurthy and V. Soots, J. Raman Spectr. 6, 221 (1977).
[180] B. Orel, D. Hadzi and F. Cabassi, Spectrochimica Acta 31A, 169 (1975).
[181] R. Poprawski, S. Matyjasik and Yu.V. Shaldin, Materials Science 13, 203 (1987).

[182] A. Miniewicz, J. Lefebvre, H. Fontaine and Y. Marqueton, J. Raman Spectr. 1989 (in press).
[183] A. Miniewicz, C. Ecolivet and Y. Marqueton, Materials Science 13, 169 (1987).
[184] D.F. Nelson, Electric, optic and acoustic interactions in dielectrics, J. Wiley, New York 1979.
[185] C. Ecolivet, A. Miniewicz and M. Sanquer, (in preparation).
[186] A. Miniewicz, M. Samoć, J. Dziedzic and R. Poprawski, [in:] Proc. 11th Mol. Cryst. Symposium, p.198, Lugano, Switzerland 1985
[187] A. Miniewicz, A. Samoć and J. Sworakowski, J. Mol. Electronics 4, 25 (1988).
[188] A. Miniewicz, R. Nowak, M. Samoć and J. Sworakowski, Acta Phys. Polonica A60, 715 (1981).
[189] M. Samoć, A. Miniewicz and D.F. Williams, Potsdamer Forschungen, 1, 132 (1983).
[190] A. Miniewicz, M. Samoć and D.F. Williams, Mol. Cryst. Liq. Cryst. 111, 199 (1984).
[191] A. Miniewicz, M. Samoć and D.F. Williams, Acta Phys. Polonica A74, 91 (1988).
[192] G. Briegleb and J. Czekalla, Z. Elektrochem. 59, 184 (1955).
[193] S.P. McGlynn and J.D. Bogus, J. Am. Chem. Soc. 80, 5096 (1958).
[194] D.S. Brown, S.C. Wallwork and A. Wilson, Acta Crystallogr. 17, 168 (1964).
[195] F. Iwasaki and Y. Saito, Acta Crystallogr. B26, 251 (1970).
[196] I. Bar and J. Bernstein, Acta Crystallogr. B34, 3438 (1978).
[197] A.W. Hanson, Acta Crystallogr. 19, 19 (1965).
[198] F.H. Herbstein, M. Kapon and G.M. Reisner, Acta Crystallogr. B42, 181 (1986).
[199] F. Bechtel, D. Chasseau and J. Gaultier, Cryst. Struct. Commun. 5, 297 (1976).
[200] A. Miniewicz, M. Samoć, J. Sworakowski, B. Jakubowski, Z. Zboiński and A. Cehak, Chem. Phys. Lett. 76, 442 (1980).
[201] A. Miniewicz, M. Samoć, J. Sworakowski and B. Jakubowski, [in:] Proc. 9th Molecular Crystal Symposium, p.175, Mittelberg -Kleinwalsertal, FRG, 1980
[202] A. Miniewicz, J. Sworakowski and D.F. Williams, Ferroelectrics 55, 271 (1984).
[203] A. Miniewicz, J. Sworakowski and D.F. Williams, [in:] Proc. Polish Molecular Crystals Conference, p.79, Kraków, Poland 1983 (in Polish).
[204] A. Miniewicz, J. Sworakowski, D.F. Williams, D.J. Cameron and J. Umemura, Spectrochimica Acta 41A, 1305 (1985).

[205] L. Toupet and A. Miniewicz, Acta Crystallogr. B, (submitted)
[206] C. Ecolivet, A. Miniewicz and M. Sanquer, J. Phys. Chem. Solids 50, 651 (1989).
[207] H.Tsuchiya, F.Marumo and F. Saito, Acta Crystallogr. B28, 1935 (1972).
[208] J.J. Stezowski, J. Chem. Phys. 73, 538 (1980).
[209] J. Lefebvre, G. Odou, M. Muller, A. Mierzejewski and T. Luty, Acta Crystallogr. B45, 323 (1989).
[210] S. Kumakura, F. Iwasaki and F. Saito, Bull. Chem. Soc. Jpn. 40, 1826 (1967).
[211] J.J. Stezowski, R.-D. Stigler and N. Karl, J. Chem. Phys. 84, 5162 (1986).
[212] M.C. Couldwell and C.K. Prout, J. Chem. Soc. Perkin II, 160 (1978).
[213] W. Mühle, J. Krzystek, J.V. von Schütz, H.C. Wolf, R.-D. Stigler and J.J. Stezowski, Chem. Phys. 108, 1 (1986).
[214] C.K. Prout, T. Morley, I.J. Tickle and J.D. Wright, J. Chem. Soc. Perkin II, 523 (1973).
[215] J.D. Wright, K. Yakushi and K. Kuroda, Acta Crystallogr. B34, 1934 (1978).
[216] T. Luty and B. Kuchta, J. Chem. Phys. 85, 4032 (1986).
[217] T. Luty, Order-disorder in Solids 6, 27 (1988).
[218] E. Erdle and H. Möhwald, Solid State Commun. 26, 327 (1978).
[219] J.C.A. Boyens and A.H. Reddoch, J. Chem. Phys. 74, 1519 (1981).
[220] A. Mierzejewski, C. Ecolivet, G.S. Pawley, T. Luty, A. Girard and M.H. Lemée, Solid State Commun. 65, 431 (1988).
[221] L. Toupet, A. Miniewicz and C. Ecolivet, Acta Crystallogr. C45, 1044 (1989).
[222] E.A. Lawton and D.D. McRitchie, J. Org. Chem. 24, 26 (1959).
[223] A.I. Kitajgorodski, Molecular crystals, PWN, Warszawa 1976 (in Polish).
[224] L. Toupet and A. Miniewicz, unpublished results
[225] J. Lefebvre, A. Miniewicz and R. Kowal, Acta Crystallogr. C45, 1372 (1989).

Received January 12, 1990

In revised form January 22, 1990

W POSZUKIWANIU MOLEKULARNO-JONOWYCH I MOLEKULARNYCH KRYSZTAŁÓW WYKAZUJĄCYCH FERROELEKTRYCZNE I ELEKTROOPTYCZNE WŁAŚCIWOŚCI

Monografia zawiera opis wyników badań eksperymentalnych wybranych własności fizycznych kryształów, których strukturę scharakteryzować można istnieniem zarówno molekularnych jak i jonowych oddziaływań. Obiektem badań były związki z trzech grup: organiczno-nieorganicznych halidków, kwaśnych ftalanów i organicznych kompleksów z przeniesieniem ładunku (CT).

Wstęp do pracy zawiera opis polarnych własności kryształów ze szczególnym uwzględnieniem nieliniowych własności optycznych. Badania podstawowe prezentowane w tej monografii mają na celu zrozumienie mikroskopowych aspektów struktury materiałów i jej wpływu na własności makroskopowe. Autor poszukuje i bada zjawiska ferroelektryczności, piroelektryczności i nieliniowe efekty optyczne w wybranych związkach.

Opisano szczegółowo metody badania współczynnika piroelektrycznego i liniowego efektu elektrooptycznego (efektu Pockelsa). Inne techniki eksperymentalne, takie jak rozpraszanie Ramana, rozpraszanie Brillouina, spektroskopia w podczerwieni, kalorymetria, badania rentgenowskie struktury czy metody dielektryczne są omawiane przy okazji prezentacji wyników badań poszczególnych związków. Przejścia fazowe obserwowane w niektórych kryształach są dyskutowane w ramach istniejących teorii a mechanizmy tych przejść rozważane na poziomie molekularnym.

Najciekawsze wyniki uzyskano dla grupy soli organicznych, a w szczególności klasy organiczno-nieorganicznych halidków. Pokazano, że $((CH_3)_3NH)_3Sb_2Cl_9$ (TMACA) i $(CH_3NH_3)_5Bi_2Br_{11}$, które są ferroelektrykami w temperaturze pokojowej, mogą być wykorzystane do budowy wydajnych detektorów piroelektrycznych. Oba te związki wykazują także własności elektrooptyczne. Badania mikroskopowe oraz badania rozpraszania Ramana i Brillouina dla dwóch izomorficznych kryształów $((CH_3)_2NH_2)_2Sb_2Cl_9$ (DMACA) i $((CH_3)_2NH_2)_2Sb_2Br_9$ (DMABA) wykazały istnienie interesujących ferroelektrycznych przejść fazowych.

Doskonałej jakości optycznej kryształy kwaśnych ftalanów hodowane z roztworu posiadają znaczące nieliniowe własności optyczne, co umożliwia ich zastosowanie jako modulatorów światła.

W grupie organicznych kompleksów CT tylko kryształ kompleksu karbazol-trinitrobenzen nie zawiera środka symetrii. Badania strukturalne w grupie kompleksów tetracyjanobenzenu wykazały istnienie kompleksu polarnego akrydyna-TCNB, ale ze względu na statystyczny nieporządek w podsieci akrydyny kryształ ten nie nadaje się do zastosowań.

ПОИСКИ МОЛЕКУЛЯРНО-ИОННЫХ И МОЛЕКУЛЯРНЫХ КРИСТАЛЛОВ ИНТЕРЕСНЫХ СЕГНЕТОЭЛЕКТРИЧЕСКИХ И ЭЛЕКТРОНИЧЕСКИХ СВОЙСТВ

Настоящая работа содержит описание результатов экспериментальных исследований разных физических свойств кристаллов, которых структуру можно охарактеризовать существованием как молекулярных, так и ионных взаимодействий. Объектом исследований были соединения, происходящие из трех групп: органично-неорганических галогенидов, кислых фталатов и органических комплексов с переносом заряда (СТ). Введение содержит описание полярных свойств кристаллов с особенным учетом нелинейных оптических свойств. Целью основных исследований, представленных в настоящей работе, является понять микроскопические аспекты структуры материалов и ее влияния на микроскопические свойства. Автор исчет и исследует явления сегнетоэлектричества, пироэлектричества и нелинейные оптические эффекты в избранных соединениях.

Подробно описаны методы исследования пироэлектрического коэффициента и линейного электрооптического эффекта (Покельса). Многие другие экспериментальные техники, как: комбинационное и бриллюэновское рассеяния, спектроскопия в инфракрасной области, калориметрия, рентгеноструктурные исследования или диэлектрические методы обсуждаются по поводу представления результатов исследований для отдельных исследований. Фазовые переходы, наблюдаемые в некоторых кристаллах, обсуждаются в рамках существующих теорий, а механизмы этих переходов рассуждаются на молекулярном уровне.

Самые интересные результаты были получены в группе органических солей, а в особенности в классе органично-неорганических галогенидов. Было показано, что $((CH_3)_3NH)_3Sb_2Cl_9$ (TMACA) и $(CH_3NH_3)_5Bi_2Br_{11}$, которые являются сегнетоэлектриками в комнатной температуре, могут быть использованы для строения эффективных пироэлектрических детекторов. Оба эти соединения обнаруживают также хорошие электрооптические свойства. Микроскопические исследования и исследования рамановского и бриллюэновского рассеяний в двух изоморфных кристаллах $((CH_3)_2NH_2)_2Sb_2Cl_9$ (DMACA) и $((CH_3)_2NH_2)_2Sb_2Br_9$ (DMABA) обнаруживали существование интересных фазовых сегнетоэлектрических переходов.

Кристаллы хорошего оптического качества кислых фталатов, разводимых из раствора, имеют существенные нелинейные оптические свойства, что способствует их применению в качестве модуляторов света.

В группе органических комплексов СТ лишь комплекс карбазол-тринитробензол не содержит центра инверсии. Структурные исследования в группе комплексов тетрацианбензола обнаружили существование полярного соединения акридин-TCNB, но из-за статического беспорядка в подсети акридина этот материал не подходит для применения в электрооптике.

CONTENTS

PRACE NAUKOWE INSTYTUTU CHEMII ORGANICZNEJ
I FIZYCZEJ
(wydane w latach 1986—1989)

Nr 30, Monografie nr 15, J. Skarżewski, *Kataliza międzyfazowa i micelarna w utlenianiu związków aromatycznych jonami metali*, Wrocław 1986 75,—

Nr 31, Monografie nr 16, G. J. Ashwell, *The pyridinum 7,7,8,8-tetracyano-p-quinodimethanide salts (from a low-temperature metal to a potential molecular rectifier)*, Wrocław 1986 50,—

Nr 32, Monografie nr 17, M. Soroka, *Wybrane problemy chemii kwasów aminofosfonowych*, Wrocław 1987 140,—

Nr 33, Konferencje nr 8, *Endocrinological Frontiers in Physiological Insect Ecology*, Wrocław 1988 1850,—

Nr 34, Monografie nr 18, L. Syper, *Zastosowanie związków selenu w reakjach utleniania cząsteczek organicznych*, Wrocław 1988 200,—

Nr 35, Monografie nr 19, B. Lejczak, *Aktywność biologiczna aminofosfonianów i fosfonopeptydów*, Wrocław 1988 160,—

Nr 36, Monografie nr 20, P. Kafarski, *Fosfonopeptydy — synteza i stereochemia*, Wrocław 1989 140,—

Subscription should be sent (at any time of the year) to:
„Ars Polona"
Krakowskie Przedmieście 7, 00-068 Warszawa
Bank account number: PBK XIII Oddz. W-wa 370044-1195-139-11
Zamówienia na prenumeratę można składać:
OR PAN, PKiN, 00-901 Warszawa
Nr konta bankowego: PBK IX Oddz. W-wa, 370031-4792

Wydawnictwa Politechniki Wrocławskiej
są do nabycia w:
P.P. „Dom Książki"
Księgarni Wr 49
Wybrzeże Wyspiańskiego 27
oraz kiosku przy Wydawnictwie Politechniki Wrocławskiej
Plac Grunwaldzki 13, 50-377 Wrocław
(budynek D-1 PWr.)

ISSN 0324-976X